Revealing surface charge transport in thin films of topological Weyl metal $SrRuO_3$

Dr. Wei-Li Lee

Institute of Physics, Academia Sinica, Nankang, 11529, Taipei, Taiwan

Outline

- ❑ **Review of the topological Weyl semimetal and ferromagnetic Weyl metal SrRuO3 (SRO) system:**
  - Brief review of magnetic Weyl semimetal and Bulk-surface correspondences in topological Weyl metal SRO.
  - Adsorption control growth of SRO thin films using oxide MBE facility at IoPAS.
- ❑ **Weyl-orbit quantum oscillation effect (WOE):**
  - Structural charac. of low defect level and untwinned SRO thin films.
  - "Thickness" dependent quantum oscillations and comp. to simulated Weyl-orbit QO.
- ❑ **Nonreciprocal and nonlinear charge transports (NRTE) in SRO thin film:**
  - Fabrication of sunbeam devices from an untwinned SRO thin film for anisotropy measurements.
  - Observation of NRTE and nonlinear Hall effect in SRO thin film at low temperatures.
- ❑ **Conclude and future outlooks**

Kar *et al.* Sci. Rep. 11, 16070 (2021).
Kar *et al.* npj Quantum Materials 8, 8 (2023).
Kar et al. arXiv:2307.04482, submitted.

NSTC 國家科學及技術委員會 National Science and Technology Council

Acknowledgements for outside collaborators

Weyl-orbit QO. in Weyl metal SrRuO3

NSRRC Director Chia-Hung Hsu

Prof. Steffen Wiedmann

Dr. Song Yang

Chun-Yen Lin

NSRRC Hsinchu
(TPS 09A and TLS 07A)
High precision X-ray charac.

Dr. Yu-Te Hsu

M. Berben

Radbound univ. and HMFL-Nijmegen
(Magnetotransport up to 35 T
SRO t = 9, 13.7, 18.7 nm)

NRTE and nonlinear Hall

Prof. Wei-Cheng Lee

Binghamton Univ. -SUNY
(theoretical band Cal.)

NCTS Director/Chair Prof.
Dr. Peram S.V. Reddy

NTU
(theoretical band Cal.)

Prof. I-Chun Cheng

EE, NTU
(Device Fabrication)

Prof. Dave Hsieh
Dr. Cinwei Li
Yungjoon Han

Caltech
(optical SHG)

Acknowledgements (cont.)

Dr. Wei-Li Lee's group, Dr. Akhilesh Singh, Dr. Bipul Das, S.T. Kuo, U. Kar, Joyce Lin and Ender Cheng.

IoP, Academia Sinica, Taipei

1. **Magnetotrasnsport measurements up to 14 T**
2. **SRO thin film growths and device fabrication**
3. **Operation and maintenance of oxide MBE facility IoPAS**
4. **X-ray, LEED and RHEED structural charac.**

Special thanks to **Dr. H. Nair** and **Prof. D. Schlom** for sharing experience on adsorption controlled growth using an oxide MBE

Brief review of Weyl semimetal (WSM)

Selected for a Viewpoint in *Physics*

PHYSICAL REVIEW B **83**, 205101 (2011)

Topological semimetal and Fermi-arc surface states in the electronic structure of pyrochlore iridates

Xiangang Wan,[1] Ari M. Turner,[2] Ashvin Vishwanath,[2,3] and Sergey Y. Savrasov[1,4]
[1]*National Laboratory of Solid State Microstructures and Department of Physics, Nanjing University, Nanjing 210093, China*
[2]*Department of Physics, University of California, Berkeley, California 94720, USA*
[3]*Materials Sciences Division, Lawrence Berkeley National Laboratory, Berkeley, California 94720, USA*
[4]*Department of Physics, University of California, Davis, One Shields Avenue, Davis, California 95616, USA*
(Received 23 February 2011; published 2 May 2011)

Minimum model of a WSM with one pair of non-overlapped Weyl nodes:
Unusual n = 0 chiral Landau levels under applied magnetic field

$$\varepsilon_{n=0} = \pm \hbar v_F \vec{k} \cdot \hat{B}$$

$$\partial_\mu j_5^\mu = \frac{e^2}{4\pi^2\hbar^2} \vec{E} \cdot \vec{B}$$

$$j_5^\mu = j_+^\mu - j_-^\mu$$

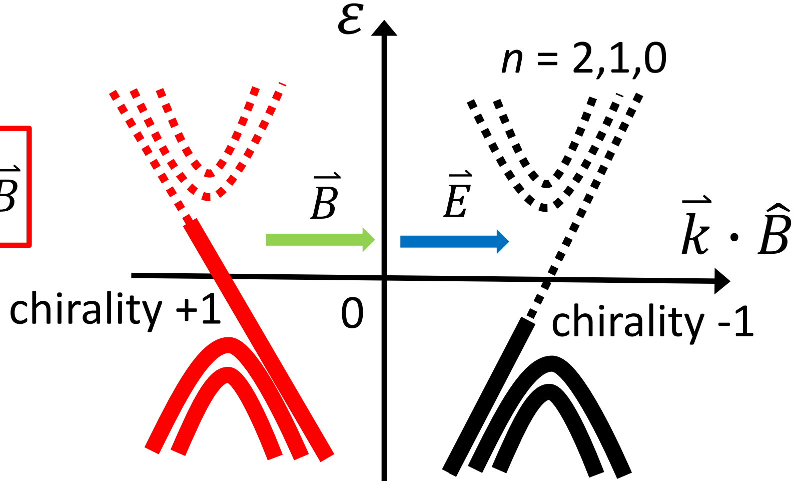

Chiral anomaly: non-conserved axial current
(neutral pion decay: $\pi^0 \rightarrow 2\gamma$: Adler-Bell-Jackiw anomaly in 1968)
Axion fields and chiral magnetic effect in cosmology/astrophysics.

For $\tau_{inter} >> \tau_{intra}$ and $\vec{E} \parallel \vec{B}$, additional conductivity

$$\sigma_{chiral} \propto \frac{B^2 \tau_{inter}}{\varepsilon_F^2}$$

Son & Spivak PRB 88, 104412 (2013)
Ong & Liang Nat. Rev. Phys 3, 394 (2021)
Yip, arXiv:1508.01010

Negative longitudinal MR for $\vec{E} \parallel \vec{B}$

Huang *et al.* PRX 5, 031023 (2015)

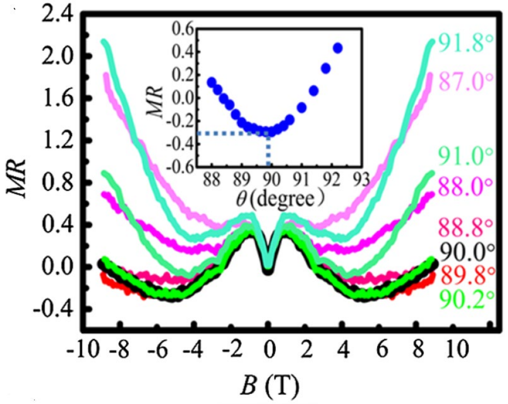

Inversion asymm. Weyl **TaAs**

Xiong *et al.* Science 350, 413 (2015)

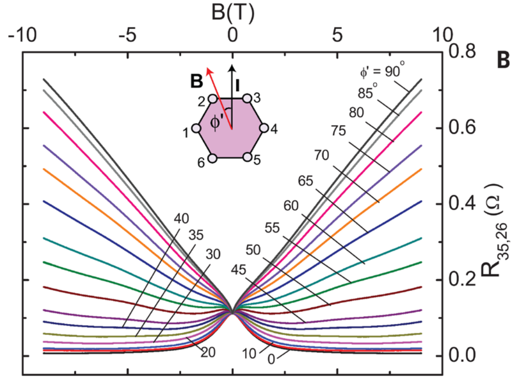

Field breaking of chiral symm. in Dirac **Na3Bi**

Suppressed TEP for $\vec{E} \parallel \vec{B}$: 1D n = 0 chiral LL (D.O.S. indep. of energy.)

Jia *et al.* Nat. commun. 8, 13741(2016)

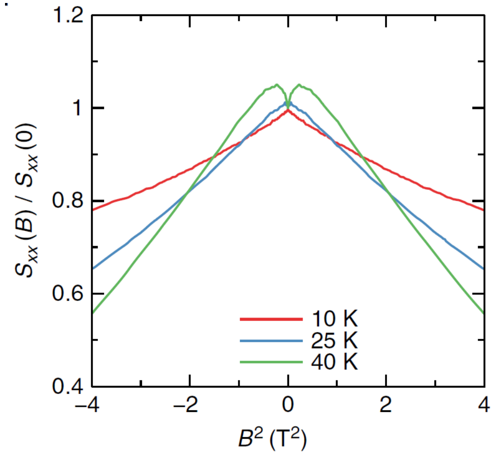

Broken chiral symm. by field in Dirac **Cd3As2**

Hirschberger *et al.* Nat. Mat. 15, 1161 (2016)

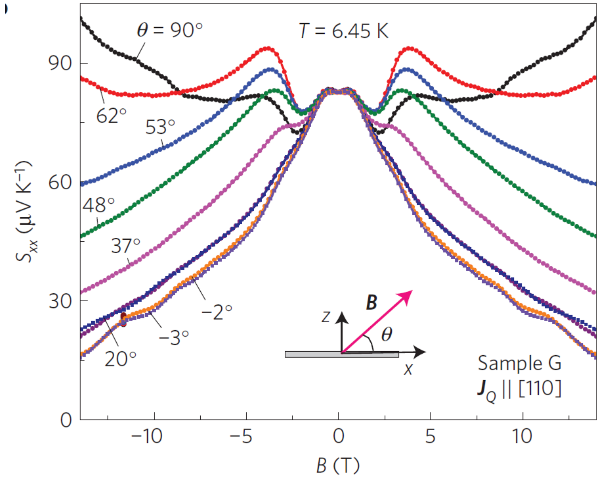

Field induced Weyl in magnetic **GdPtBi**

Fermi arc surface states in a topological Weyl semimetal

Wan *et al.* PRB 83, 205101 (2011)
Armitage *et al.* RMP 90, 015001 (2018)
Nandkishore *et al*. PRB 89, 245110 (2014)
Wilson *et al.* PRB 97, 235108 (2018)

A minimum model of a Weyl SM: one Weyl-node pair

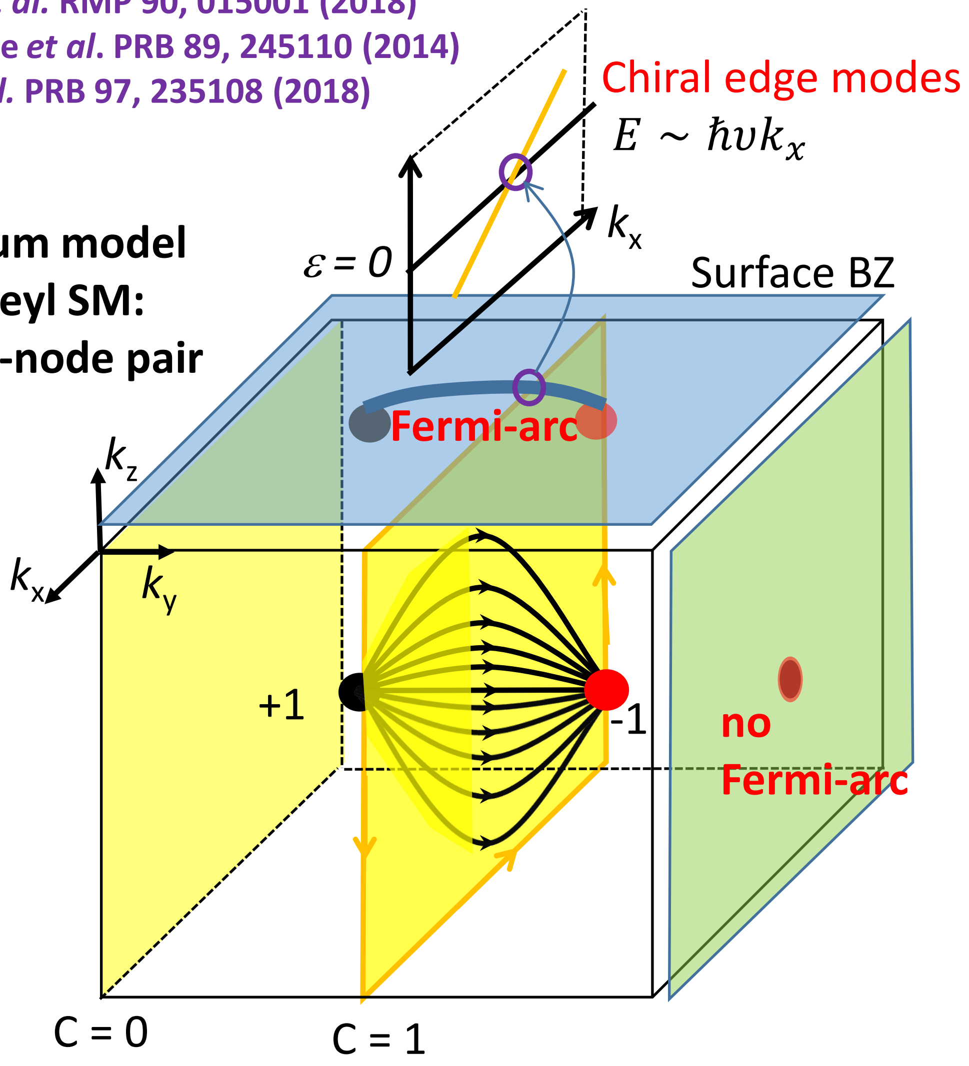

- Any sliced 2D plane between a Weyl-node pair has a total Berry flux of 2π (C =1): Chiral edge modes at the boundary

$$\text{Chern number } C = \underbrace{\frac{1}{2\pi}\oint \vec{\Omega}\left(\vec{k}\right)\cdot dS_{\vec{k}}}_{\text{Berry flux}}$$

- Fermi-arc surface states are unusual "one-way" chiral zero modes (ε = 0) but may not be robust against disorder: bulk-surface hybridization + rare region effect in disordered Dirac/Weyl.
  (high quality crystals and thin films are needed !)

- Fermi-arc surface states: connecting projected non-overlapping Weyl-node pairs.

- Unique bulk-surface correspondence between Weyl-node bulk states and Fermi-arc surface states.

Unique thickness dep. Weyl-orbit quantum oscillations in Weyl semimetal

Potter *et al.* Nat. Commun. 5, 5161 (2014)

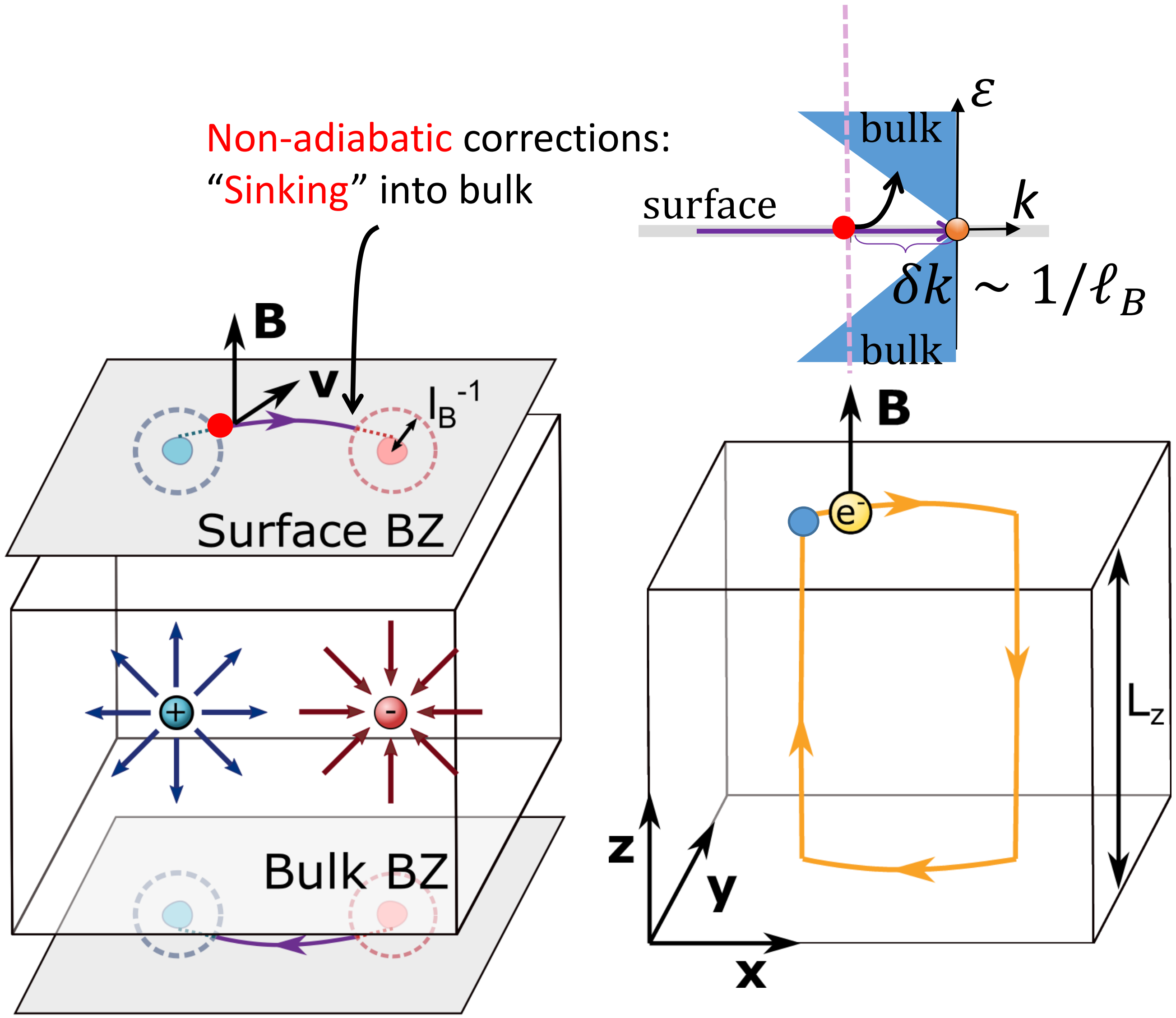

- Distinct nonlocal cyclotron orbit driven by B_z

Top Fermi-arc

Bulk Weyl-node (+1) ⇄ Bulk Weyl-node(-1)

Bottom Fermi-arc

- Quantized energy of nonlocal Weyl-orbit

$$\varepsilon_n \cdot 2\left(\frac{\hbar k_0}{evB} + \frac{L_z}{v}\right) = 2\pi n\hbar.$$

n is LL index, and k_0 is the length of Fermi-arc.

- Unique thickness dep. QO ($\varepsilon_n = \mu$)

$$\frac{1}{B_n} = \frac{e}{\hbar k_0'}\left[\frac{\pi\hbar v n}{\mu} - L_z\right].$$

$k_0' \equiv k_0(1 - 4\alpha/k_0\ell_B)$, and

α is non-adiabatic correction param.

$\ell_B \equiv \sqrt{\hbar/eB_n}$ is the magnetic length

- Reduced effective Weyl-orbit area due to α.

- Only sensitive to B_z : a 2D-like Fermi-pocket.

First demonstration of Weyl-orbit quantum oscillations in Dirac semimetal Cd3As2

Transport evidence for Fermi-arc-mediated chirality transfer in the Dirac semimetal Cd_3As_2

Philip J. W. Moll[1,2], Nityan L. Nair[1], Toni Helm[1,2], Andrew C. Potter[1], Itamar Kimchi[1], Ashvin Vishwanath[1] & James G. Analytis[1,3]

Moll *et al.* Nature 535, 266 (2016)

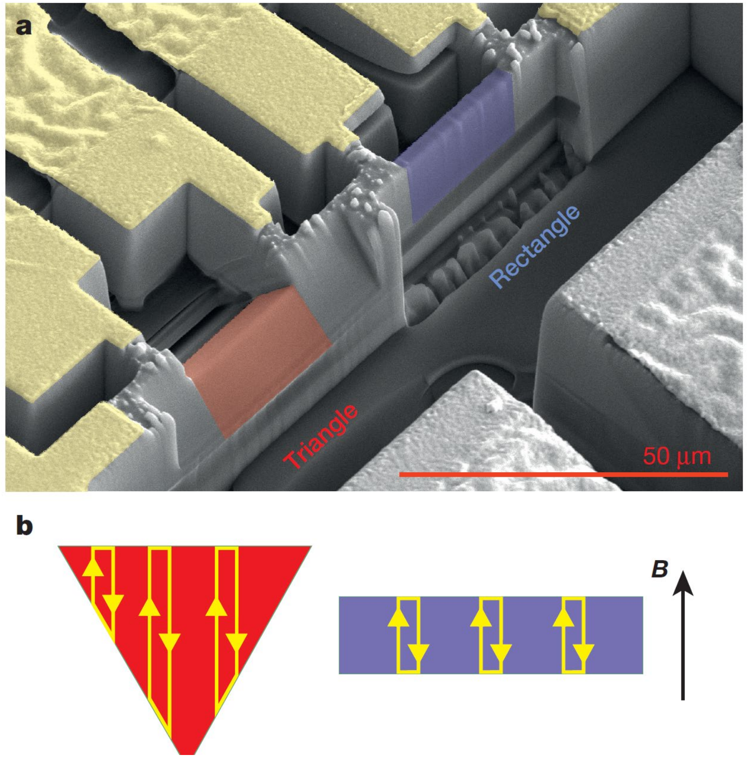

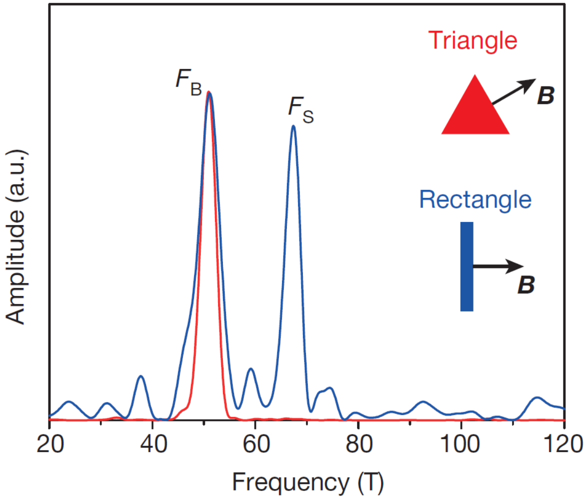

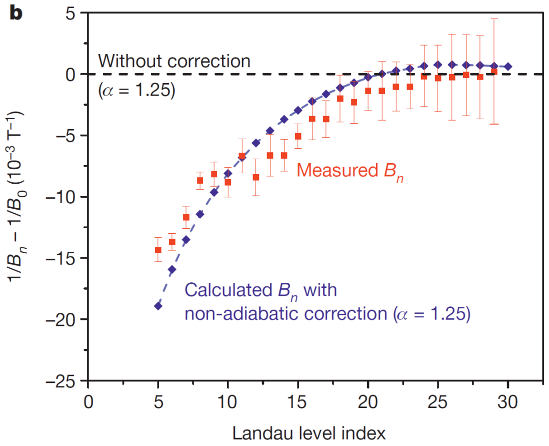

- FIB-machined thin flakes of Cd_3As_2, thickness > 150 nm (<< bulk mean free path ~ 1000 nm)
- Field-splitting of the Weyl-node pair
- The absence of Weyl-orbit QO in wedge shaped Cd_3As_2
- The presence of the non-adiabatic correction.

- A number of more recent reports in Cd_3As_2 thin films and other microcrystal devices:
  Zhang *et al.* Nat. Commun. 8, 13741 (2017) & Nature 565, 331 (2019)
  Schumann *et al.* PRL 120, 016801 (2018),
  Nishihaya *et al.* Nat. Commun. 2, 2572 (2021)
  …
- Extrinsic (surface) defect from ion-implantation ? Density variation effect ? Surface Fermi-loop or Fermi-arcs ?
  Galletti *et al.* PRB 99, 201401 (2019)
  Lin *et al.* PRL 122, 036602 (2019) …

> Quest for further tests in other Dirac/Weyl semimetal systems, particularly in high quality thin-film form !

Emergent property of SRO as a magnetic Weyl

- Orthorhombic SRO is a metallic and ferromagnetic oxide with a Curie temp ~ 165 K.
- Moderate correlated material : Fermi-liquid at low temp and asym. tunneling spectrum
- Slightly distorted orthorhombic SRO films on SrTiO3 (001) compressive strain of - 0.4% with magnetic easy axis along $[110]_o$.

Koster *et al.* Rev. Mod. Phys. 84, 253 (2012)

- The presence of the Weyl nodes near Fermi surface:
  - ✓ $\sigma_{xy} \simeq -180\ \Omega^{-1}\mathrm{cm}^{-1}$ (close to $\frac{e^2}{ha} \sim 500\ \Omega^{-1}\mathrm{cm}^{-1}$)
  - ✓ Non-monotonic anomalous Hall conductivity with magnetization
  - ✓ Spin wave gap and softening of the magnon mode at low temp.
- DFT + U (J = 0.2U) calculations show d-p hybridization and complex band crossings around the Fermi surface (> 100 crossings), inferring a Weyl phase. **Chen *et al.* PRB 88, 125110 (2013)**
- The growth of high crystalline SRO film is difficulty due to the high volatility of RuOx and thus the presence of Ru vacancies.
- High sensitivity of disorder on charge transport in ruthenates.

Capogna *et al.* *PRL* 88, 076602 (2002)

- **Achieving growth of SRO films by oxide MBE with low level of Ru vancancies.**

  Adsorption controlled technique: Nair *et al.* APL mater. 6, 046101 (2018)

  Machine learning assisted: Takiguchi et al. Nat. commun. 11, 4969 (2020)

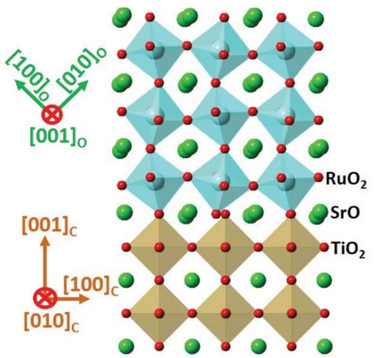

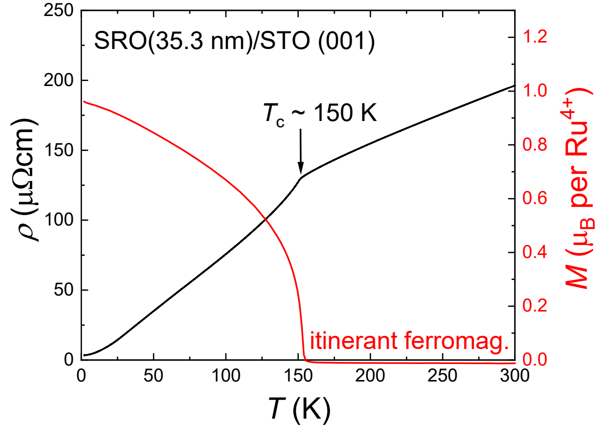

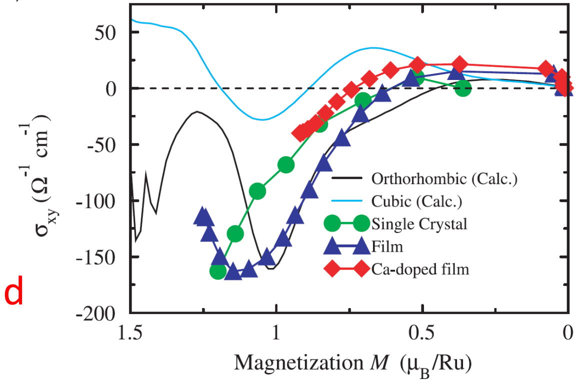

Fang *et al.* Science 302, 92 (2003)

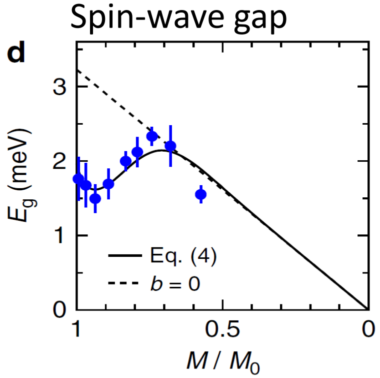

Itoh *et al.* Nat. commun. 7, 11788 (2016)

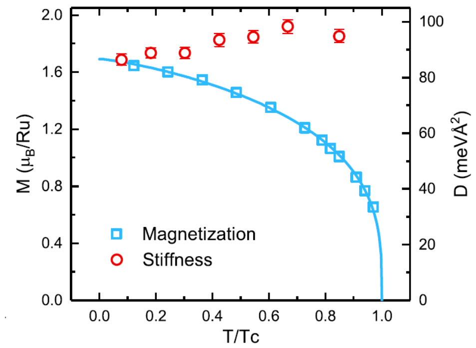

Jenni *et al.* PRL 123, 017202 (2019)

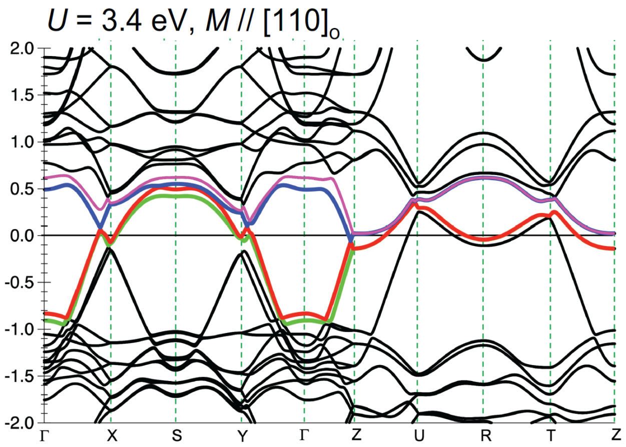

Adsorption control growth of films using MBE with volatile elements

- The growth of GaAs : excess As_2/As_4 flux and growth rate determined by Ga flux.

Foxon J. Vac. Sci. Technol. *B* 1983.

Arrhenius plot

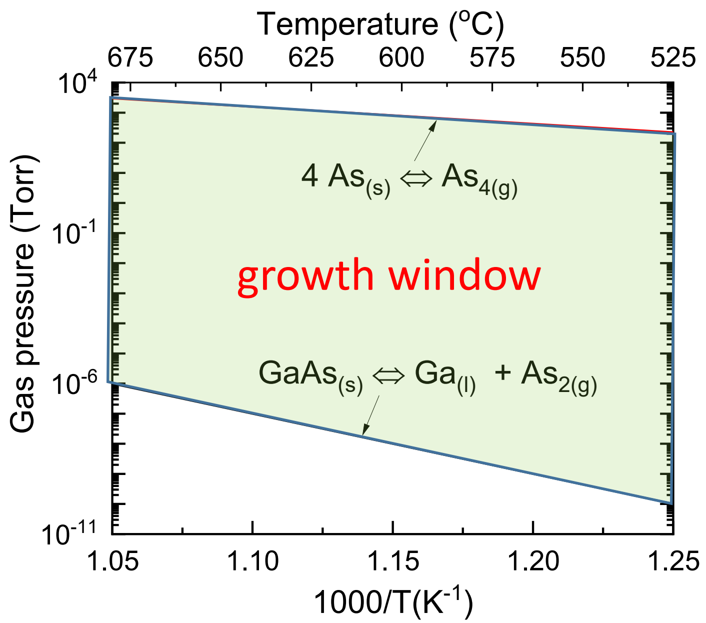

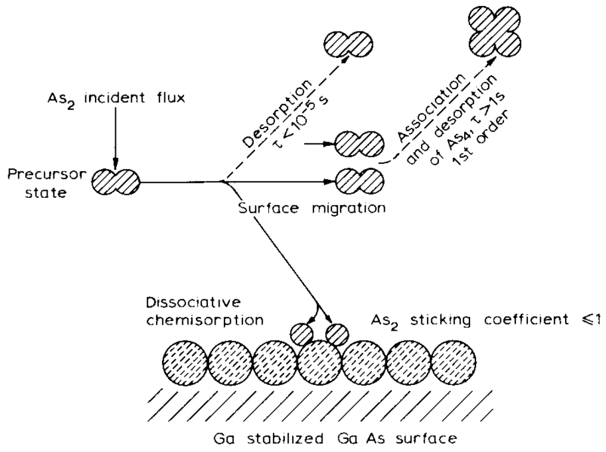

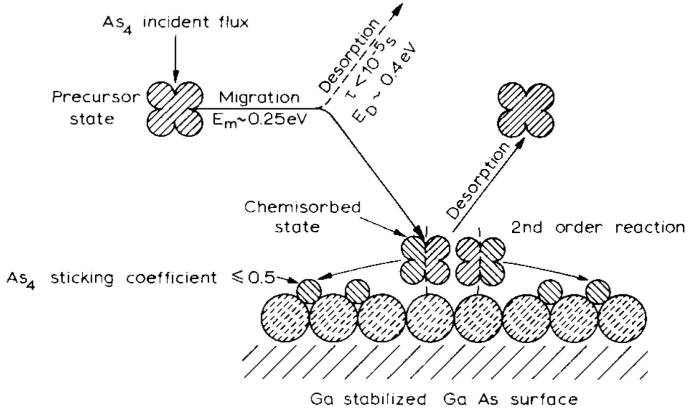

- Three temperatures approach for Bi_2Se_3: excess Se flux and $T_{Bi\ cell} > T_{substrate} > T_{Se\ cell}$.

Chen *et al.* Adv. Mater. 2011.

- The advantage of thermodynamically self-adjusted stoichiometry in the resulting films: resemble bulk single crystal growth process !

Adsorption control growth of oxide epitaxial thin films

- Growth of several oxides films: $PbTiO_3$, $LuFe_2O_4$, $SrRuO_3$, Sr_2RuO_4 …etc.
  Theis *et al.* Thin Solid films 325, 107 (1998), Brooks *et al.* APL 101, 132907 (2012), Nair *et al.* APL mater. 6, 046101 (2018)
- Thermodynamics of MBE (TOMBE phase diagram) for Ruthenates $Sr_{n+1}Ru_nO_{3n+1}$: open system with excess Ru flux in ozone environment ideal for the growth of ruthenates thin films to minimize the Ru vacancies.
- Large growth window for $SrRuO_3$ phase and tunable by Ru flux: thermodynamically-adjusted Stoichiometry of the oxide films.

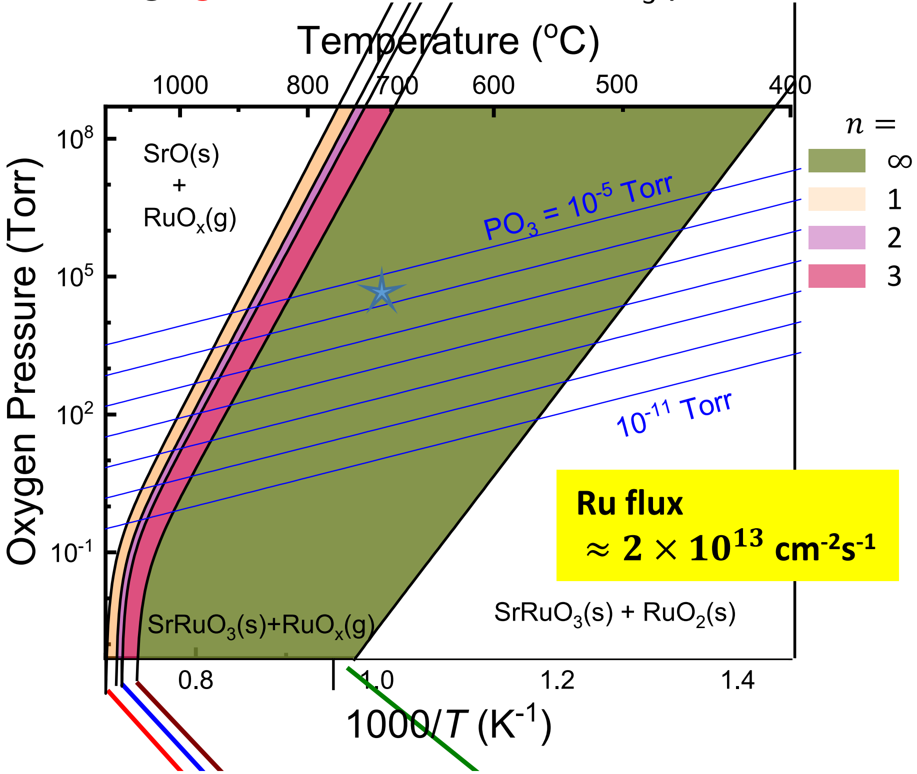

Films by MBE adsorption-controlled growth

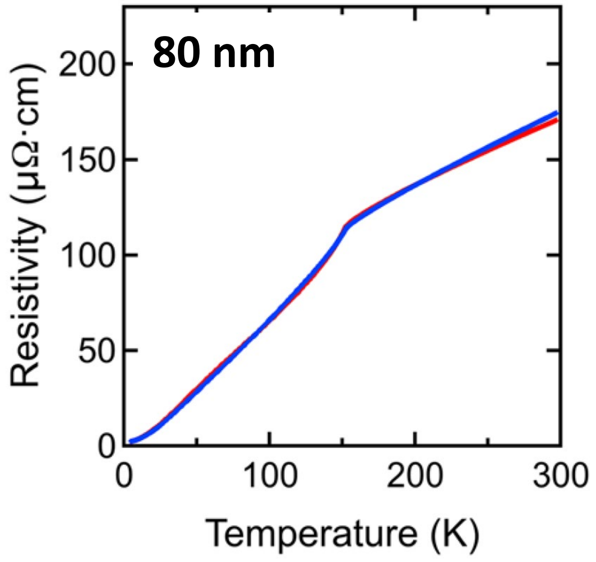

$\rho(4K)$ ~ 2 $\mu\Omega$cm
RRR ~ 80.

Cf.

Single-crystal by F.Z.	Films By PLD
$\rho(4K)$ ~ 1.05 $\mu\Omega$cm RRR ~ 192.	$\rho(4K) > 120$ $\mu\Omega$cm RRR << 10

- In principle, it can further apply to other oxide growth with proper metal-organic source.

Ex: the growth of $SrTiO_3$ using the metal-organic source of Titanium tetra-isopropoxide [$Ti(OC_3H_7)_4$ or TTIP] **Jalan *et al.* APL 95, 032906 (2009)**

Single crystal SRO by floating zone

Kikugawa *et al.* Crys. Growth De. 2015.

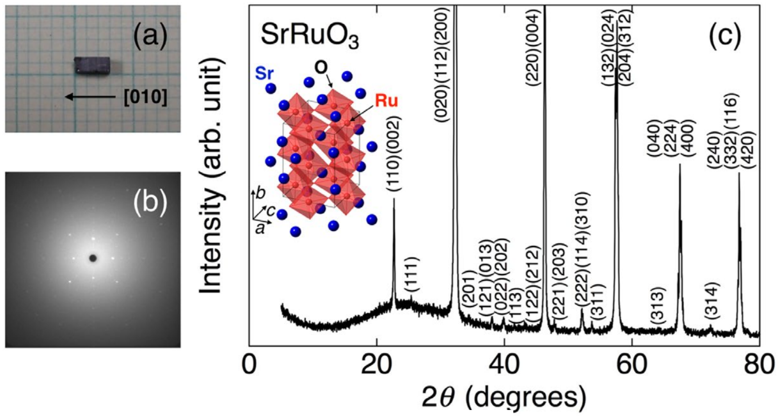

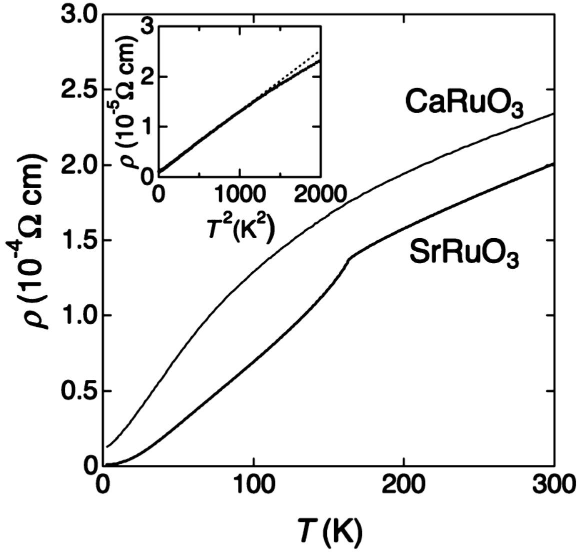

ρ(4K) ~ 1.05 $\mu\Omega$cm

RRR≡ ρ(300K)/ρ(4K) ~ 192.

SRO films grown by pulsed laser deposition (PLD)

Siemons *et al.* *PRB* 2007.

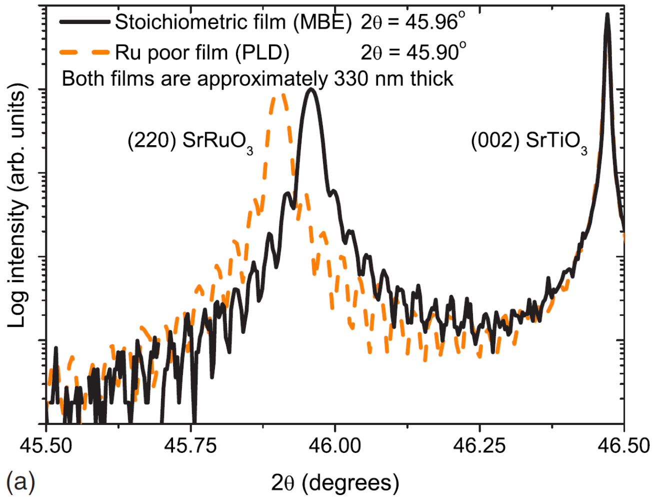

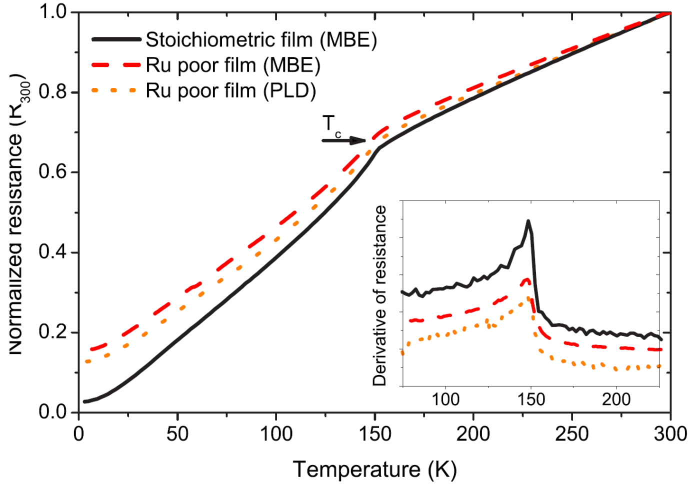

PLD SRO films

ρ(4K) > 120 $\mu\Omega$cm

RRR << 10

- X-ray alone may not be sensitive to random point defects in SRO films, but low temperature residual resistivity does !
- In ruthenate, low temp. charge transport is largely influenced by the Ru vacancies that were common in PLD films.
- Adsorption-controlled growth using MBE was developed to overcome Ru-vacancy problem.

Capogna *et al.* *PRL* 2002.

Several transport issues at low temp. in SRO films can be revisited !

Oxide MBE at IoP installed in Nov. 2014

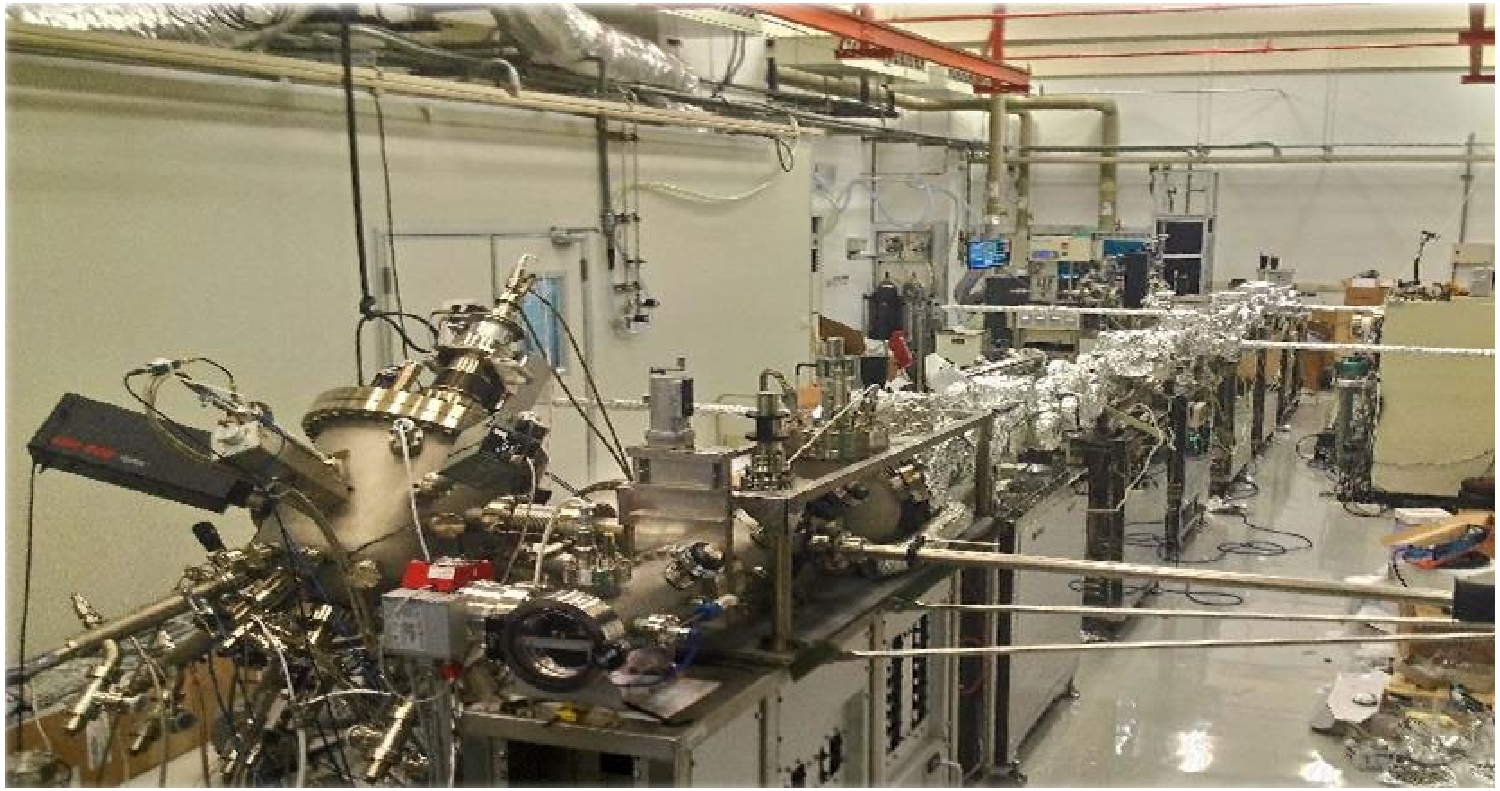

Sources:

10 effusion cells

4 pockets EB evap.

***Ex-situ* charac.:**

- **RBS**
- **X-ray (IoP AS)**
- **STEM-EELs (CCMS NTU)**
- **XPS (NSRRC, Hsinchu)**
- **….**

Characterization:

RHEED

RGA

Pyrometer

QCM

Active group members

PI: Dr. Wei-Li Lee

Post-doc:

Dr. Akhilesh Singh

RA :

Elisha Lu

Trent yang

Jyoti Verma

Ph.D. student:

Uddipta Kar

Master students (collab.):

T.W. Kuo C.Y. Chen

Special thanks to:

Prof. Ivan Bozovic

Prof. Harold Hwang

Prof. Donglai Feng

Dr. D.W. Shen

Dr. Rob Moore

Dr. Wei-Sheng Lee

Dr. Ben Bensaoula

….

Oxide MBE facility at IoPAS with ozone distiller


Dr. Wei-Li Lee


Dr. Akhilesh Singh

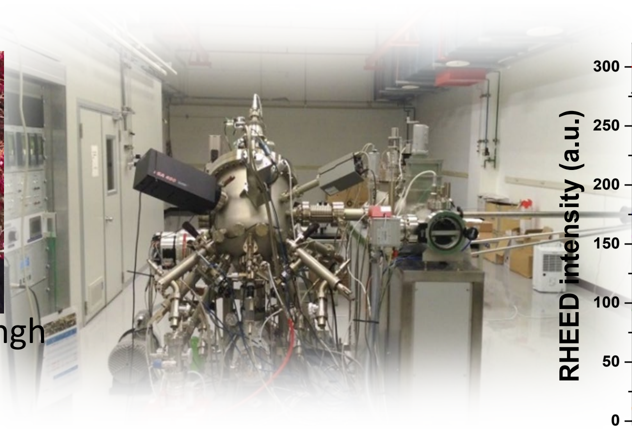

In-situ RHEED monitor

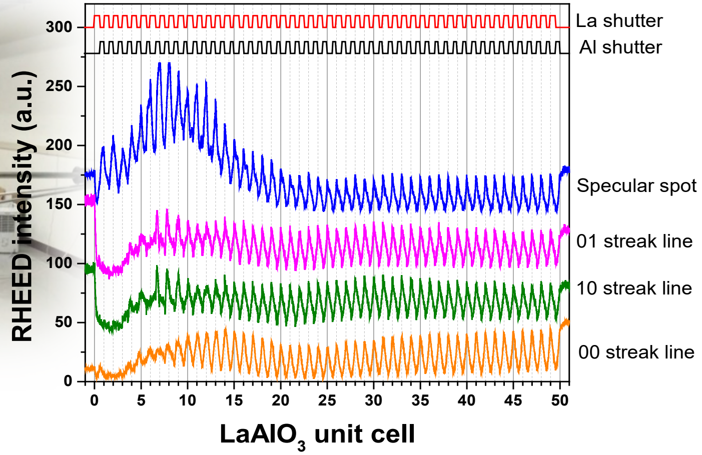

Spin-polarized in-gap states in surface-reconstructed SrTiO3

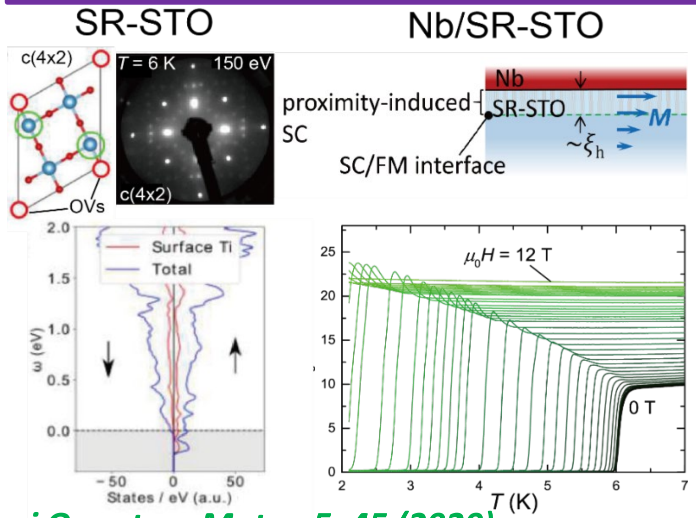

npj Quantum Mater. 5, 45 (2020)

Quasi-two-dimensional hole gas at complex oxide interface

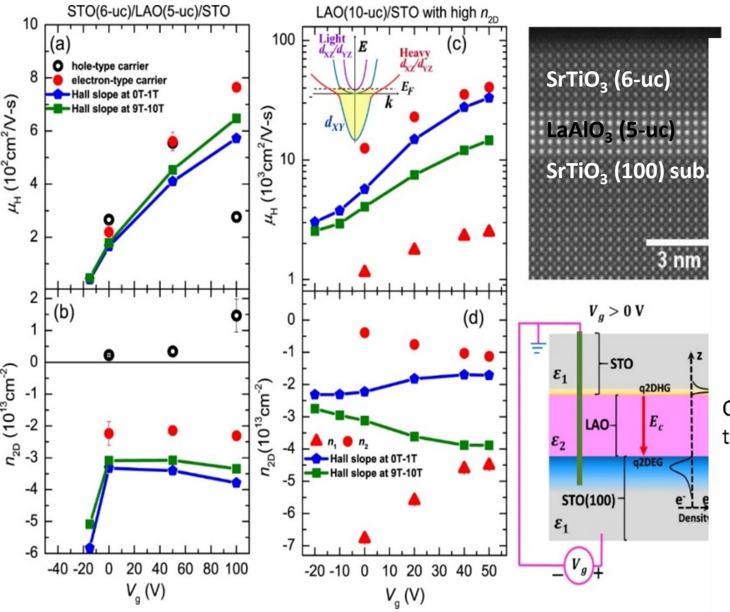

Phys. Rev. Materials 2, 114009 (2018)

Phys. Rev. Materials 3, 075003 (2019) (Dr. MW Chu)

Orbital selectivity for Cooper pairing at superconducting interface

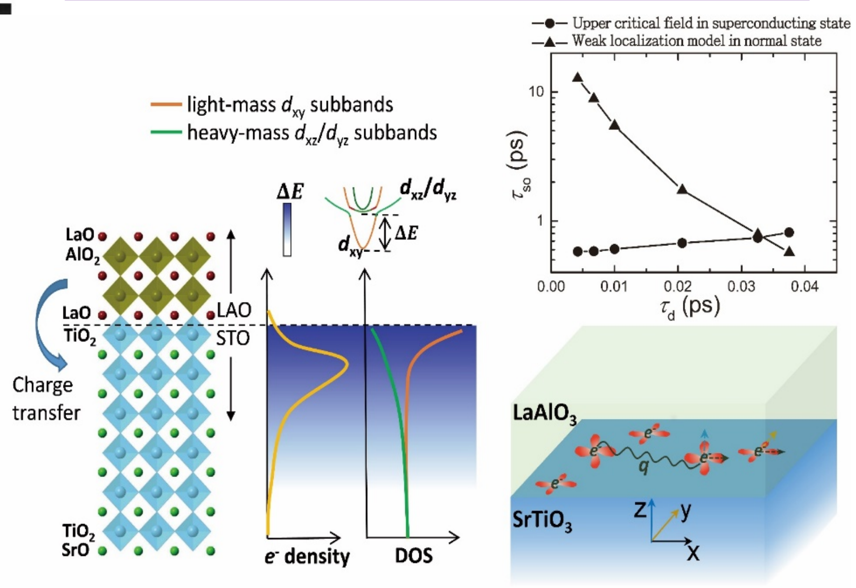

Phys. Rev. Research 2, 013311 (2020)

Weyl-orbit quantum oscillation in topological Weyl semimetal SrRuO3

Single domain SRO film

Weyl orbit

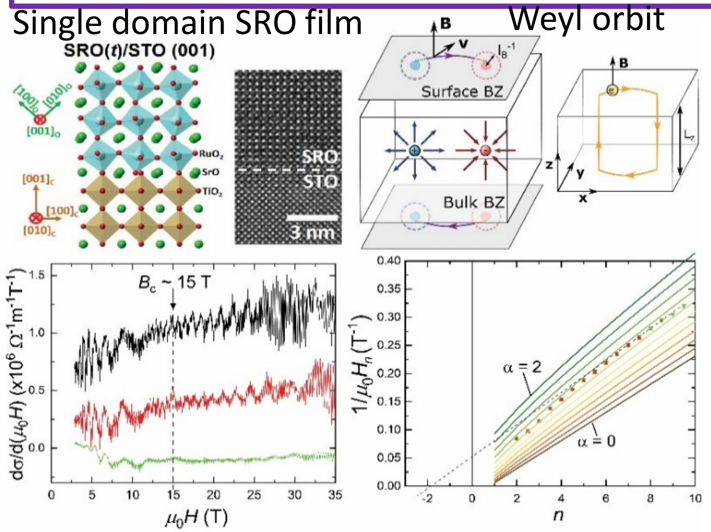

Kar *et al.* Sci. Rep. 11, 16070 (2021)

Kar *et al.* npj Quantum Materials 8, 8 (2023).

Revealing surface charge transport in thin films of topological Weyl metal $SrRuO_3$

Dr. Wei-Li Lee

Institute of Physics, Academia Sinica, Nankang, 11529, Taipei, Taiwan

Outline

❑ **Review of the topological Weyl semimetal and ferromagnetic Weyl metal SrRuO3 (SRO) system:**

- Brief review of magnetic Weyl semimetal and Bulk-surface correspondences in topological Weyl metal SRO
- Oxide MBE facility at IoPAS since 2014 and adsorption control growth of SRO thin films.

❑ **Weyl-orbit quantum oscillation effect (WOE):**

- Structural charac. of low defect level and untwinned SRO thin films.
- "Thickness" dependent quantum oscillations and comp. to simulated Weyl-orbit QO.

❑ **Nonreciprocal and nonlinear charge transports (NRTE) in SRO thin film:**

- Fabrication of sunbeam devices from an untwinned SRO thin film for anisotropy measurments
- Observation of NRTE and nonlinear Hall effect in SRO thin film at low temperatures.

❑ **Conclude and future outlooks**

Kar *et al.* Sci. Rep. 11, 16070 (2021)
Kar *et al.* npj Quantum Materials 8, 8 (2023).
Kar et al. arXiv:2307.04482, submitted

NSTC 國家科學及技術委員會 National Science and Technology Council

Determination of domain populations in SRO films on miscut STO (001) sub.

- Slightly distorted Orthorhombic-phase:
  - ✓ Reciprocal space mapping (**RSM**)
  - ✓ Observable $(221)_o$ reflection

- Excellent thickness uniformity :
  - ✓ Crystal truncation rods (**CTR**)
  - ✓ AFM Surface roughness < 0.3 nm

- Distinguish domains via X-ray (0 2 ±1) reflections
  - ✓ Four possible orthorhombic twin domains
  - ✓ The volume fraction for each domain is highly sensitive to the substrate's miscut angles (α ,β)
  - ✓ Dominant domain A with $[001]_o$ // STO$[010]_c$

Orthorhombic twin domains

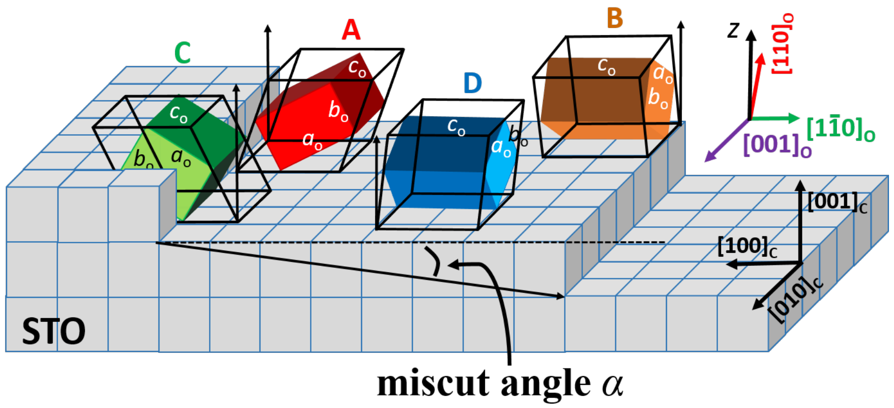

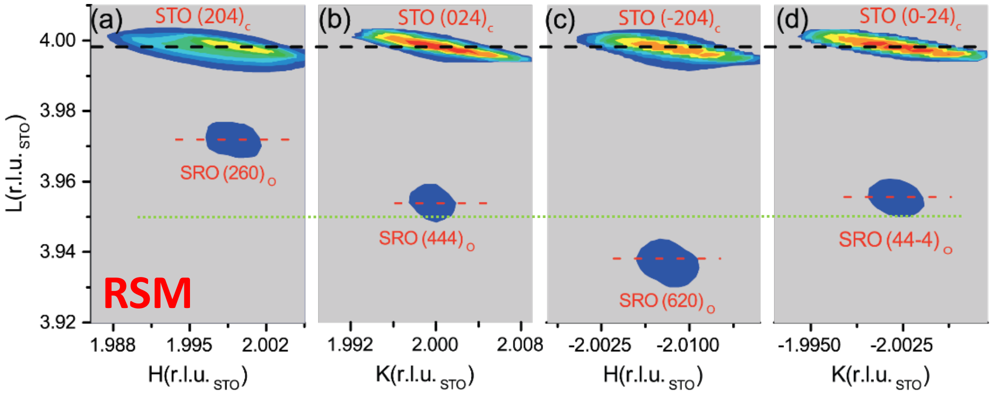

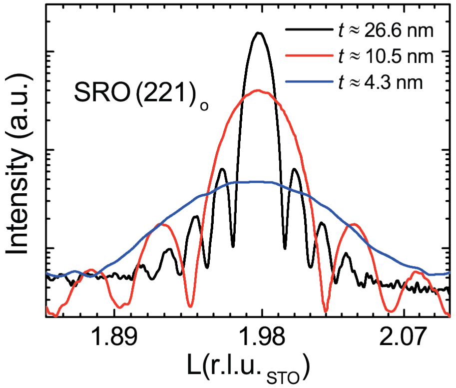

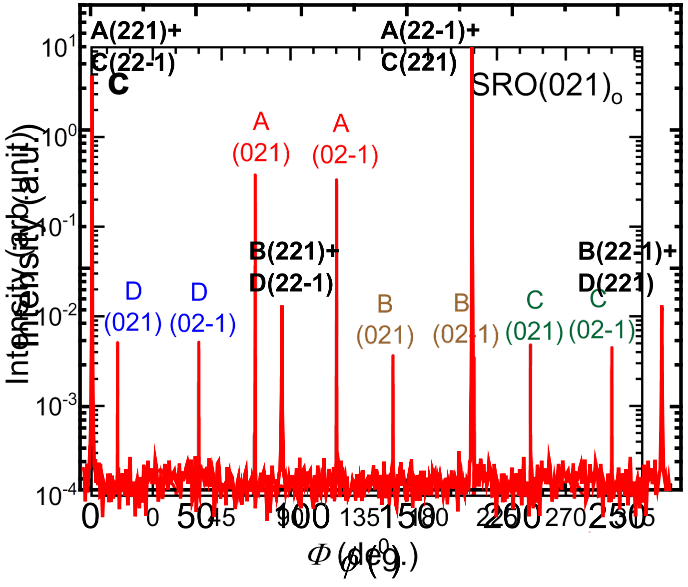

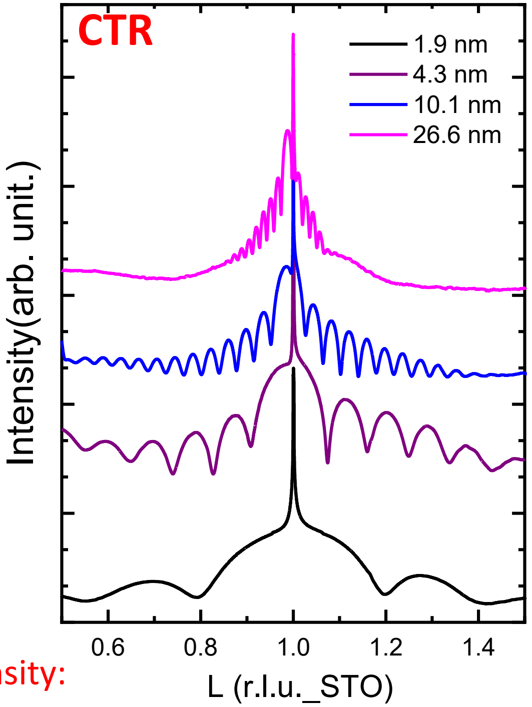

Domain volume fraction from integrated peak intensity:

Domain A = 94.1 %, Domain B = 1.7%,

Domain C = 2.0%, and Domain D = 2.2%.

Kar *et al.* Sci. Rep. 11, 16070 (2021)

The growth of untwinned SRO films with low residual resistivity

Kar *et al.* Sci. Rep. 11, 16070 (2021)

- Untwinned SRO films using miscut STO (001) sub. with a small miscut angles (α = 0.1°, β=0°) : dominant **A** domain with a volume fraction more than 90% for 7.7 nm < t < 40 nm.
- The metallic and ferromagnetic nature survives down to t = 1.2 nm of SRO.
- RRR reduces from 77.1 for $t \approx$ 28.5 nm to 2.5 for $t \approx$ 1.2 nm, while ρ(5K) increases from 2.5 μΩcm for $t \approx$ 28.5 nm to 131.0 μΩcm for $t \approx$ 1.2 nm.
- High RRR and low residual resistivity are close to that of single crystal SRO !

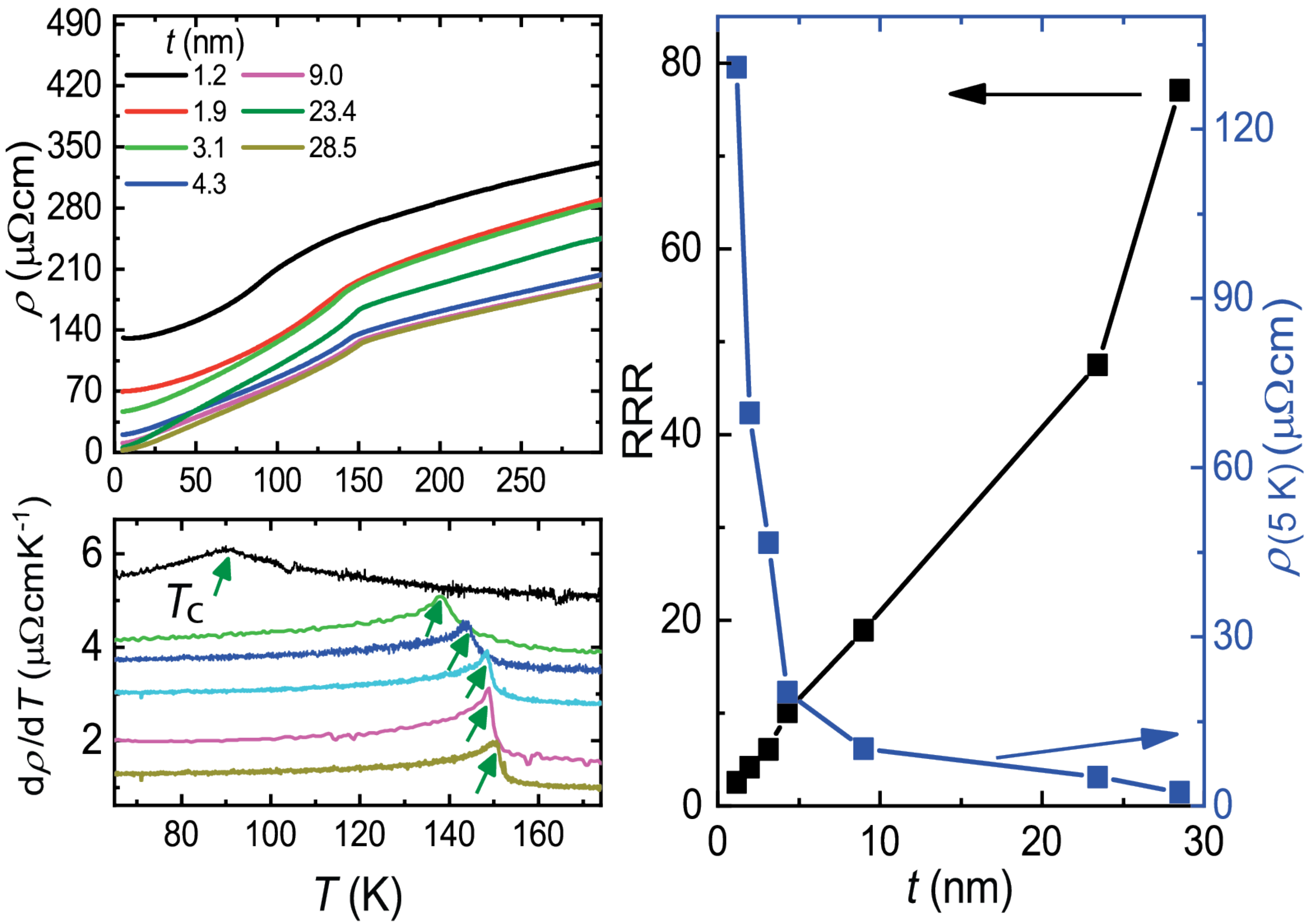

Resistivity anisotropy in untwinned $SrRuO_3$

SRO t = 13.7 nm
sunbeam device

+B // - $\hat{z}$ ⊗

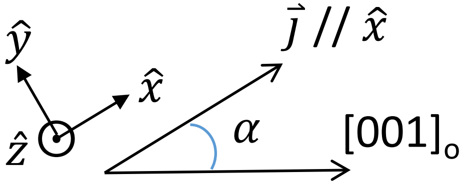

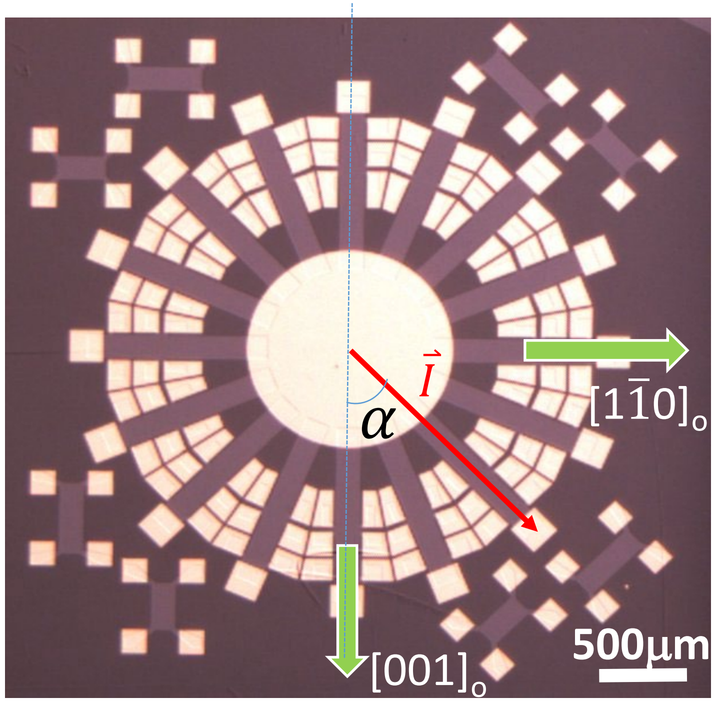

α: angle between
bias current $\vec{I}$ & $[001]_o$

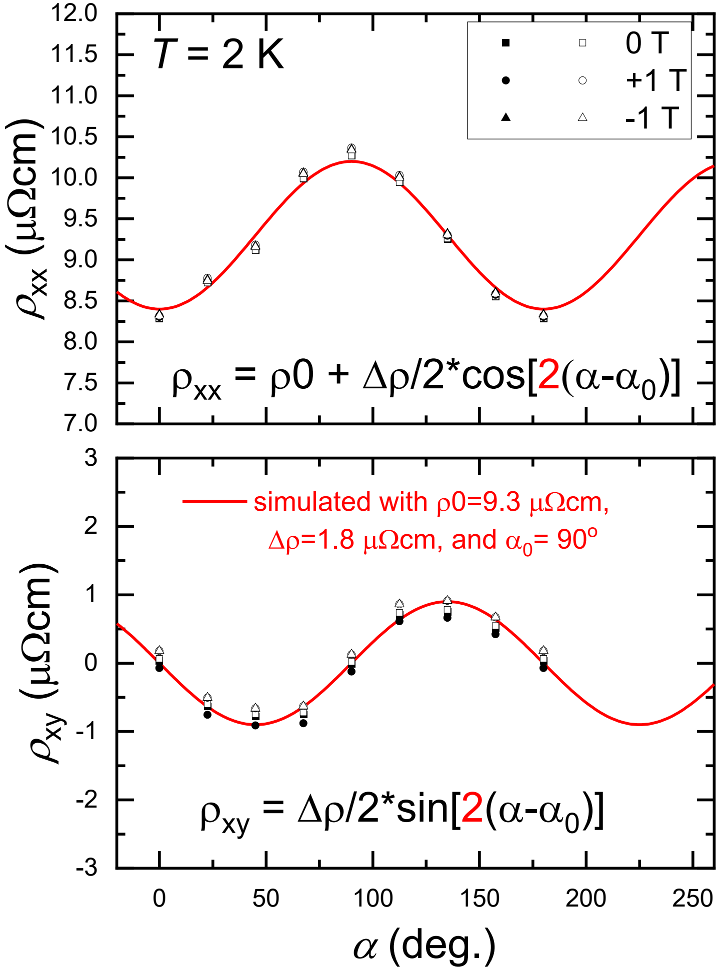

- SRO film was patterned to have exactly the same Hall bar geometry to minimize the leads misalignment artifact.
- Agree well with the simulated ρ anisotropy: justifying the single-domain/untwinned SRO films

$$\vec{E}_a = \Delta\rho\,(\hat{a}\cdot\vec{J})\,\hat{a}, \text{ and } \hat{a} \mathbin{//} [1\bar{1}0]_o.$$

- The magnetic coercive field (Hc) ~ 0.3 T, and thus the ρ variation is NOT "magnetization" effect ! (ex: AMR/PHE), $\vec{M} \perp \vec{I}$ is always satisfied.
- For the following quantum oscillation measurements for SRO films with different thicknesses (t), same measurement geometry of $\vec{I}$ // $[1\bar{1}0]_o$ to avoid complication due to anisotropy effect.

Thickness dependent magnetotransport in untwinned SRO films on miscut SrTiO3 (001) sub.

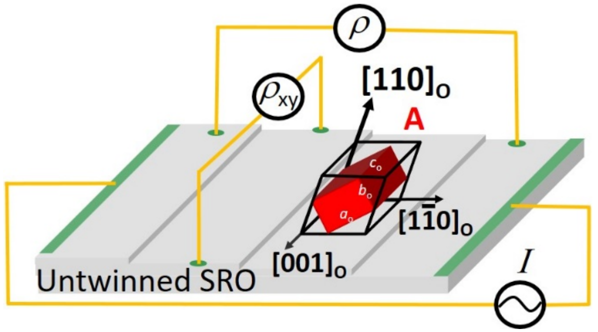

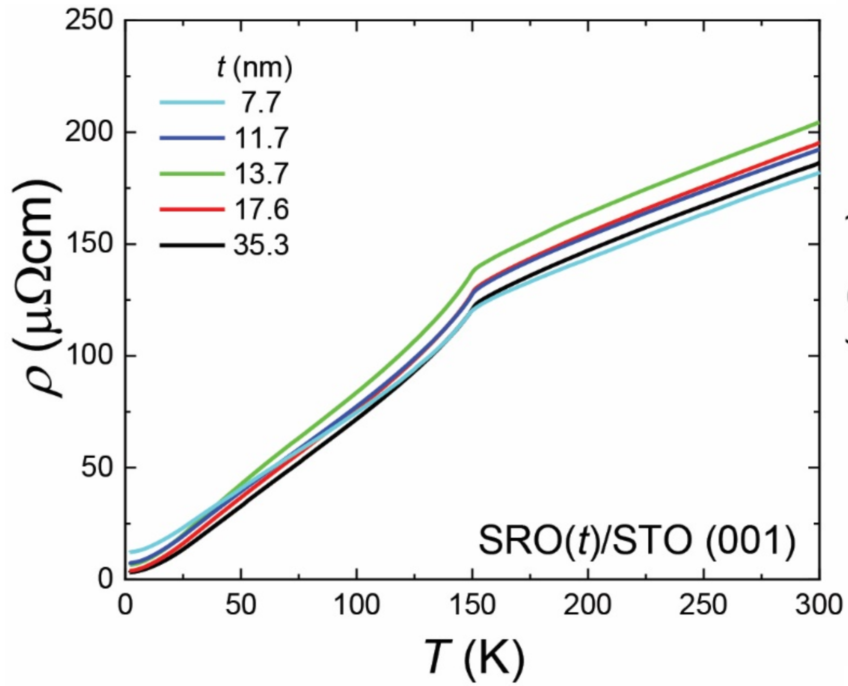

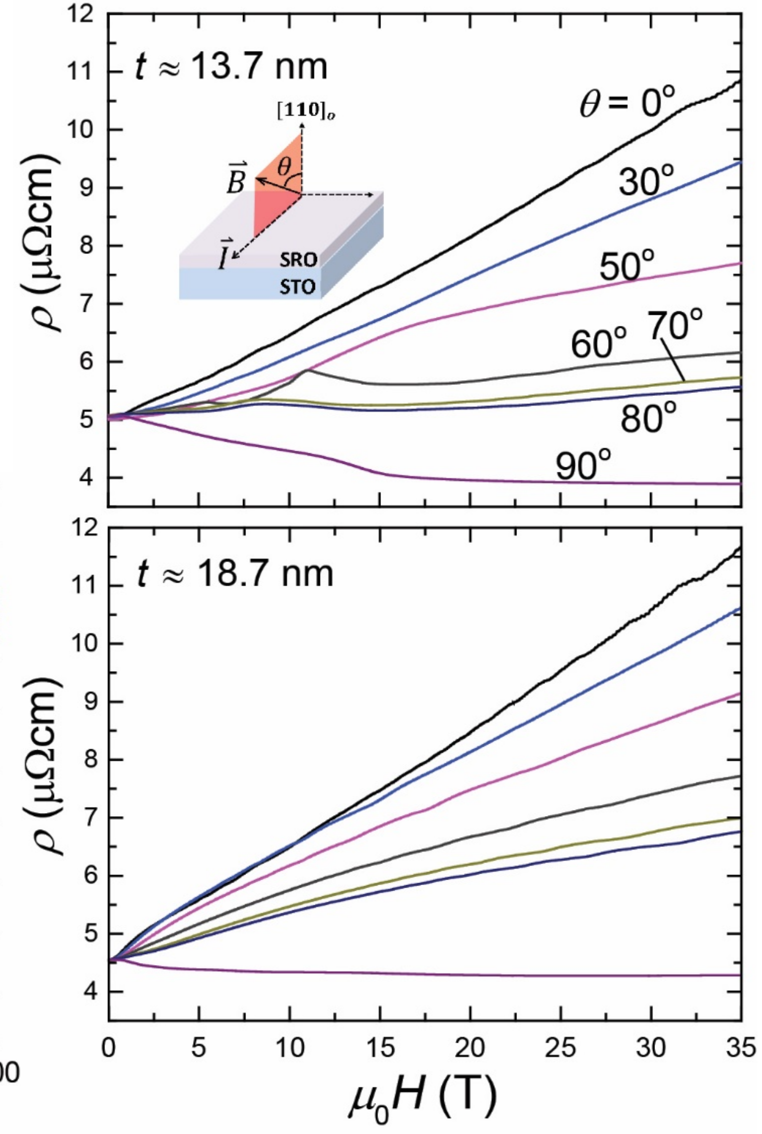

Adsorption-controlled growth by oxide MBE
Dominant A domain with a volume fraction more than 90% for 7.7 nm < t < 35.3 nm

Kar *et al.* Sci. Rep. 11, 16070 (2021)

- Use same transport geometry for all untwinned SRO films with different ts
  $\vec{I} \parallel [1\bar{1}0]_o \perp [001]_o$
- For thickness t : 7.7 to 35.3 nm
  RRR ($\rho(300K)/\rho(5K)$): 14.4 to 51.6
  RR (2.5K): 12.31 to 3.24 $\mu\Omega$cm
- Consistent MR behavior for a WSM
  - ✓ Large and nonsaturating positive MR (θ = 0°)
  - ✓ Negative longitudinal MR (θ = 90°): Chiral anomaly.

Current jetting or Chiral anomaly ?

Liang *et al*. PRX 8, 031002 (2018)

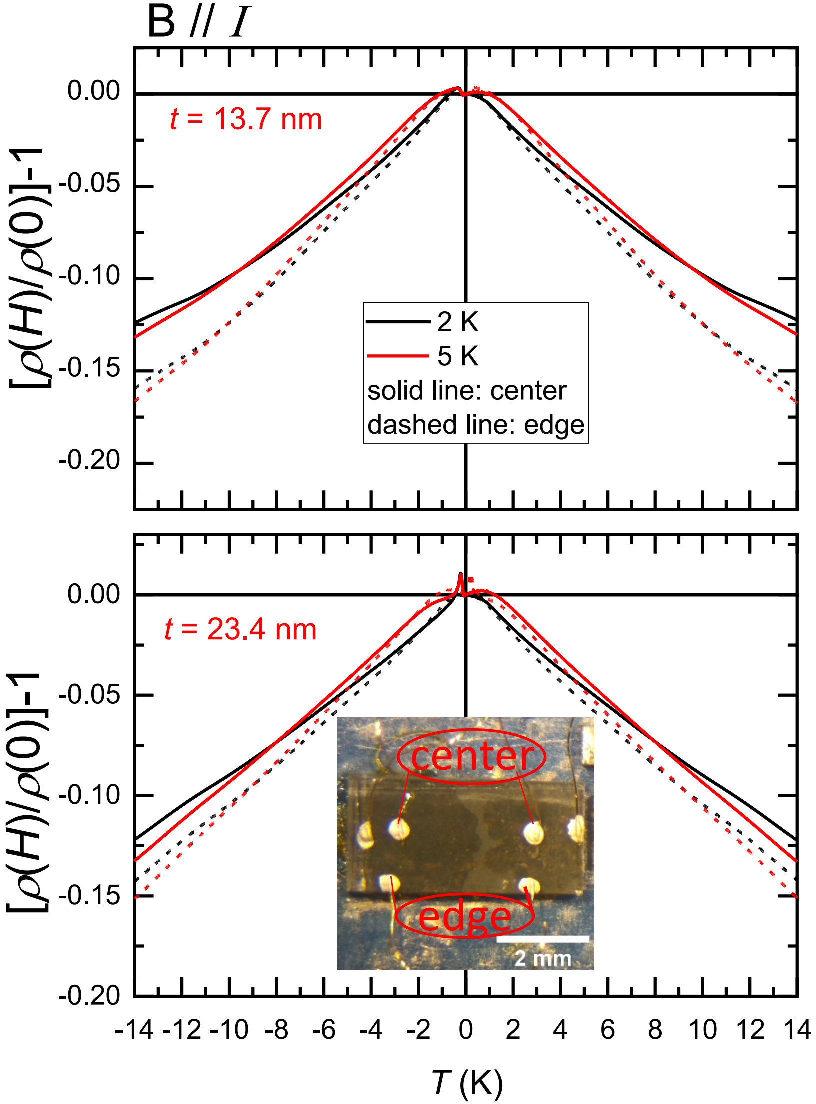

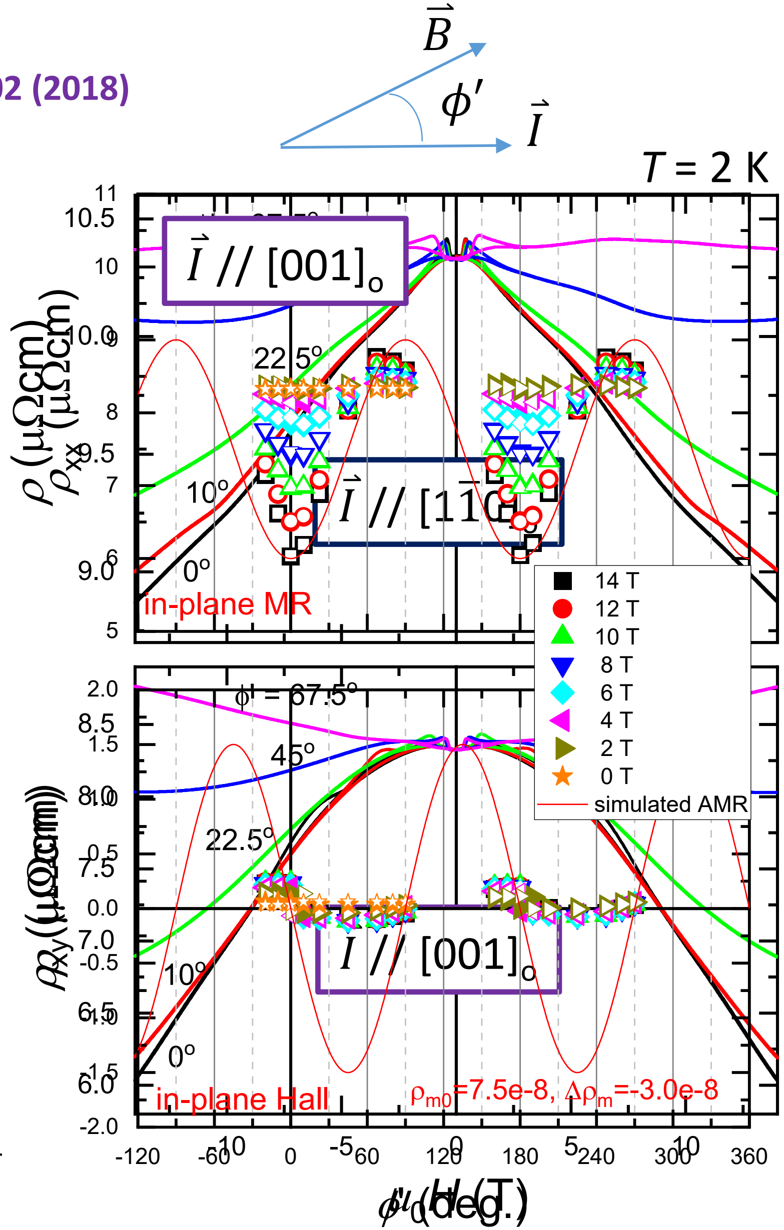

- Varying contact locations: consistent negative MR behavior.
- Same negative MR for B // I for I// [001]$_o$.
- B_{cyc} ~ 16 T: using mobility μ_e~ 3,000 cm^2/Vs, and set $\mu_e B_{cyc} \sim 5$.
- Quantum limit field B_Q ~ 15 T for a single spin subband with a pocket size of F = 30 T.
- $B_{cyc} \sim B_Q$, current jetting may not be significant.
- More rigorous ϕ'-dep. MR, the large negative MR for $\phi' \approx 0$ can not be simply due to anisotropy MR (or planar Hall effect) in a magnet.

High field quantum oscillations in untwinned SRO films

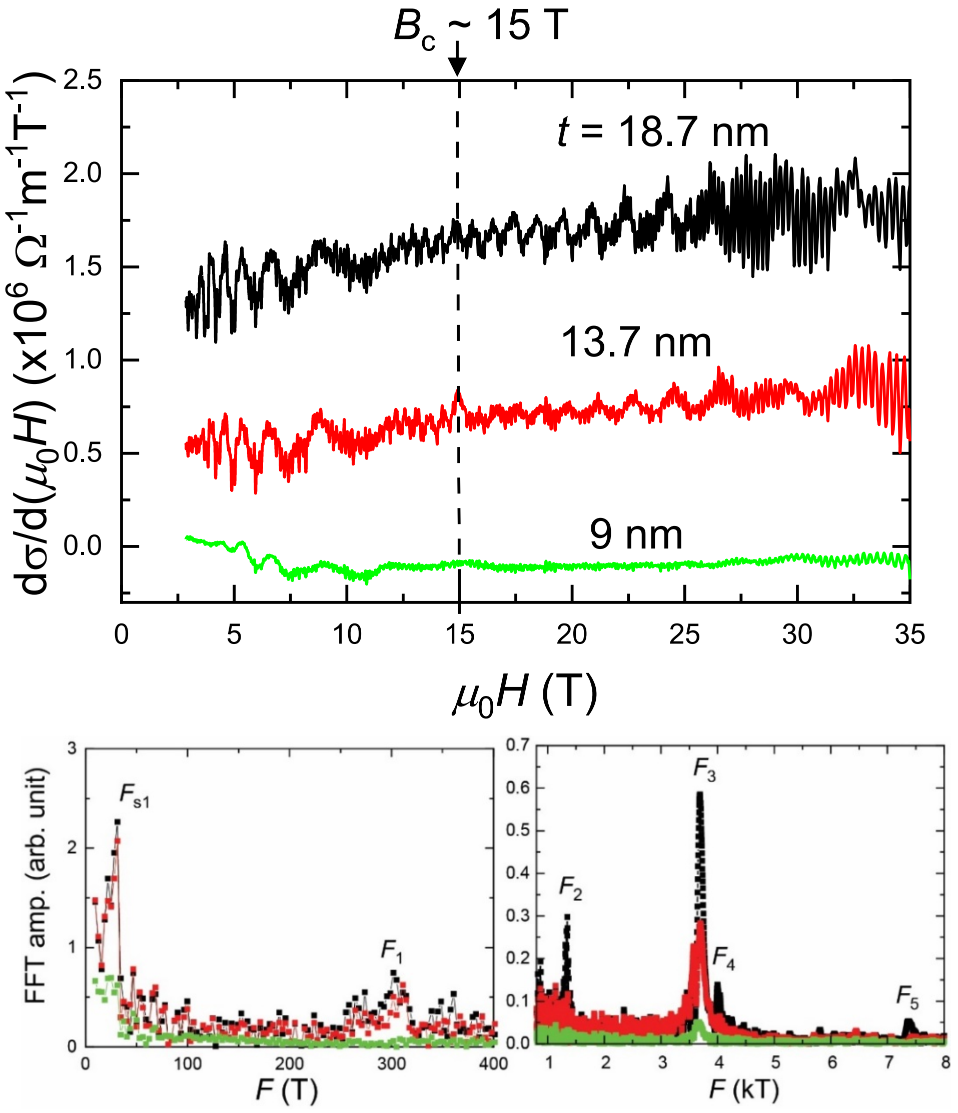

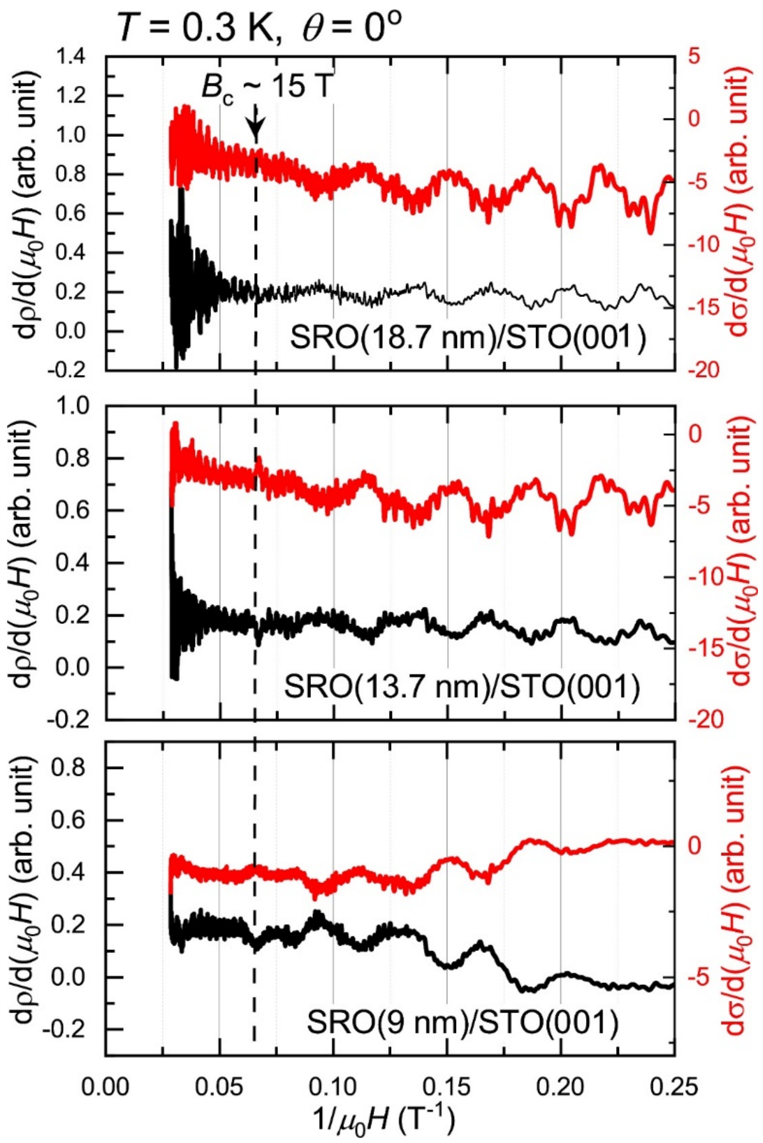

- For $\mu_0 H$ > 3T, F_{s1} ~ 30 T appears.
- For $\mu_0 H$ > 12T, F_{1-5} from 300 T to 7,500 T appears with ampl. Increase with t.
- F_{s1} ~ 30 T appears to vanish above B_c ~ 15 T for aLL three samples !

Thickness dep. quantum oscillation

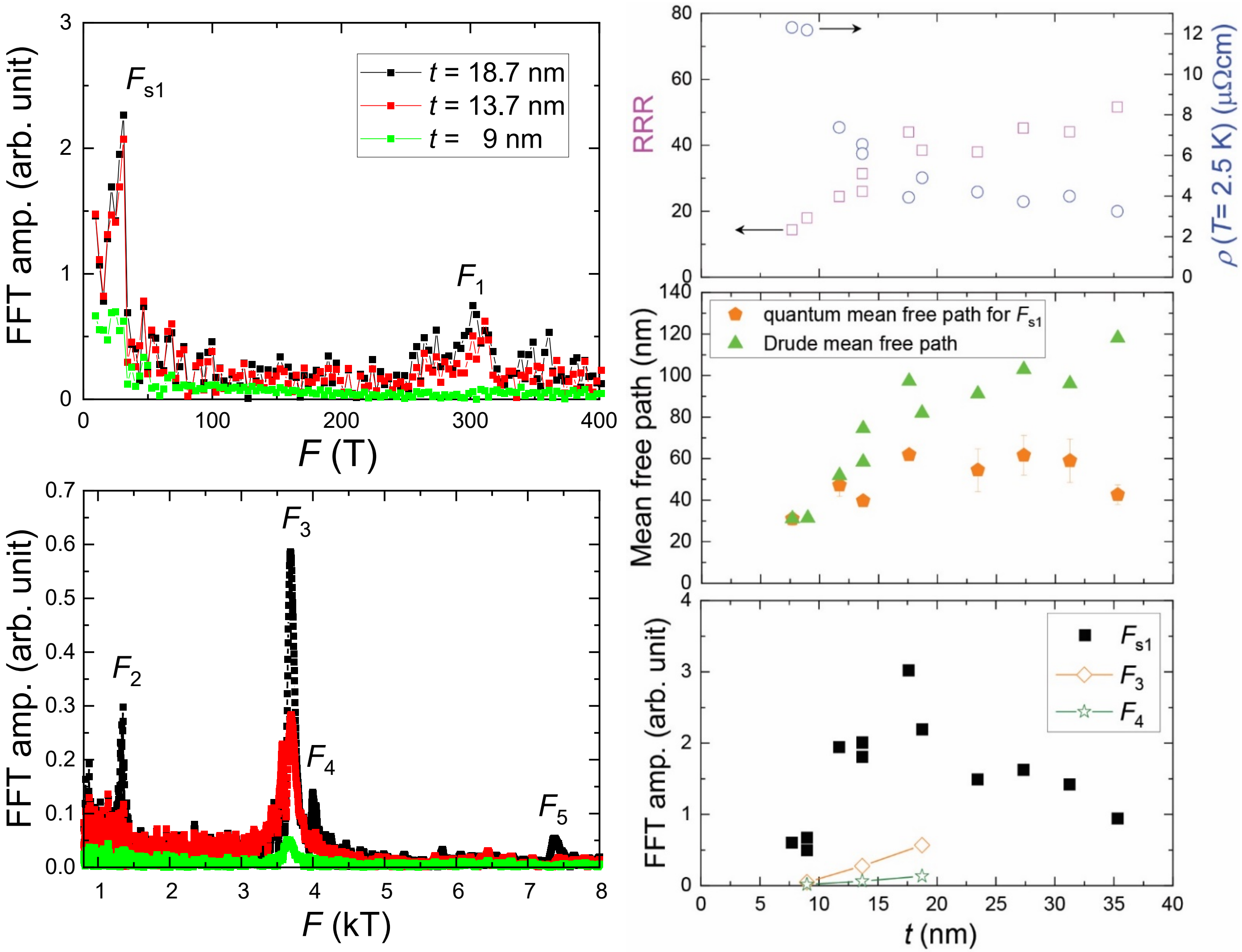

- The extracted quantum lifetime for F_{s1} shows relatively weak t-dep.
  (Cf. progressive increases of Drude MFP with t)

- Non-monotonic t-dep. FFT amplitude for F_{s1}
(Cf. F_3, F_4 show progressive increases of FFT amplitude with t as expected)

- F_{s1} does not appear to be largely affected by the bulk scattering: surface origin ?

- From temp.-dep. QO data:
  $F_{1\text{-}5}$ from 300 T to 7,500 T
  (3 m_e and 5 m_e for F_1 and F_3)
  F_{s1} ~ 30 T with $m^* \approx 0.3\ m_e$

- For doped-SrTiO3: m* ~ 0.7 - 1.5 m_e for light Ti d_{xy}

Kozuka *et al.* Nature 462, 487 (2009)
Wang *et al.* Nat. mater. 15, 835 (2016)

θ and γ angular dependent quantum oscillations for F_{s1} ~ 30 T

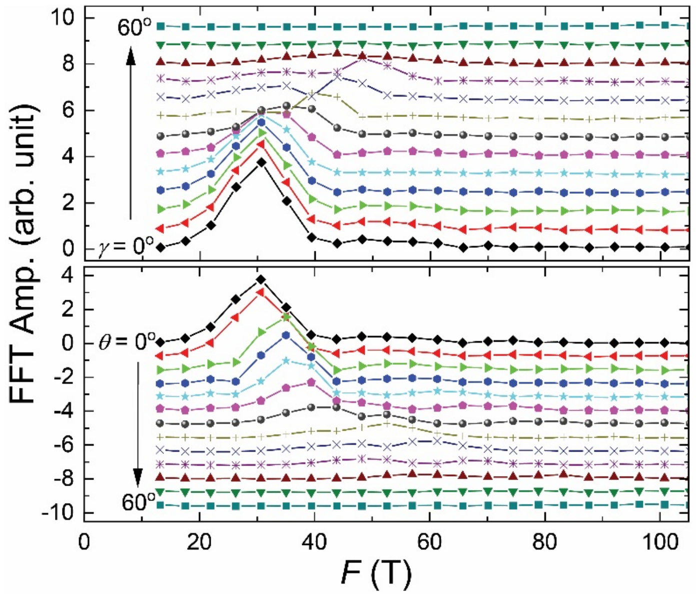

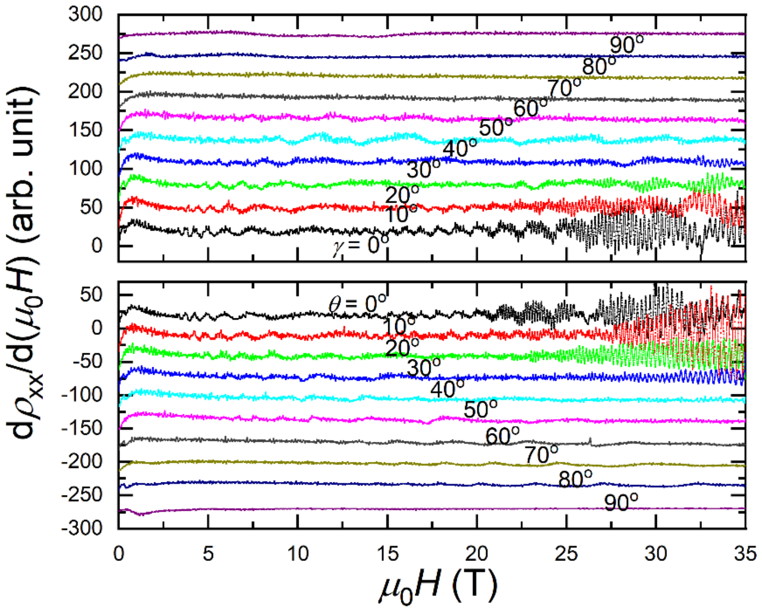

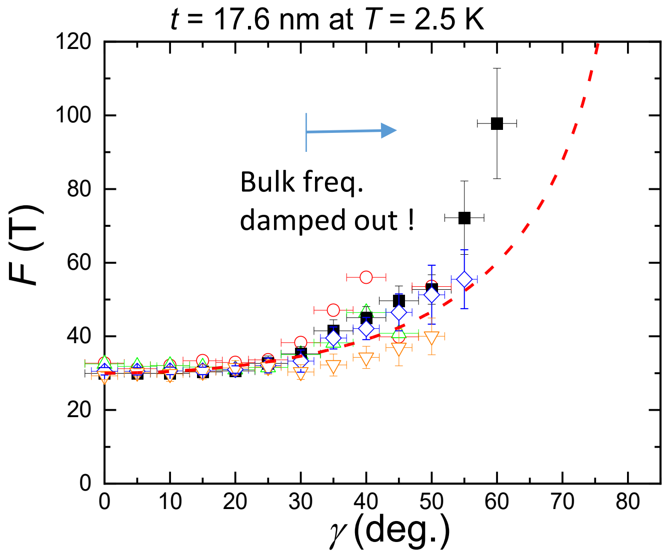

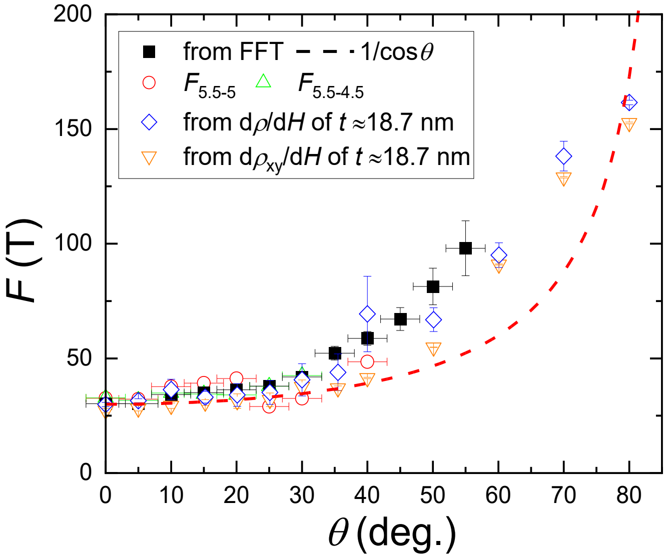

- Splitting of F_{s1} in FFT spectra at intermediate angles may infer competing QO contributions: 3D bulk Fermi pockets, 3D Weyl nodes and surface-origin effect (Weyl-orbit QO).

- As θ and γ increases above ~ 30°, bulk freq. $F_{1\text{-}5}$ damped out faster due to surface/interface scatterings.

Drude ℓ_d (≈ 100 nm) >> t (≈13.7 nm) ≈ ℓ_B (4.7 nm @ 30 T)

- For the QO of F_{s1}, 1/cos(angles) dependences are observed for both θ and γ rotations, inferring a 2D-like Fermi pocket for F_{s1}.

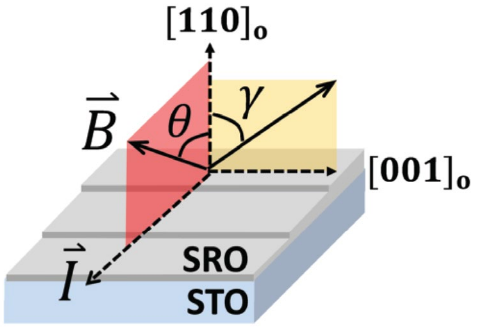

c.f. Kaneta-Takada et al. npj QM 7, 102 (2022)

Unique thickness dep. of the QO phase for F_{s1} ~ 30 T

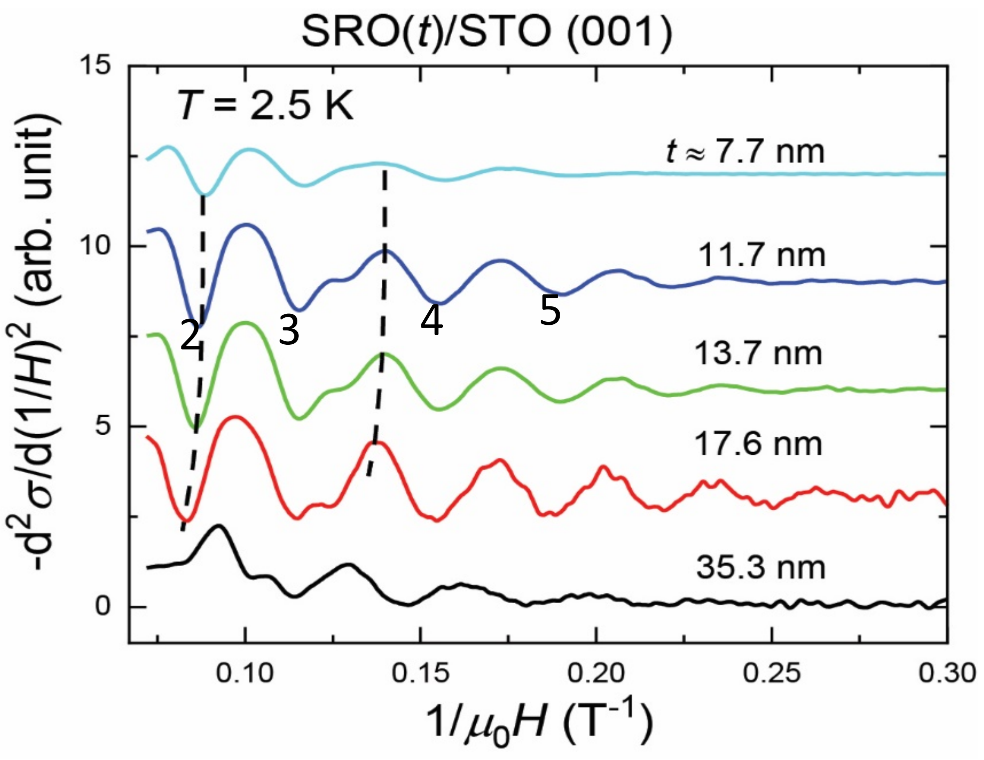

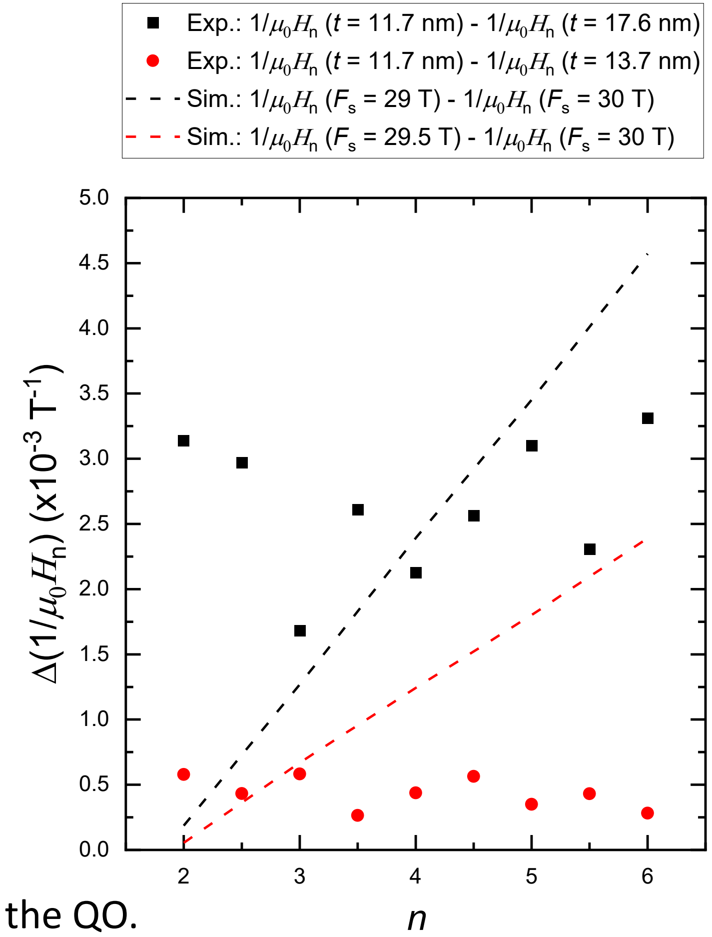

- Using derivatives ($d\sigma/dH$ or $-d^2\sigma/d(1/H)^2$) to avoid possible distortions to the QO.
- σ_{xx} minima or ρ_{xx} maxima: integer LL index n (**Xiong *et al.* PRB 86, 045314 (2012)**)

  For a 3D system with coexistence of bulk conductivity, and $\rho_{xx} = \sigma_{xx}/[{\sigma_{xx}}^2 + {\sigma_{xy}}^2] \sim 1/\sigma_{xx}$.
- Oscillation ampl. is largest for 10 nm < t < 20 nm.
- Thickness dep. QO: progressive shifts of the peak/valley to lower $1/\mu_0 H_n$ value when t goes from 7.7 to 17.6 nm.

  Weyl-orbit QO: $\frac{1}{\mu_0 H_n} = \frac{e}{\hbar k_0'}\left[\frac{\pi \hbar \upsilon n}{\mu} - L_Z\right]$.
- The amount of phase shift is nearly "n"-indep.: phase shift due to small density variation can be excluded.

Unique concave downward feature for F_{s1} ~ 30 T

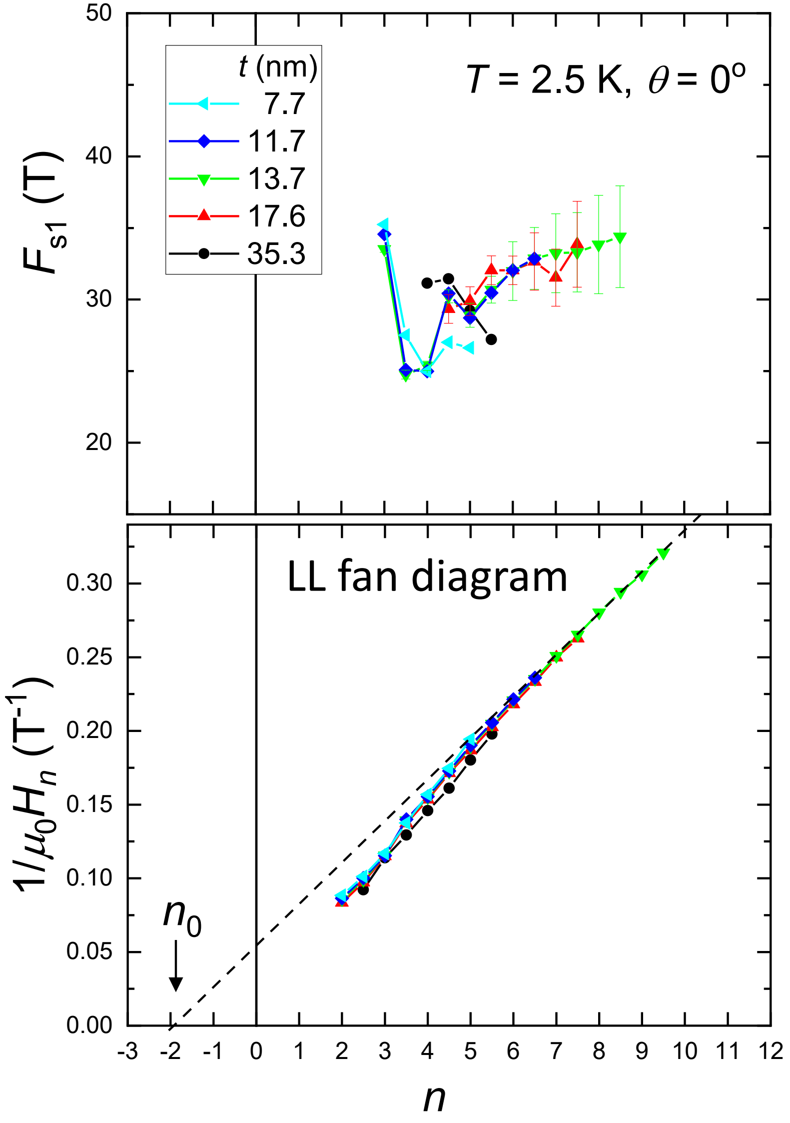

concave downward !

LL spectrum of a conical band:

$$E_n = \upsilon_F\sqrt{(2ne\hbar B + \underbrace{(g\mu_B B/2\upsilon_F)^2}_{\text{Zeeman term}})}$$

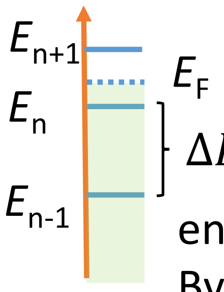

enhanced ΔE_n
By Zeeman term

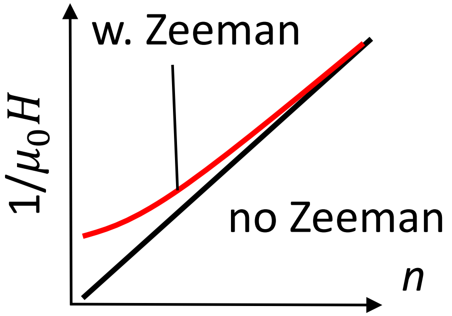

concave upward !

- LL fan diagram shows an unique and unusual concave downward curvature, and thus the extracted F_{s1} value gradually decreases with LL index n.

Cf. Zeeman coupling energy gives an opposite curvature (concave upward) !

- If treating B_c~ 15 T as the field for the quantum limit, an unusual large intercept $n_0 \approx -2$ was observed.

Cf. For a typical 3D band,

$$n_0 = \begin{cases} \pm\frac{1}{8}, \text{trivial band.} \\ \pm\frac{5}{8}, \text{ conical band } (\pi \text{ Berry phase}). \end{cases}$$

Xiong *et al.* PRB 86, 045314 (2012)
Wang *et al.* PRL 117, 077201 (2016)

- Demagnetization field, H_d :

$$\mu_0 H_d = -D_t M_{sat} \approx 0.3 \text{ T}$$

(Coercive field $H_c \sim 0.3\ T$)

The influence of non-adiabatic corrections to Weyl-orbit quantum oscillations

Non-adiabatic corrections:
"Sinking" into bulk

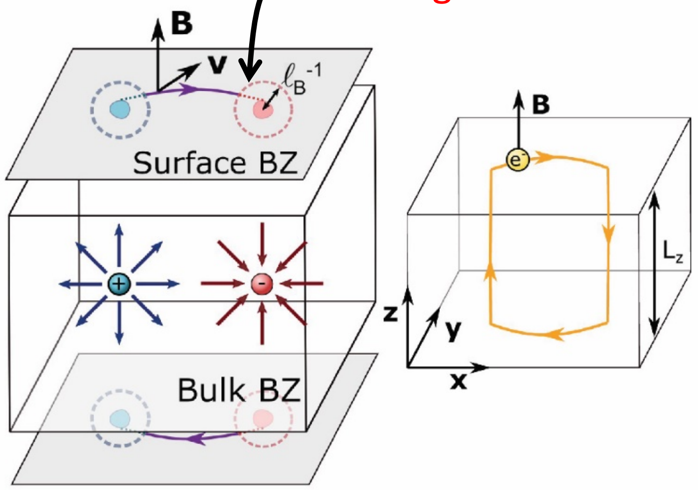

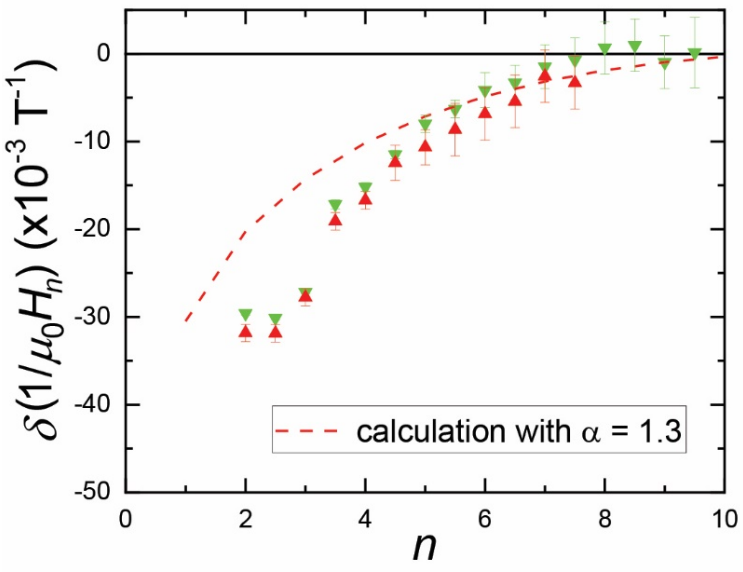

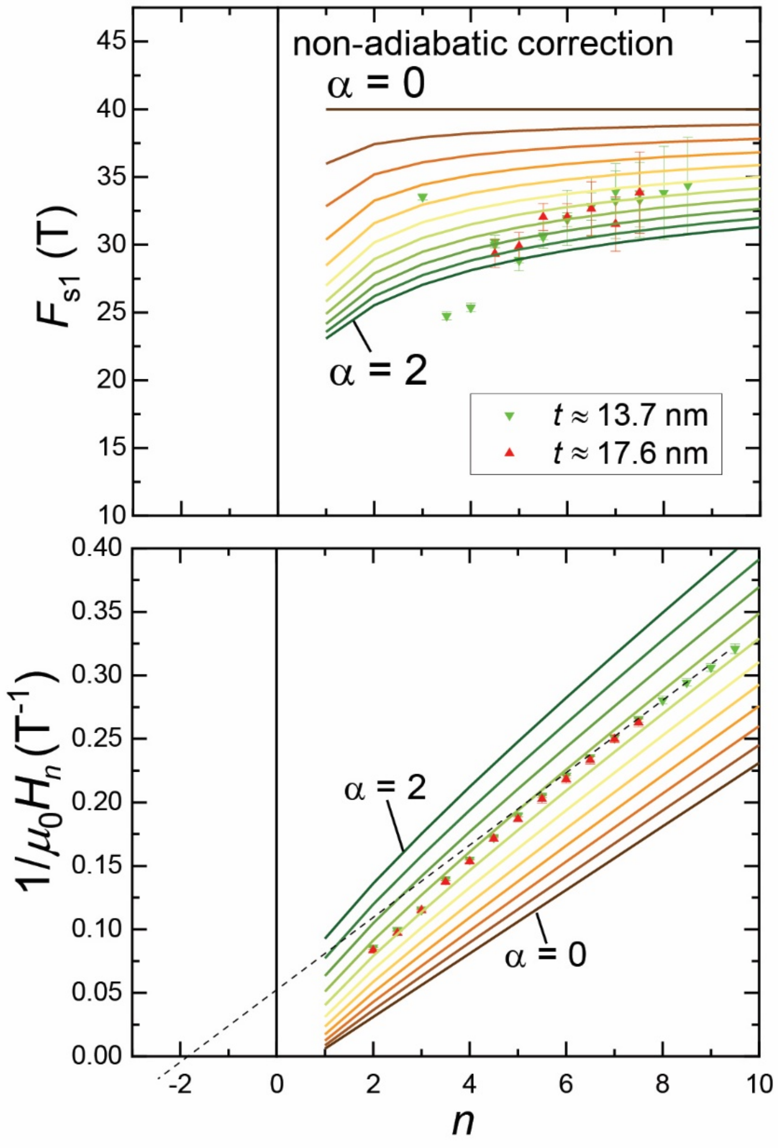

- "Sinking" into the bulk states before reaching the projected nodes: reduced area enclosed by Weyl-orbit with a relevant length scale of $1/\ell_B$ in k-space. (magnetic length ℓ_B(5 T) ≈ 11 nm)

Cf. Surface-bulk connectivity via nodes revealed in QPI STM (**Inoue *et al.* Science 351, 1184 (2016), Batabyal *et al.* Sci. adv. 2, e1600709 (2016)**)

- Non-adiabatic correction factor α:

$$\frac{1}{\mu_0 H_n} = \frac{e}{\hbar k_0'}\left[\frac{\pi\hbar v n}{\mu} - L_Z\right].$$

$k_0' \equiv k_0(1 - 4\alpha/k_0\ell_B)$, and α is non-adiabatic correction param.

- Simulated curves with $\boldsymbol{L_Z}$ = 13.7 nm (NO any other adjusting param. !!):
  - ✓ Concave downward curvature increases with increasing α.
  - ✓ Upward shifting: a large intercept n_0.
- Extracted Weyl-orbit QO parameters:
  k_0 = 1.09 nm^{-1}, α = 1.3 ,
  μ= 15.43 meV, v = 1.34x 10^5 m/sec

- Sizable effect for α term even in low field:

$1/\ell_B$(5 T) ≈ 0.1 nm^{-1}, $k_0' \approx 0.6\, k_0$! B_{sat}~30 T > B_c.

Optimum thickness of 10 ≤ t ≤ 20 nm for the Weyl-orbit QO effect

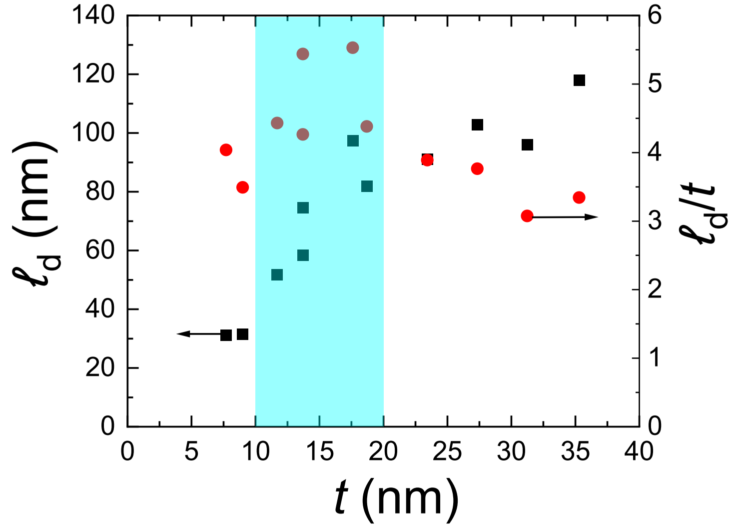

Simulated WOE Landau fan diag.

Thickness dep. WOE

$$\frac{1}{\mu_0 H_n} = \frac{e}{\hbar k_0'}\left[\frac{\pi\hbar \upsilon n}{\mu} - L_Z\right]$$

k_0 = 1.09 nm^{-1}
α = 1.3
μ= 15.43 meV
υ = 1.34x10^5 m/sec

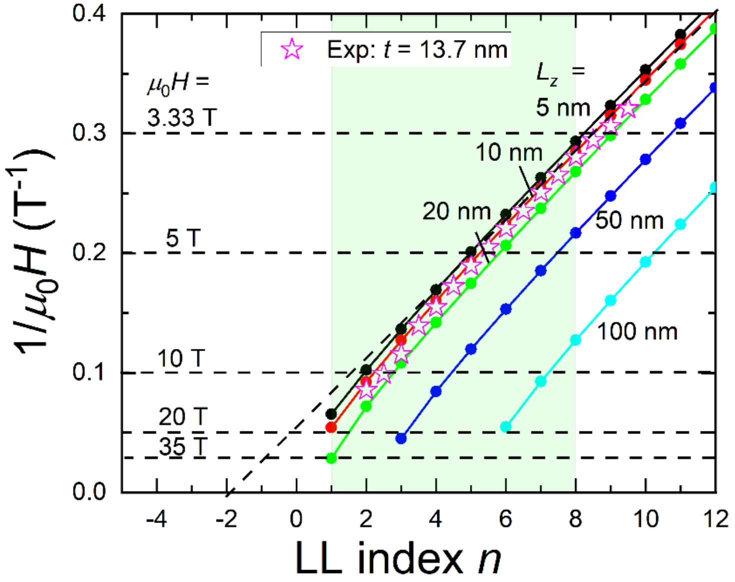

- The ratio of ℓ_d/t governs the bulk tunneling amplitude in the Weyl-orbit QO: (Drude MFP ℓ_d with a bulk density n_{3D} = 6.1x10^{21} cm^{-3})
  - ✓ The Weyl-orbit QO is favorable for ℓ_d/t >1.
  - ✓ Largest ℓ_d/t for 10 ≤ t ≤ 20 nm: Weyl-orbit QO may be maximized to dominate over 3D bulk QO for $\mu_0 H$ < 15T. (note: $F_{1\text{-}5}$ from 300 T to 7,500 T appears for $\mu_0 H$ > 12T.
- t ≤ 20 nm can reveal Weyl-orbit QO within a relatively lower field range, where its ampl. can dominate over that from other 3D bulk pockets, and both large n_0 and downward concave feature can be clearly identified !

- Competition between Bulk 3D pockets, tunnel ampl. and disorder-induced suppression of Fermi-arcs/WSM phase
  - ➢ For t >> 20 nm:
  - Further decline of the bulk tunneling ampl. (exp(-t/ℓ_d)) !
  - $1/H_n$-n curve shift downward: need higher field for the WO QO !
  - Increased QO contribution from the bulk 3D pockets.
  - ➢ For t << 10 nm:
  - Rapid drop of the ℓ_d due to increased surface scattering plus increased disorder in ultra-thin SRO films.
  - Suppression of both Weyl-orbit and bulk 3D Weyl nodes QO.

Wilson *et al.* PRB 97, 235108 (2018)

Revealing surface charge transport in thin films of topological Weyl metal $SrRuO_3$

Dr. Wei-Li Lee
Institute of Physics, Academia Sinica, Nankang, 11529, Taipei, Taiwan

Outline

- ❑ **Review of the topological Weyl semimetal and ferromagnetic Weyl metal SrRuO3 (SRO) system:**
  - Brief review of magnetic Weyl semimetal and Bulk-surface correspondences in topological Weyl metal SRO.
  - Adsorption control growth of SRO thin films using oxide MBE facility at IoPAS.

- ❑ **Weyl-orbit quantum oscillation effect (WOE):**
  - Structural charac. of low defect level and untwinned SRO thin films.
  - "Thickness" dependent quantum oscillations and comp. to simulated Weyl-orbit QO.

- ❑ **Nonreciprocal and nonlinear charge transports (NRTE) in SRO thin film:**
  - Fabrication of sunbeam devices from an untwinned SRO thin film for anisotropy measurements.
  - Observation of NRTE and nonlinear Hall effect in SRO thin film at low temperatures.

- ❑ **Conclude and future outlooks**

Kar *et al.* Sci. Rep. 11, 16070 (2021).
Kar *et al.* npj Quantum Materials 8, 8 (2023).
Kar et al. arXiv:2307.04482, submitted.

NSTC 國家科學及技術委員會 National Science and Technology Council

Nonreciprocal and nonlinear charge transport effects in single-phase materials (selected)

NRTE (current rectification)

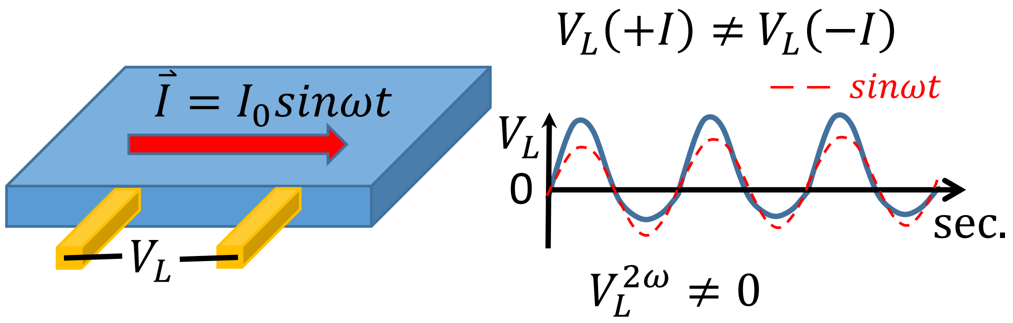

Selected examples for NRTE (incomplete)

- Magnetochiral effect: $V_L = V_{L0}(1 + \gamma I \cdot (\vec{P} \times \vec{B}))$.
  Breaking both inversion sym: $\hat{I}$ and Time-reversal sym: $\hat{T}$
- Velocity asymmetry with broken $\hat{I}$.
  Ex: TI surface state, gapped BLG with trigonal warping …
- Asymmetry scattering effect with $\hat{I}$ breaking surface states.
  Ex: between chiral edge modes of QAHE and surface states

Rikken & Wyder, PRL 94, 016601 (2005)
Tokura and Nagaosa, Nat. Commun. 9, 3740 (2018)
He et al., Nat. Phys. 14, 495 (2018)
Lu *et al.*, Phys. Rev. Research 3, 033160 (2021)
Kou *et al.* PRL 113, 137201 (2014)
Yasuda et al., Nat. nanotech. 15, 831 (2020)

Nonlinear Hall effect (NLH, Hall current rectification)

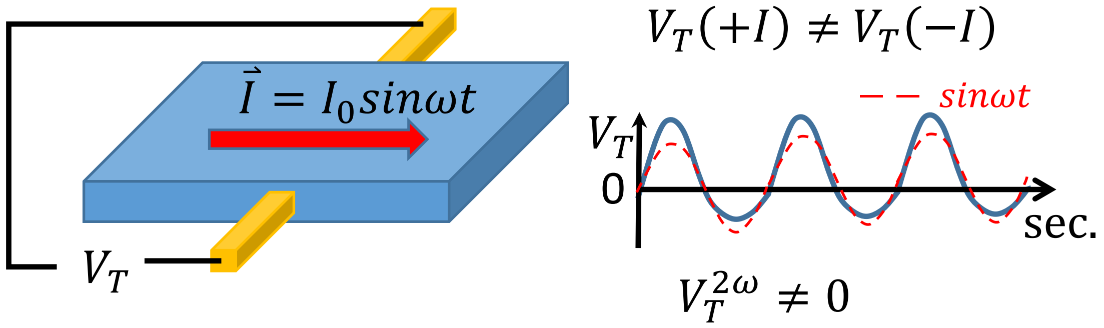

Possible mechanisms for NLH (incomplete)

- Intrinsic Berry curvature effect and quantum metric dipole (D_M): *PT* symmetric AFM BP/MnBi2Te4/BP
- Extrinsic Berry curvature dipole (D): $J_a^{2\omega} \propto \tau D_{ba} E_b^2$

$$D_{bd} \equiv \int \frac{dk^3}{(2\pi)^3} f_0 \frac{\partial \Omega_b}{\partial k_d},$$ (ex: bilayer WTe2…)

- Extrinsic skew scattering and side jump effects.
- Broken $\hat{I}$ is needed for nonzero NLH.

NRTE and NLH Can be a probe for detecting broken $\hat{I}$! (c.f. optical SHG)

Gao, Yang, Niu, PRL 112, 166601 (2014)
Gao *et al.*, Science 381, 6654 (2023).
Sodermann and Fu PRL 115, 216806 (2015).
Ma *et al.*, Nature 565, 337 (2019).
Du *et al.* Nat. Commun. 10, 3047 (2019).

Scale-Invariant Quantum Anomalous Hall Effect in Magnetic Topological Insulators beyond the Two-Dimensional Limit

Xufeng Kou,[1] Shih-Ting Guo,[2] Yabin Fan,[1] Lei Pan,[1] Murong Lang,[1] Ying Jiang,[3] Qiming Shao,[1] Tianxiao Nie,[1] Koichi Murata,[1] Jianshi Tang,[1] Yong Wang,[3] Liang He,[1] Ting-Kuo Lee,[2] Wei-Li Lee,[2,*] and Kang L. Wang[1,†]
[1]Department of Electrical Engineering, University of California, Los Angeles, California 90095, USA
[2]Institute of Physics, Academia Sinica, Taipei 11529, Taiwan
[3]Center for Electron Microscopy and State Key Laboratory of Silicon Materials, Department of Materials Science and Engineering, Zhejiang University, Hangzhou 310027, China
(Received 26 May 2014; revised manuscript received 28 July 2014; published 26 September 2014)

3D ferromagnetic topological insulator

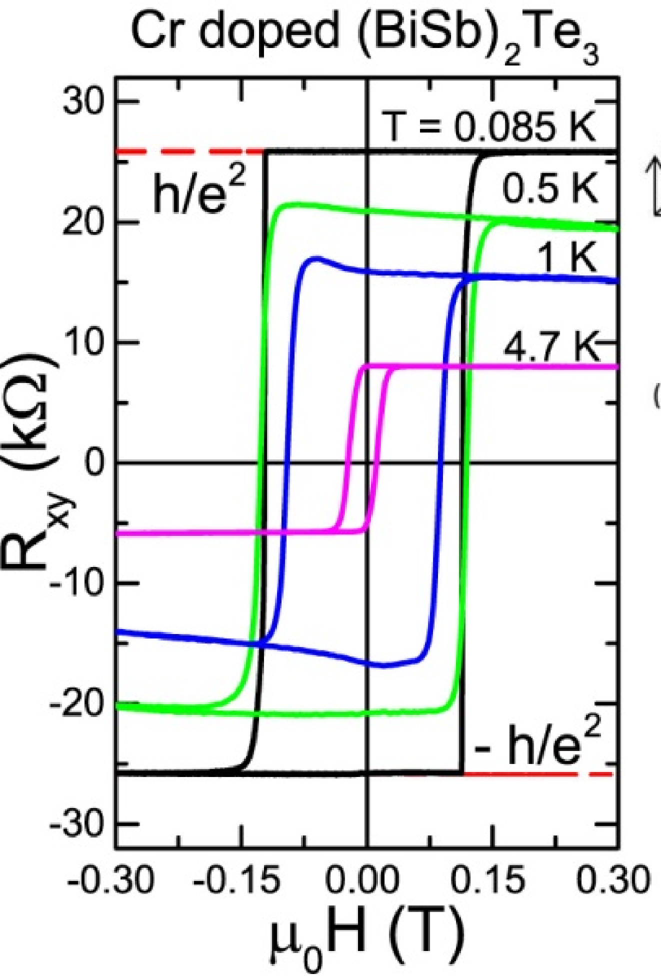

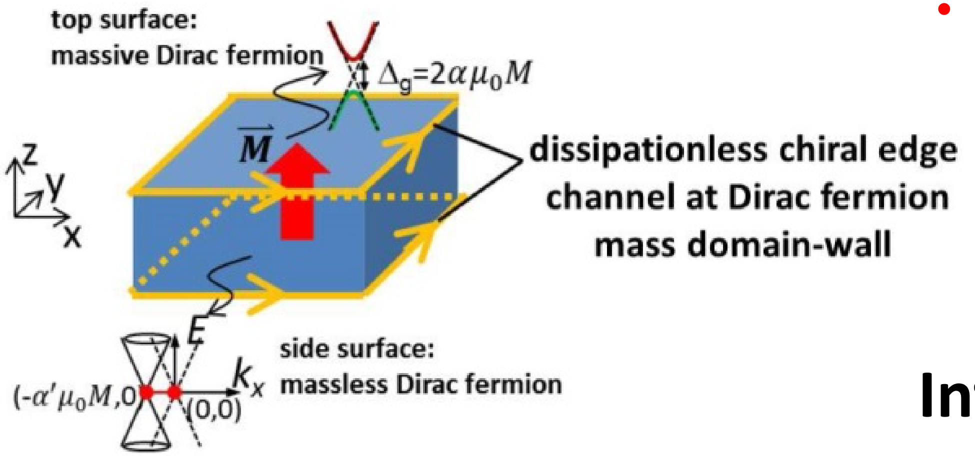

non-local measurement

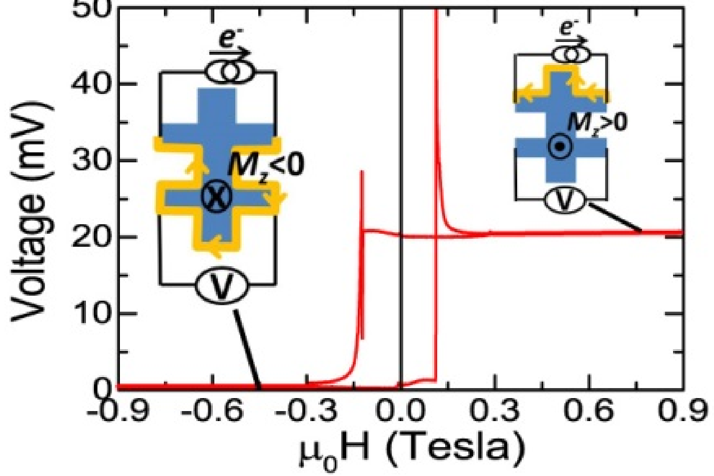

- "One-way" electron flow of QAHE chiral edge channel can be switched on and off by controlling M_z .
- Co-existence of dissipationless 1D chiral edge mode and a dissipative channel !
- **Somewhat robust topological edge/surface states against other trivial states.**

Inferring NRTE due to the coexistence of dissipationless chiral edge mode and dissipative channel for a thick magnetic TI !

Kou *et al.* PRL 113, 137201 (2014)

nature nanotechnology SUPPLEMENTARY INFORMATION
https://doi.org/10.1038/s41565-020-0733-2
In the format provided by the authors and unedited.

Large non-reciprocal charge transport mediated by quantum anomalous Hall edge states

Kenji Yasuda[1,6], Takahiro Morimoto[1,2], Ryutaro Yoshimi[3], Masataka Mogi[1], Atsushi Tsukazaki[4], Minoru Kawamura[3], Kei S. Takahashi[2,3], Masashi Kawasaki[1,3], Naoto Nagaosa[1,3] and Yoshinori Tokura[1,3,5]

Nat. nanotech. 15, 831 (2020)

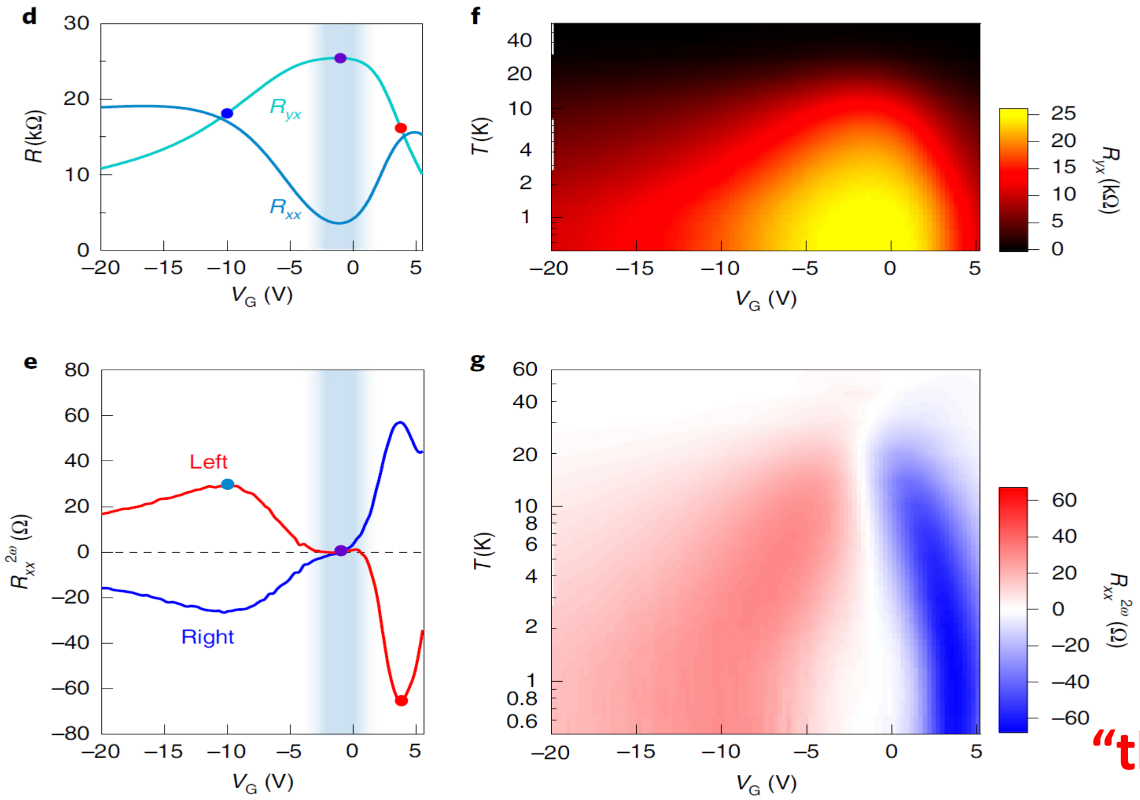

Cr-doped Magnetic topological insulator

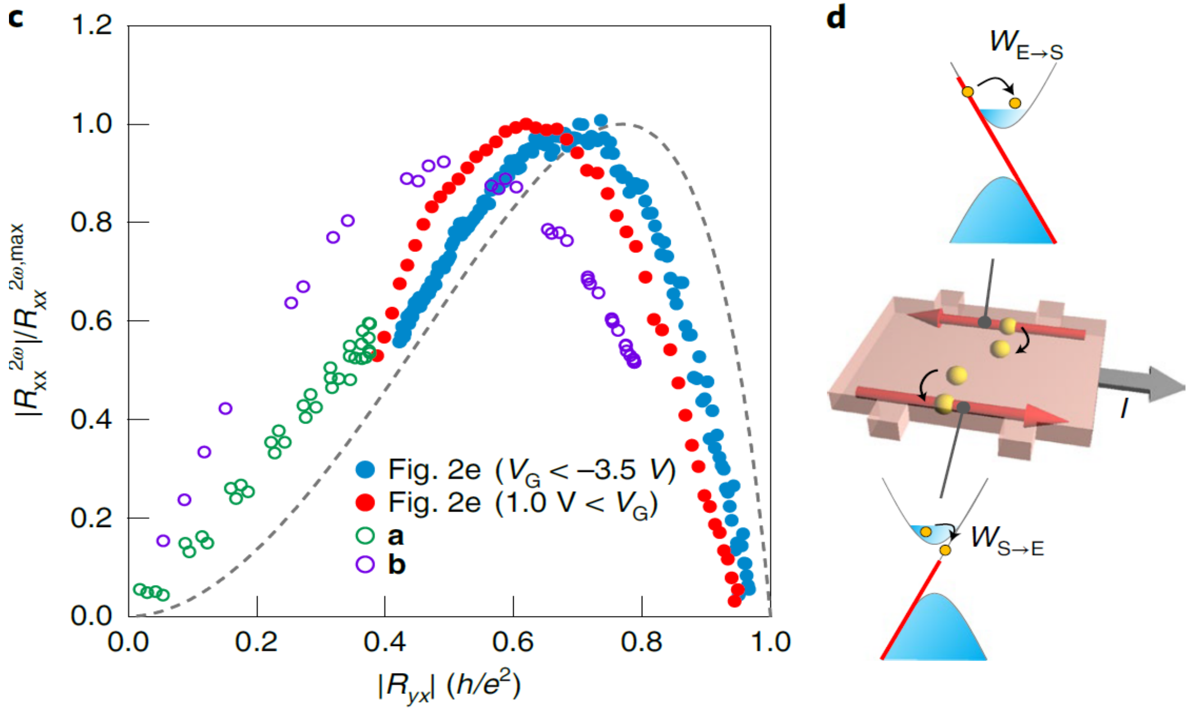

- Asymmetric scattering between dissipationless 1D chiral edge modes with dissipative surface states:

$$W_{edge-to-surface}(+I) \neq W_{surface-to-edge}(-I)$$

- NRTE of $R_{xx}^{2\omega}$ is vanishing when 1D chiral edge mode dominates the charge transport.
- The observed NRTE of $R_{xx}^{2\omega}$ persist up to 40 K ($\approx T_c$)!! (C.f. QAHE with $R_{xy} = h/e^2$ only survives up to ~ 1 K !)

"the non-reciprocal resistance measurement may work as a valuable probe to detect the existence of the edge and surface states."

Quantum Nonlinear Hall Effect Induced by Berry Curvature Dipole in Time-Reversal Invariant Materials

Inti Sodemann and Liang Fu
Department of Physics, Massachusetts Institute of Technology, Cambridge, Massachusetts 02139, USA
(Received 11 August 2015; published 20 November 2015)
PRL 115, 216806 (2015)

Observation of the nonlinear Hall effect under time-reversal-symmetric conditions

Qiong Ma[1,13], Su-Yang Xu[1,13], Huitao Shen[1,13], David MacNeill[1], Valla Fatemi[1], Tay-Rong Chang[2], Andrés M. Mier Valdivia[1], Sanfeng Wu[1], Zongzheng Du[3,4,5], Chuang-Han Hsu[6,7], Shiang Fang[8], Quinn D. Gibson[9], Kenji Watanabe[10], Takashi Taniguchi[10], Robert J. Cava[9], Efthimios Kaxiras[8,11], Hai-Zhou Lu[3,4], Hsin Lin[12], Liang Fu[1], Nuh Gedik[1]* & Pablo Jarillo-Herrero[1]*
Ma *et al.*, Nature 565, 337 (2019).

Second harmonic transverse current density:

$$j_a^{2\omega} = \chi_{abb} E_b^2$$

$$\chi_{abb} = \frac{e^3\tau}{2\hbar^2(1+i\omega\tau)} D_{bc}$$

Berry curvature dipole(BCD) $D_{bd} \equiv \int_k f_0 \frac{\partial \Omega_d}{\partial k_b}$

NLH will appear only when there is current component along $\vec{D}$

Broken $\hat{I}$ in bilayer WTe2 with a mirror plane M_a

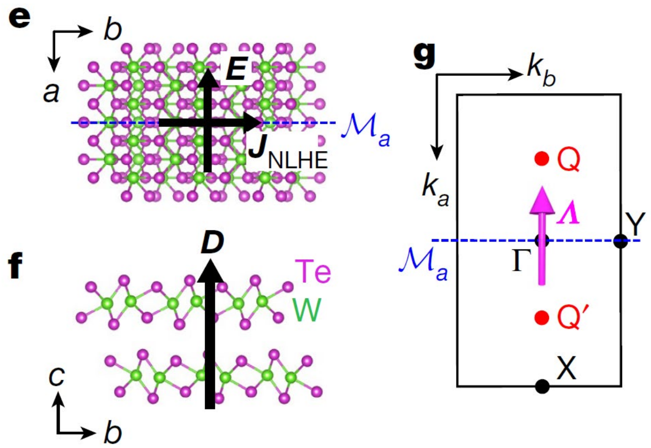

BCD along k_a

Taking into account the anisotropy effect:
ρ_a and are ρ_b are the resistivity along two principal axes and setting a BCD along $\hat{b}$

$$\chi_{abb} = -\chi_{bba} \equiv \chi_b \propto D_{bc}$$

Nonlinear Hall resistance $R_y^{2\omega} = \frac{\chi_b \rho_a \rho_b^2}{W t^2} I \sin\alpha,$

α: angle between bias current and $\hat{a}$

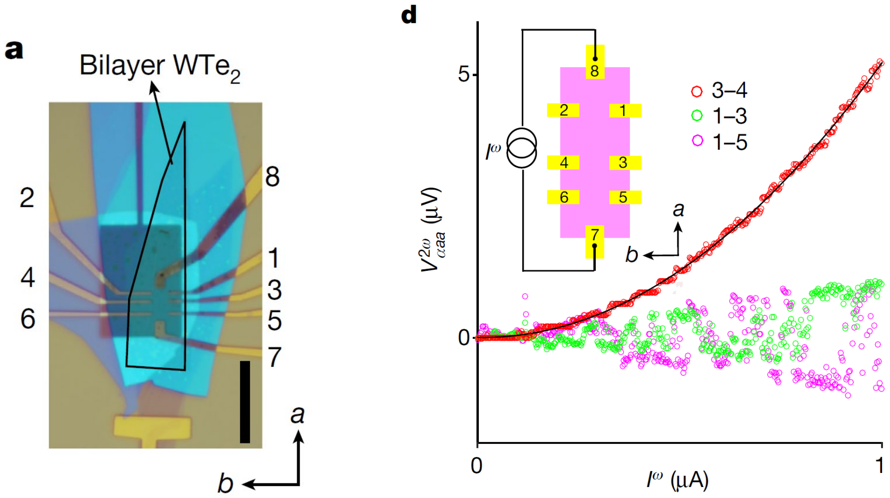

Kar *et al.* arXiv:2307.04482, submitted.

Observation of NRTE and NLH in SRO thin film for *T* < 10 K

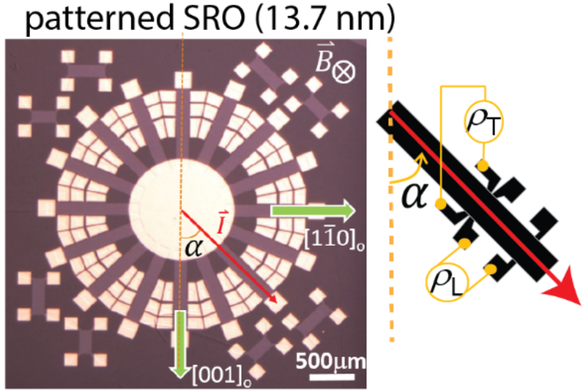

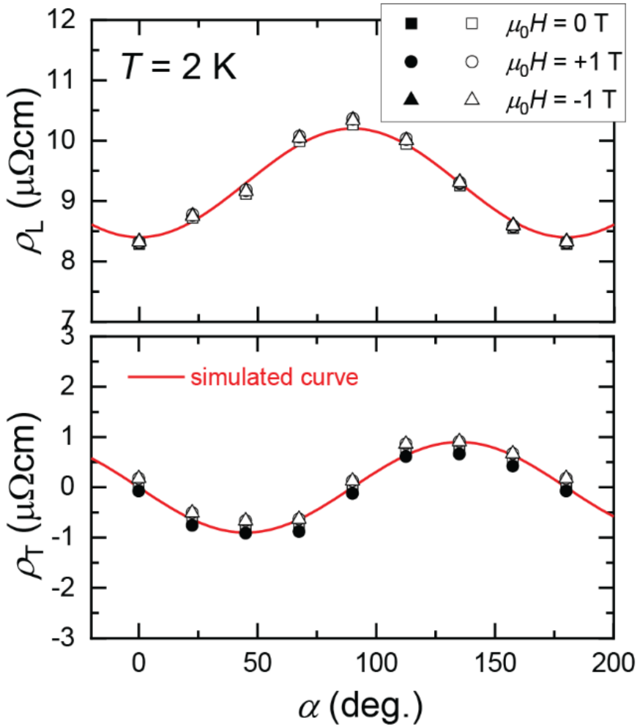

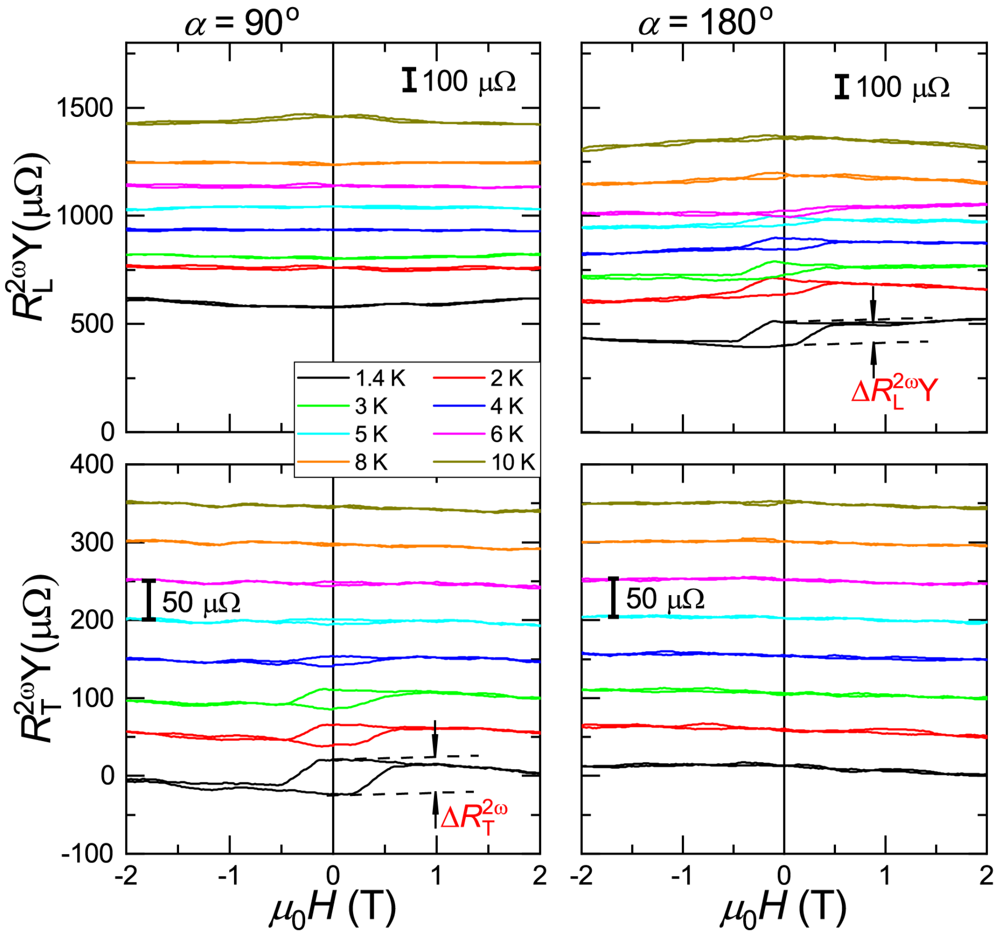

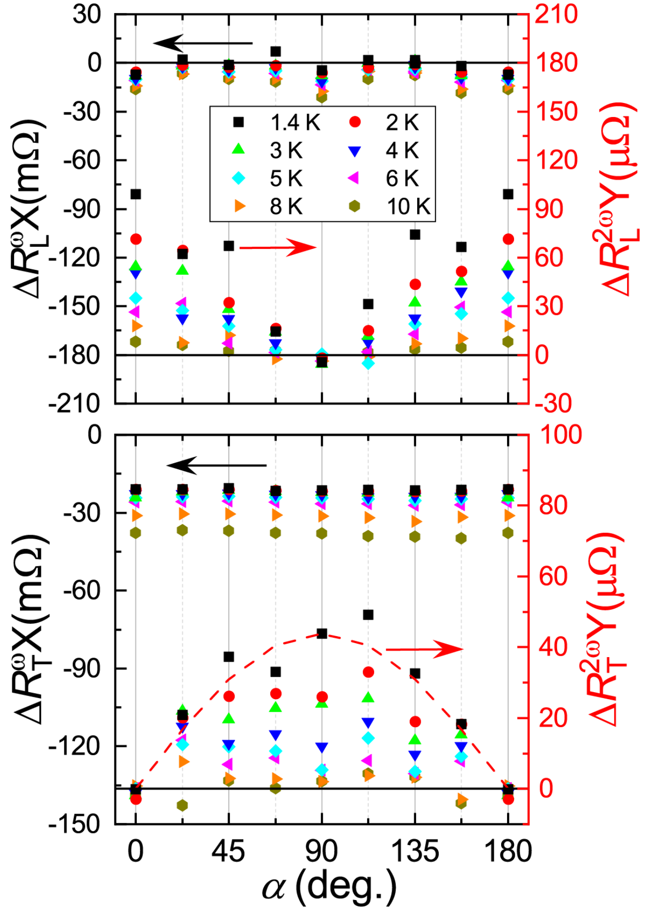

- Non-linear and non-reciprocal charge transport in both ρ_L and ρ_T in zero magnetic field.
- $\Delta R_T^{2\omega} \propto \sin\alpha$, while $\Delta R_L^{2\omega} \propto |\cos\alpha|$: orthogonality in the magnitude for $\Delta R_T^{2\omega}$ and $\Delta R_L^{2\omega}$.
- **Observed $\Delta R_T^{2\omega}$ and $\Delta R_L^{2\omega}$ are surprising since bulk SRO preserves inversion sym. !**
  space group (*P*bnm (300K), and *P*12$_1$/n1 (10K))

What's happening for T < 10 K ?

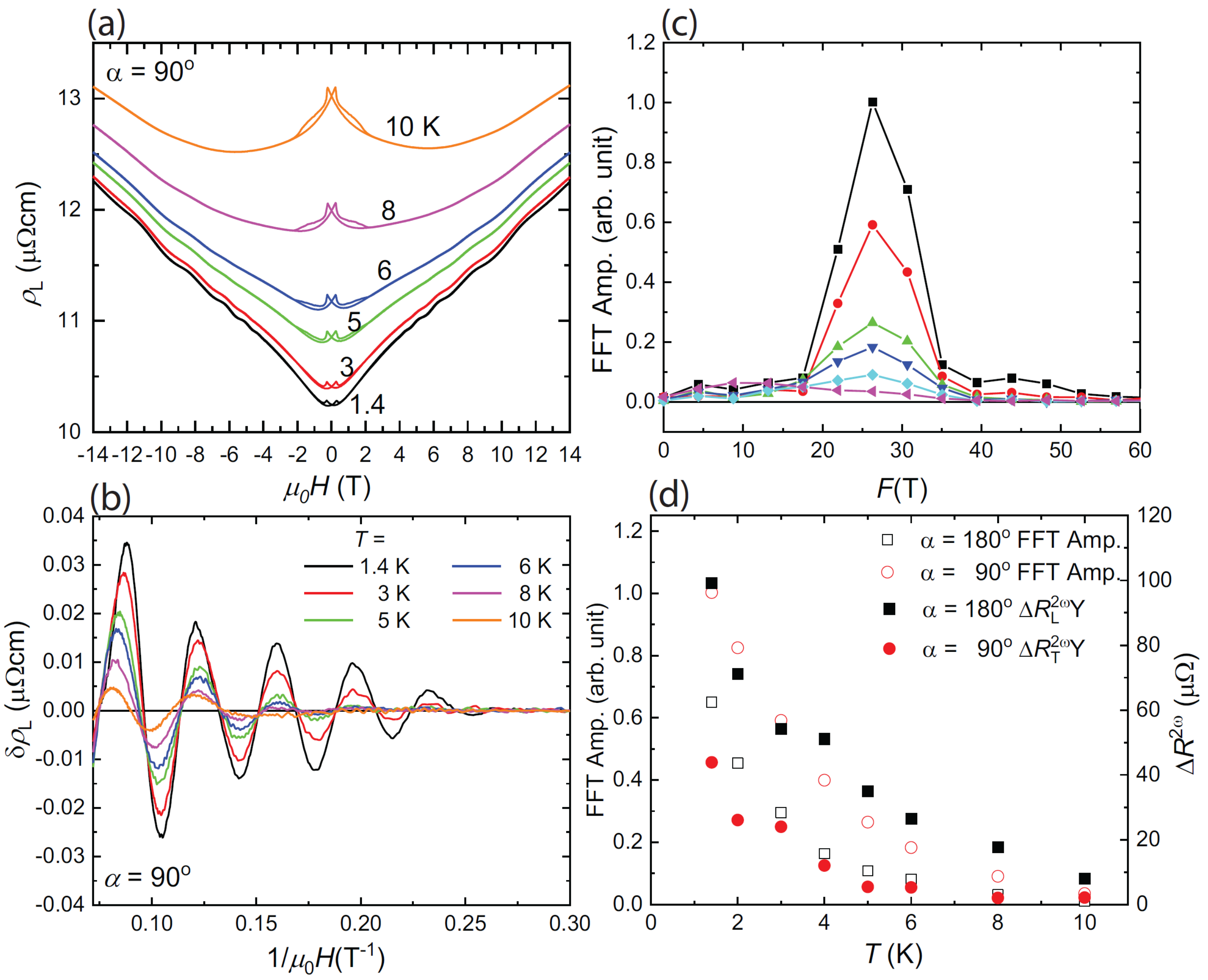

- Crossover behavior in weak field MR and nonlinear field dependent of Hall resistivity: multi-channel charge conductions
- Rapid increase of the amplitude for 2D-like quantum oscillation with a freq. ~ 30 T below 10 K (Weyl-orbit Q.O.)
- The **Observed $\Delta R_T^{2\omega}$ and $\Delta R_L^{2\omega}$** for T < 10 K is in harmonic with the emergence of the 30 T quantum oscillation and also the crossover behavior in MR and Hall resistivity.
- The **Observed $\Delta R_T^{2\omega}$ and $\Delta R_L^{2\omega}$** are thus most likely also deriving from the **edges states and surfaces states** in SRO, where **broken $\hat{I}$** is well justified !

Surface Berry curvature dipole with 1D chiral edge mode in SRO thin film

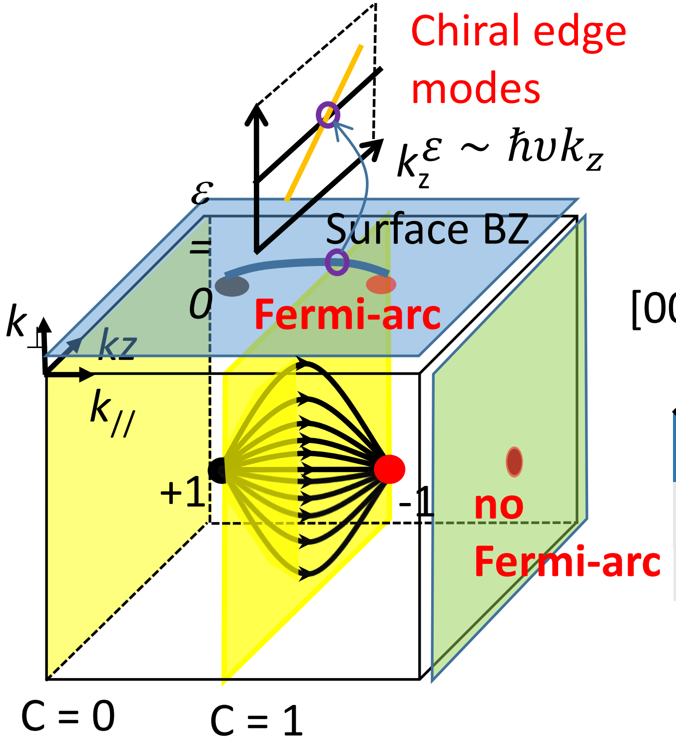

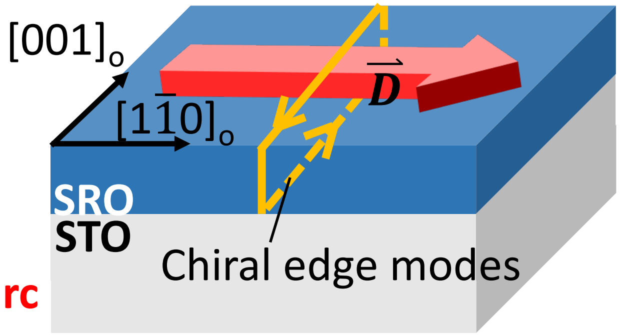

- **Observed $\Delta R_T^{2\omega}$ and $\Delta R_L^{2\omega}$** and their orthogonal α dependence: surface/edge states with broken $\hat{I}$!

surface BCD $\vec{D}$ // $[1\bar{1}0]_o$ + chiral edge modes // $[001]_o$

- Band calculations:
  - ✓ Nonzero total Berry flux for 2D slices along k_z: presence of chiral edge modes along $[001]_o$.
  - ✓ type II and tilted Weyl nodes: possible nonzero surface BCD along $k_{//}$ and thus $[1\bar{1}0]_o$.
  - ✓ Hot lines, separating surface and bulk states, with diverging BCD ?

Wawrzik *et al.* PRL 127, 056601 (2021).

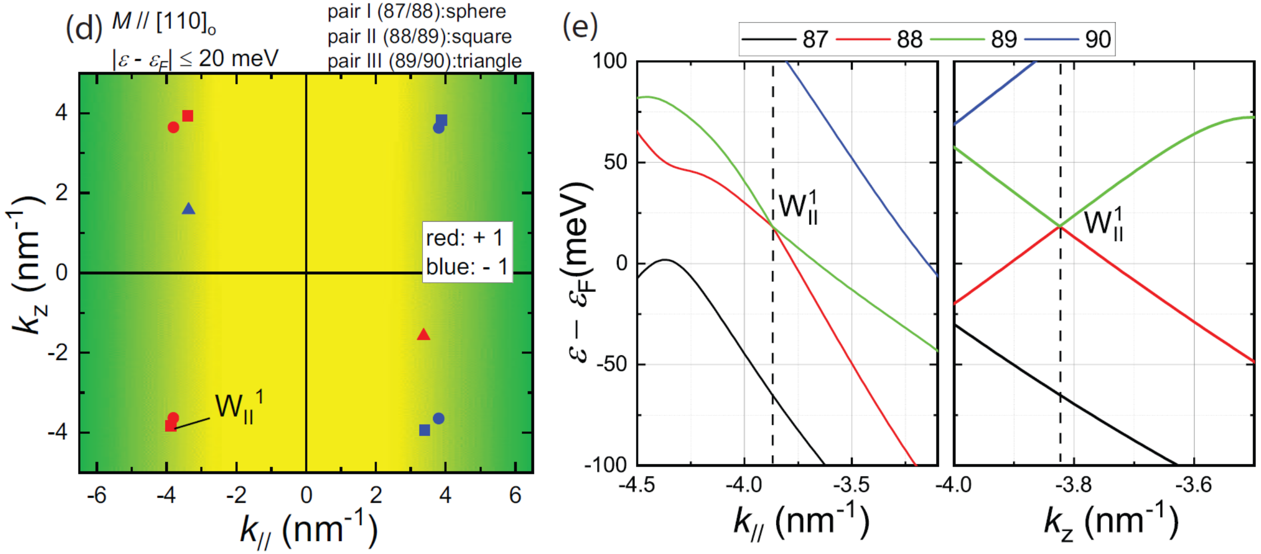

- The NRTE of $\Delta R_L^{2\omega}$ can be due to asymmetric scattering between the chiral edge models on top surface with the Fermi-arc surface states. (cf. NRTE in QAHE)

Conclusion

❑ WOE: Kar *et al.* Sci. Rep. 11, 16070 (2021) and npj Quantum Materials 8, 8 (2023)

- Adsorption-controlled growth of SRO thin films on miscut STO (001) using oxide MBE:
  - ➢ 7.7 < t < 35 nm, high RRR (~14 to 52) and low RR (~12 to 3 $\mu\Omega$cm)
  - ➢ Single-domain and untwinned epitaxial films with excellent thickness uniformity
- F_{s1} ~ 30 T with a light mass of 0.3 m_e:
  - ➢ Non-monotonic "thickness"*(t)*-dep. of FFT amplitude with largest amplitude for *t* ranging from 10-20 nm and relatively weak *t*-dep. of extracted quantum lifetime
  - ➢ F_{s1} follows 1/cos(angles) dep. (2D-like Fermi pocket)
- Simulated Weyl-orbit QO for thickness with optimum thickness of $10 \le t \le 20$ nm :
  - ➢ Unique concave downward curvature in LL fan diag.
  - ➢ Direct consequence of the non-adiabatic corrections (α term).

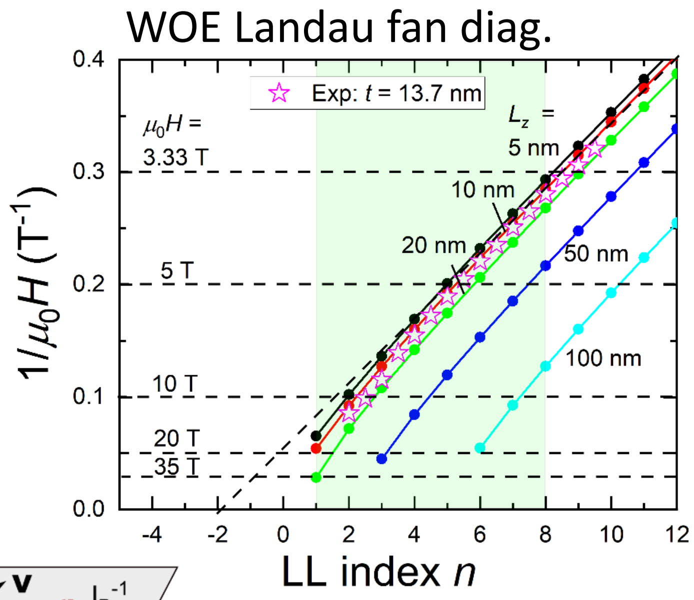

❑ NRTE and NLH in SOR: arXiv:2307.04482

- **Observed $\Delta R_T^{2\omega}$ and $\Delta R_L^{2\omega}$** and their orthogonal α dependence: surface BCD $\vec{D}$ // $[1\bar{1}0]_o$ + chiral edge modes // $[001]_o$
- Band calculations:
  - ✓ Nonzero total Berry flux for 2D slices along k_z support for the presence of chiral edge modes along $[001]_o$.
  - ✓ type II and tilted Weyl nodes: possible nonzero surface BCD along $k_{//}$ and thus $[1\bar{1}0]_o$.

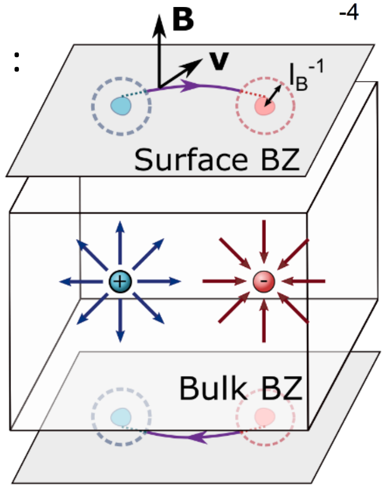

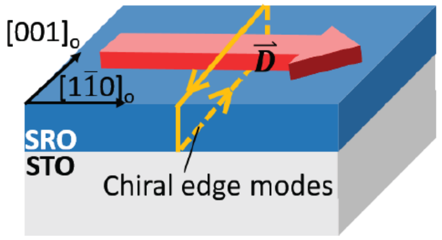

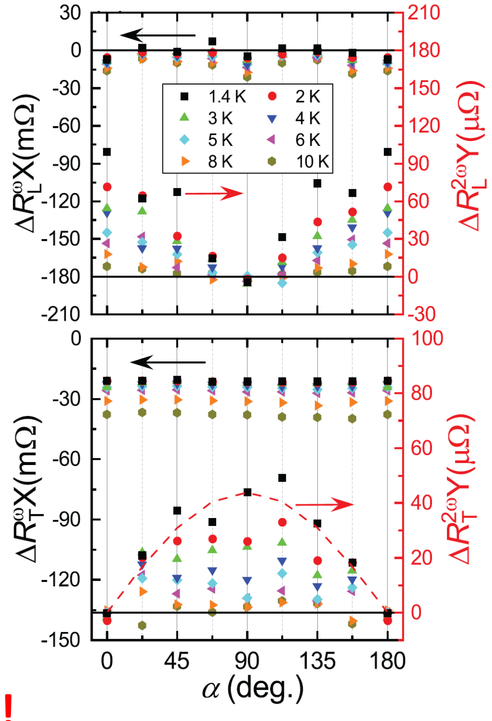

Only possible with sample in thin film form with low defect level grown by oxide MBE facility !

Outlook of future direction

- Unsettle issues for SRO:
  - ✓ The role of electron correlation at low temp ? Electronic nematicity ? ($\rho \sim T^2$ for $T \lesssim 15$ K)
  - ✓ The sustention of the Fermi-arc surface states and 1D chiral edge modes in Weyl *metals* (SRO trivial bulk states: $m^* > 3\ m_e$)
  - ✓ The NRTE and NLH in system with broken *PT.*
- Thin film of Weyl metal SRO is an ideal platform for the design and fabrication of topological electronics:
  - ✓ Further probing Fermi-arc surface states (chiral-zero modes) related physical effects: thermoelectric property, anisotropy property, SRO-based Josephson junction, superconducting proximity coupling to Fermi-arc surface states (Majorana physics ? FFLO states ?) … etc
- Strain engineering on SRO films: tuning Fermi-arc surface states.
  - ✓ Apply adsorption controlled technique to the growth of SRO on different substrates:

    Ex: $(LSAT(001)_c$, -1.6 %) , $(DyScO3(110)_o$, +0.4%)
- Extension of adsorption controlled technique to other oxides:
  - ✓ Development of metal-organic sources for Ti, Ru … etc
  - ✓ Unconventional S.C. Sr_2RuO_4, Mott insulators LaTiO3,Ca_2RuO_4 …
  - ✓ "Altermagnet" RuO_2
  - ✓ ……

Patterned SRO-device

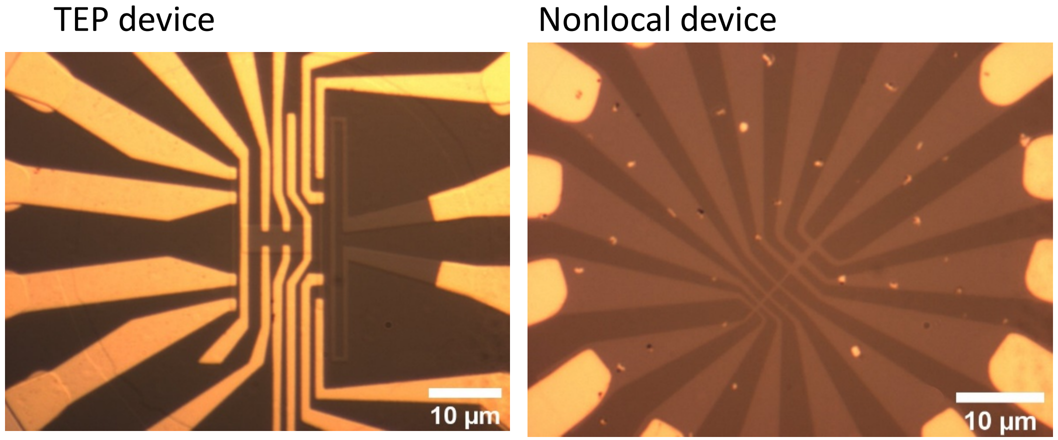

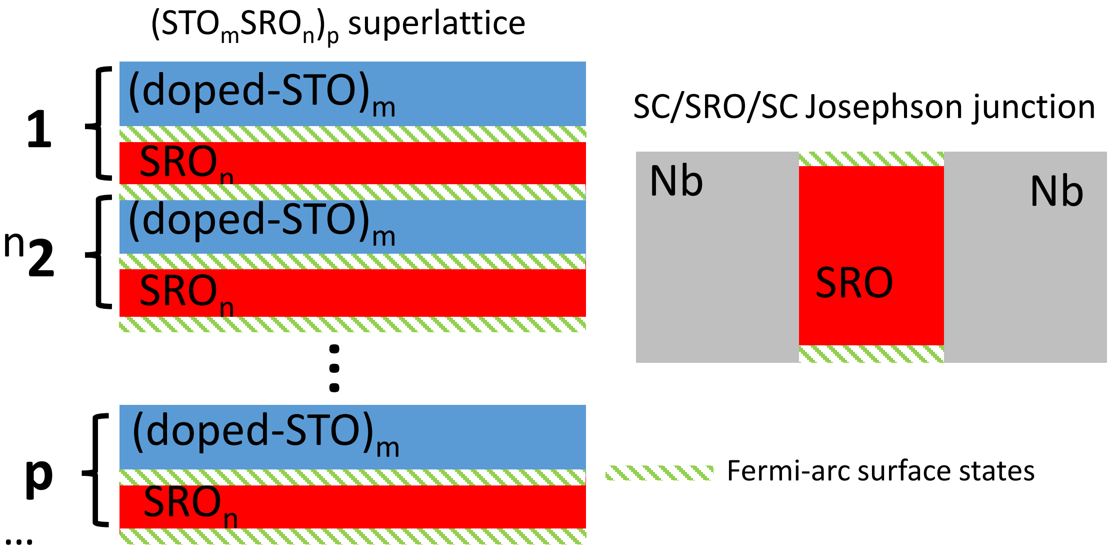

Multi-chamber UHV epitaxial thin film growth and characterization system Lab (B113-115)

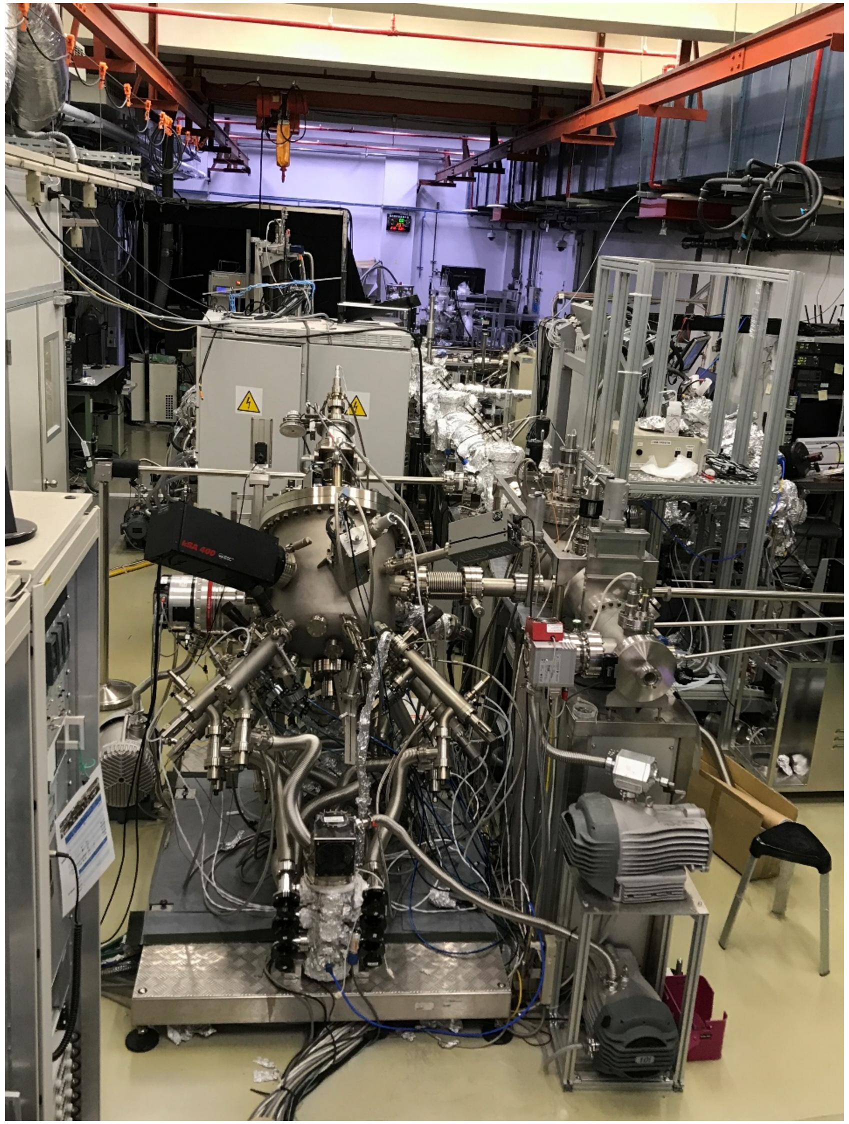

- Oxide MBE with O_3 distiller 2014 (Wei-Li Lee)
- PLD 2014 (YH Chu)
- UHV sample transfer chamber 2016 (Wei-Li Lee, Jason Chang)
- ARPES: DA 30, He-lamp, and monochromator 2017 (SJ Tang)
- Chalcogenide MBE 2017 (Yung Liou, Sankar Raman?)
- VT-STM (Jason Chang)

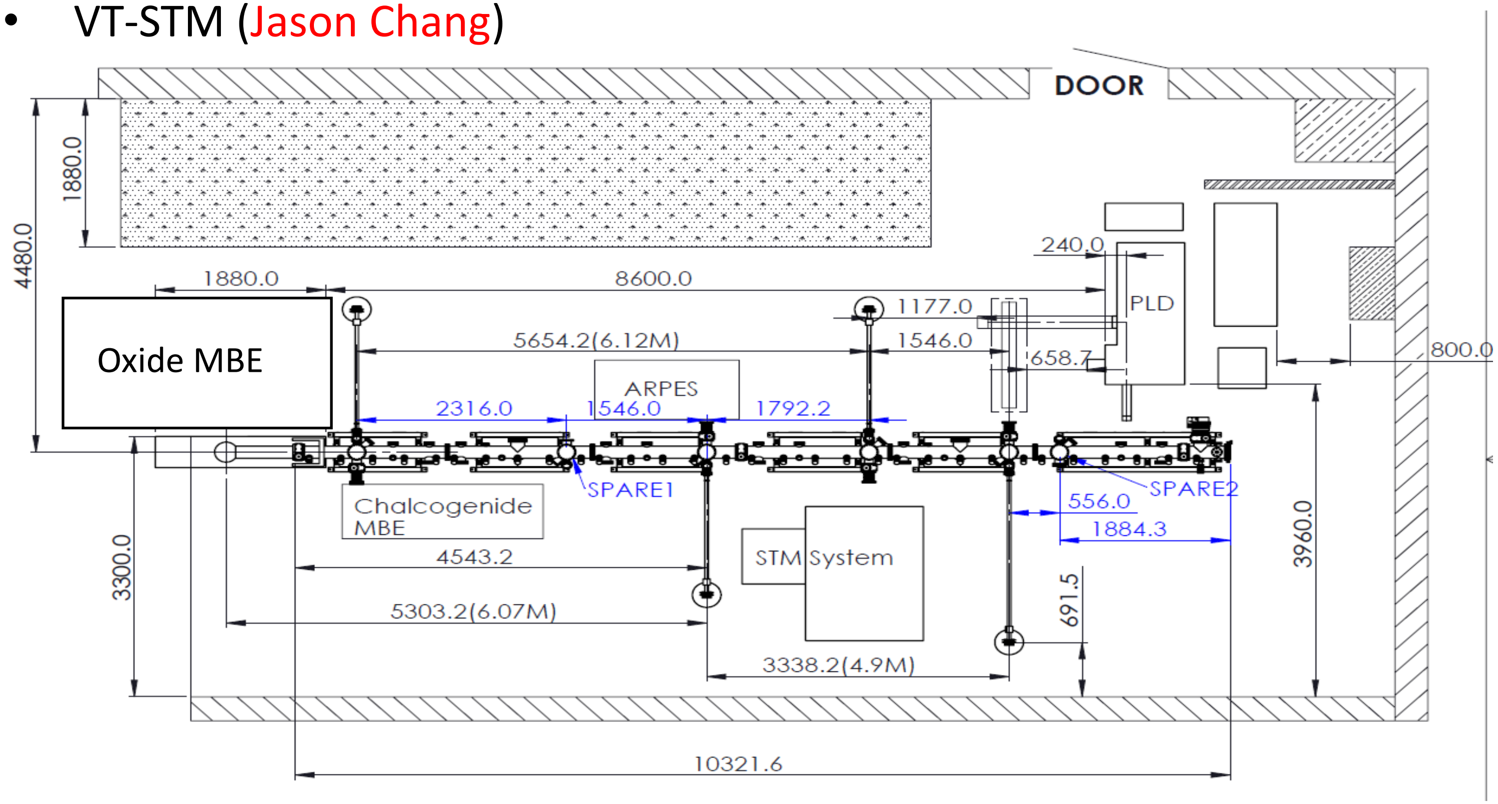

> 4M USD investments since 2014.
Oxide MBE + Chal. MBE + ARPES + PLD + VTSTM

This is NOT a plan/proposal ! Those facilities are what we already had at IoP !
Need to recruit active young PIs (ARPES, MBE) to get involved !

--THE END--

Thank you for your attention

Weyl-orbit QO.

Kar *et al.* Sci. Rep. 11, 16070 (2021)

Kar *et al.* npj Quantum Materials 8, 8 (2023).

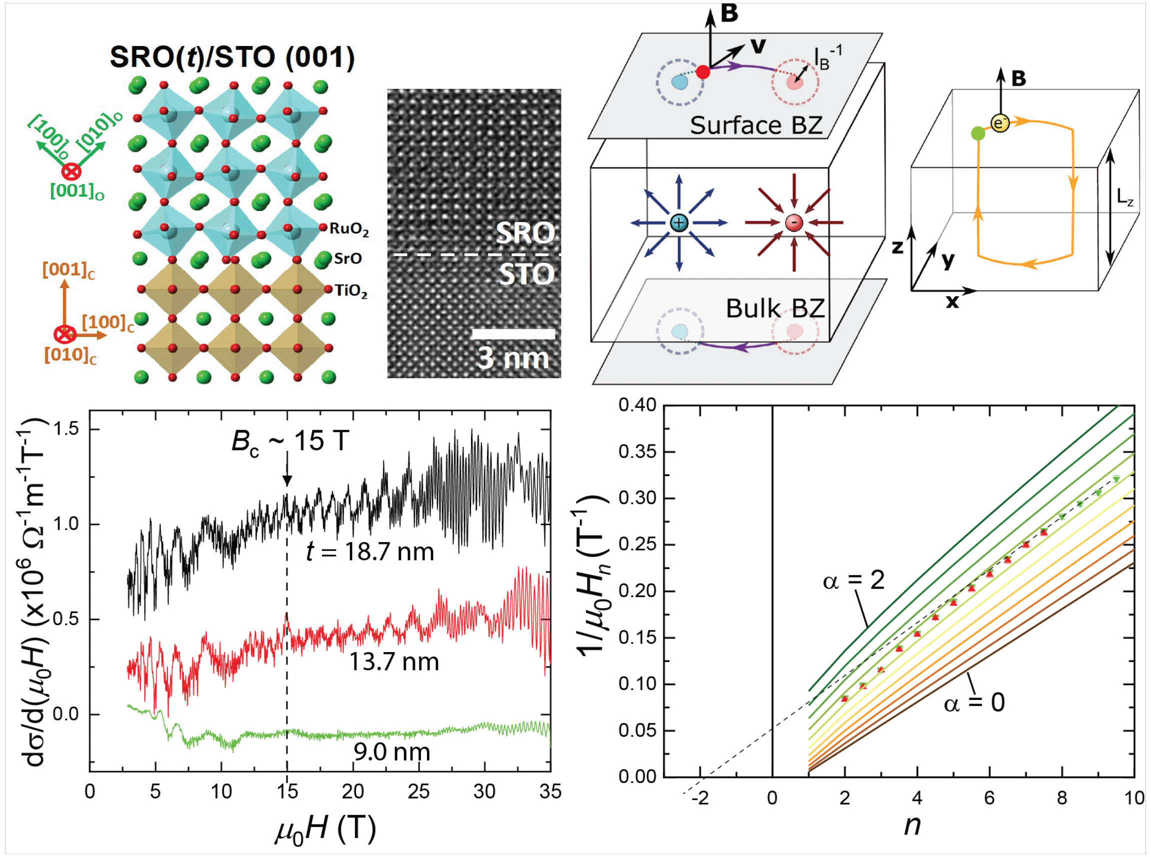

NRTE and nonlinear Hall

Kar *et al.* arXiv:2307.04482, submitted.

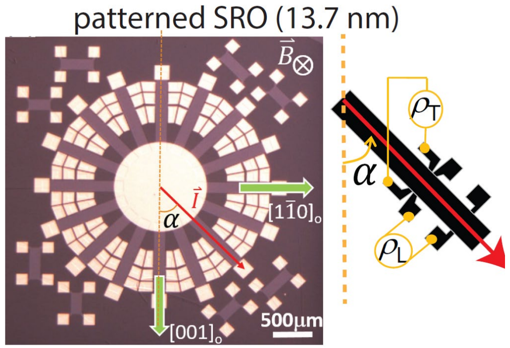

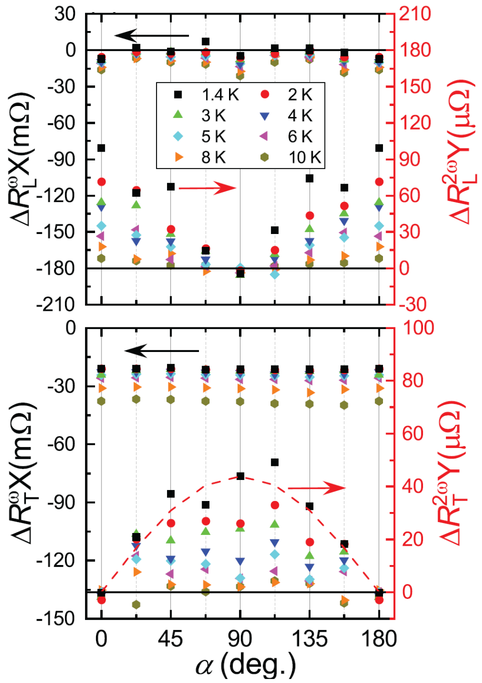

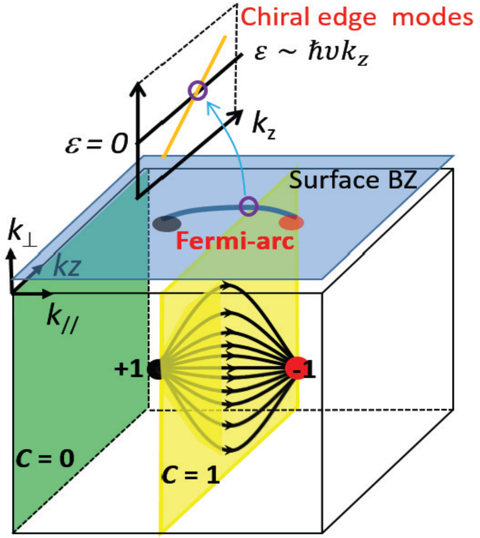

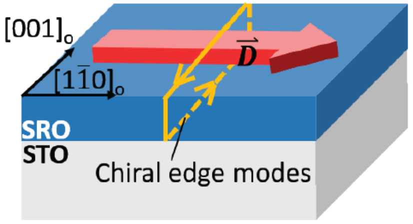

Supporting information below

Revisit of physical properties in SRO ultra thin films

SRO films grown by pulsed laser deposition (PLD)

- Critical thickness of about 3 uc for itinerant Ferromagnetic property in SRO films

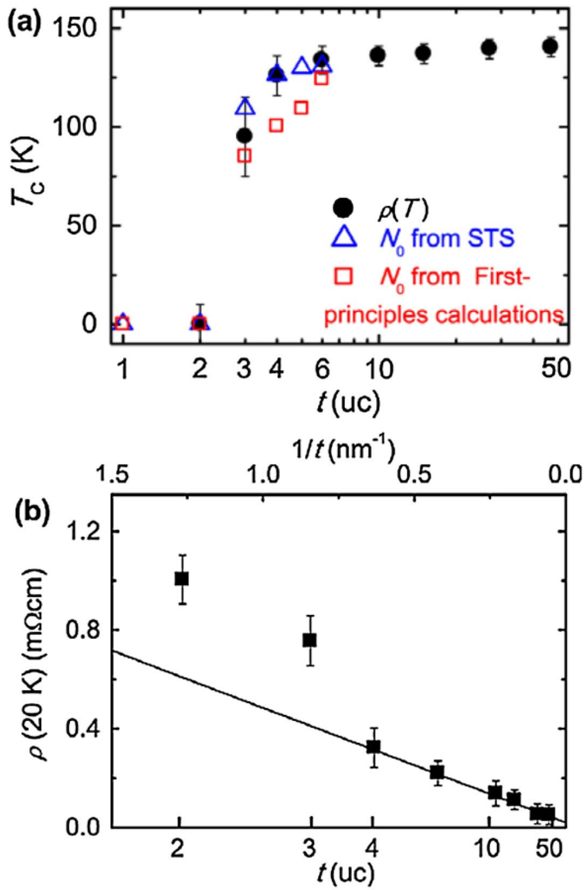

Chang *et al.* PRL 2009

SRO films grown by MBE using adsorption controlled technique

Ferromagnetism and Conductivity in Atomically Thin $SrRuO_3$

H. Boschker,[1] T. Harada,[1] T. Asaba,[2] R. Ashoori,[3] A. V. Boris,[1] H. Hilgenkamp,[4] C. R. Hughes,[1,5] M. E. Holtz,[6] L. Li,[2,3] D. A. Muller,[6,7] H. Nair,[8] P. Reith,[4] X. Renshaw Wang,[4,*] D. G. Schlom,[7,8] A. Soukiassian,[8] and J. Mannhart[1]

PHYSICAL REVIEW X **9,** 011027 (2019)

- A 2D metallic and ferromagnetic oxide

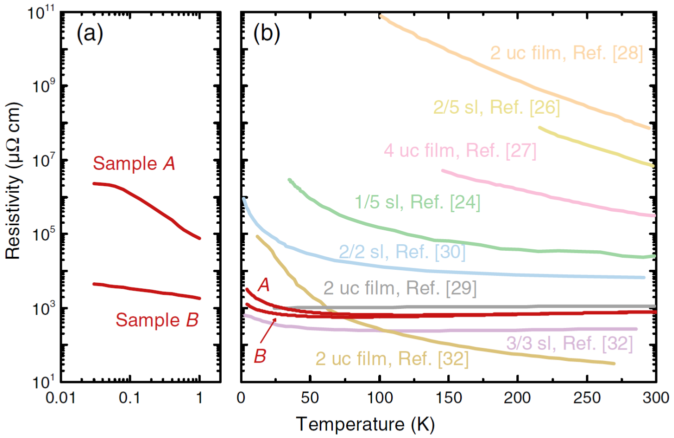

FIG. 7. Temperature dependence of the resistivities of samples *A* and *B*. (a) Temperature range below 1 K on a logarithmic scale. (b) Temperature range $2 < T < 300$ K on a linear scale. For comparison, thin-film and superlattice (sl) samples found in the literature with a comparable thickness of the $SrRuO_3$ layers are also shown. The superlattices are $\{(SrRuO_3)_1 - (SrTiO_3)_5\}_{20}$ [24], $\{(SrRuO_3)_2 - (BaTiO_3)_5\}_{36}$ [26], $\{(SrRuO_3)_2 - (LaAlO_3)_2\}_{60}$ [30], and $\{(SrRuO_3)_3 - (SrTiO_3)_3\}_{15}$ [32]. All samples are grown on $SrTiO_3$ substrates.

Torque magnetometry

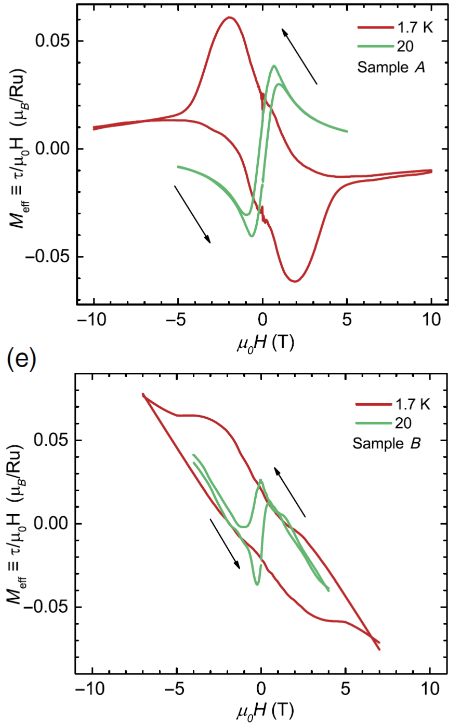

Monolayer sample A: upper bound of 0.4% two-layer SRO.(STEM)
Monolayer sample B: upper bound of 0.3% two-layer SRO.

Several transport issues at low temp. in SRO films can be revisited !

Comparison to band calculations

DFT+U, Wien2k with FP-LAPW+lo and PBE-GGA,

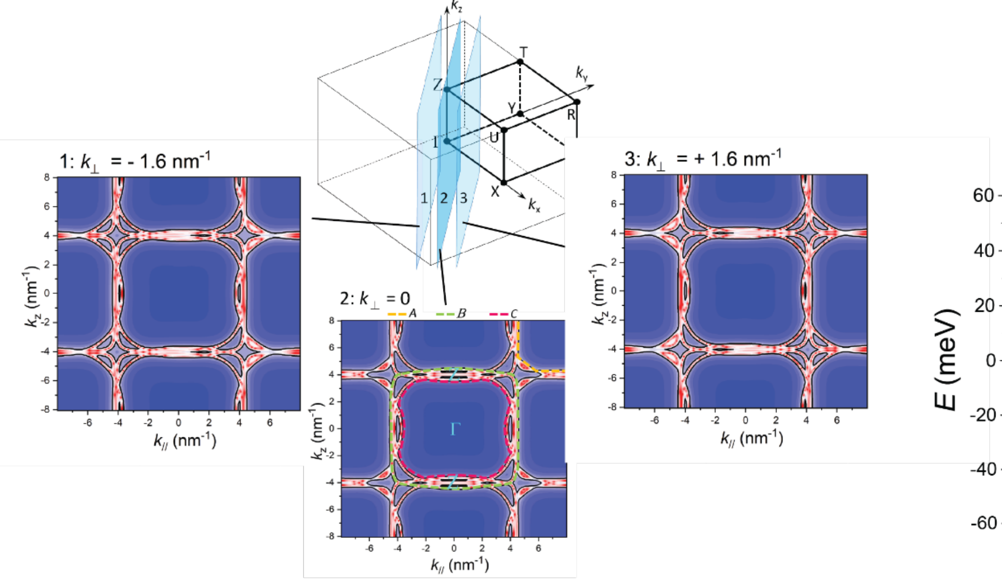

U = 3.4 eV, M // [110]$_o$, J = 0.2 U

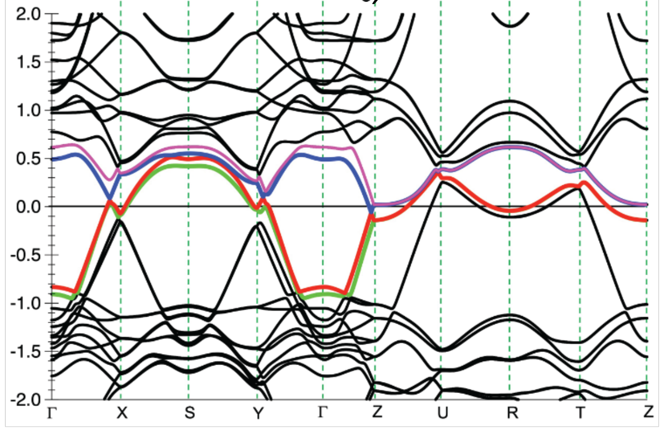

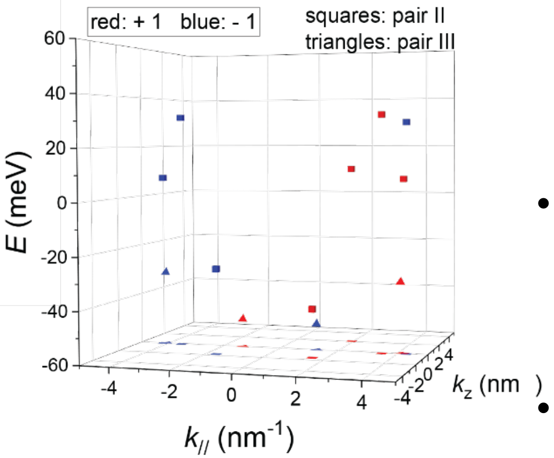

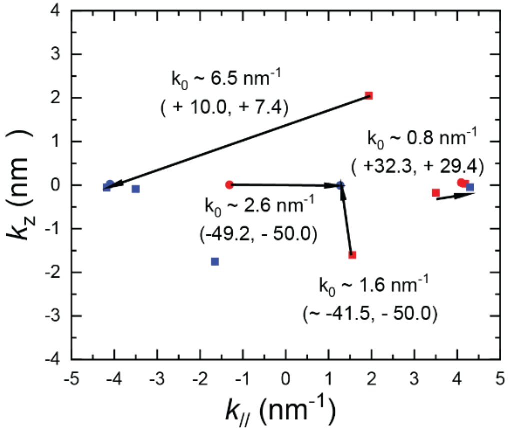

- Bulk pockets A, B, and C:

	A	B	C
Band cal. (T)	5077	7531	5517
Exp. QO (T)	3680 (F_3)	7400 (F_5)	4000 (F_4)

- Searching for Weyl-nodes from four pairs of bands near Fermi energy (with an energy window of $|E - E_F| \leqq$ 50 meV)

- The nodes are NOT at high sym. Locations, and sensitive to the band parameters (U, M)

- Non-overlapped Weyl-node pairs on (110)$_o$ plane can be identified with Fermi-arc length k_0 ranging from 0.8 to 6.5 nm^{-1}, supporting for the occurrence of Weyl-orbit QO in our untwinned SRO films.

Cf. k_0 = 1.09 nm^{-1} from experiment.

Temperature dependent XRD of the SRO 35 uc

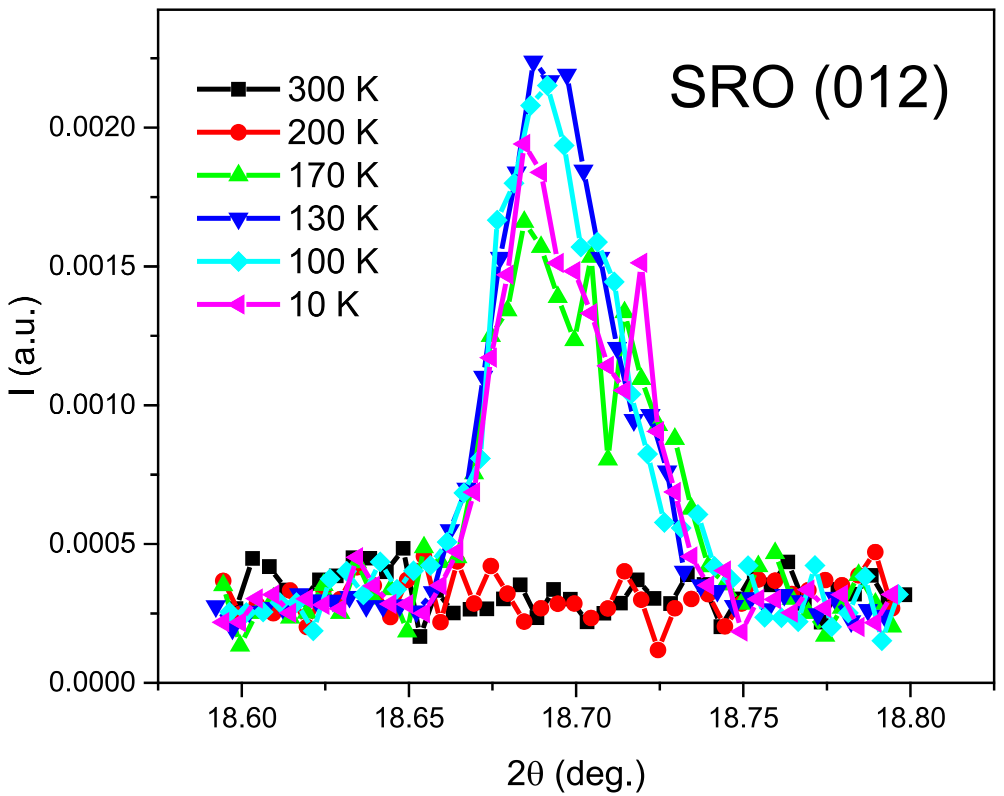

SRO space group (Pbnm) at RT

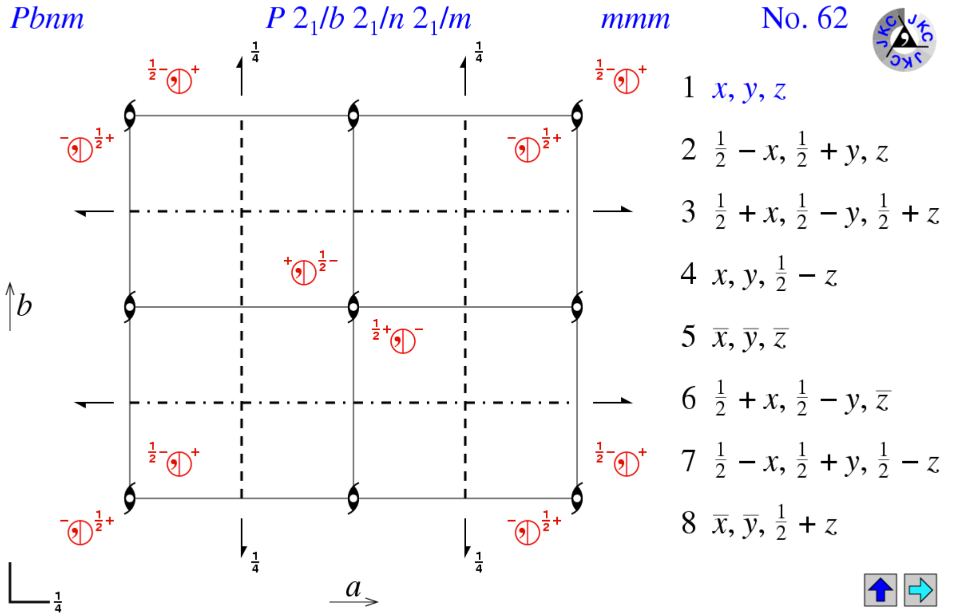

SRO space group ($P12_1/n1$) at below ~170 K

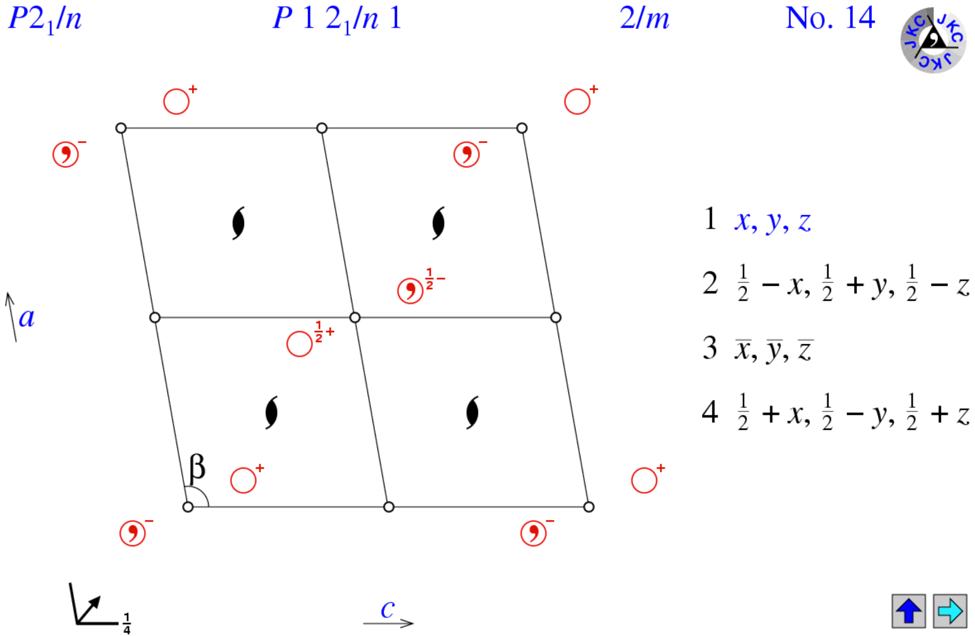

- The Pbnm SRO likely changes to the $P12_1/n$ 1 SRO after breaking the mirror symmetry.
- SRO (012) reflection is allowed in the $P12_1/n$ 1 space group.
- SRO(012) reflection is forbidden in Pbnm space group.
- SRO (012) peak were not appeared at 200 K and 300 K, revealing for the Pbnm space group.
- SRO (012) peak appeared from 170 K to 10 K suggesting for a structural transition from pbnm to likely $P12_1/n$ 1 space group.

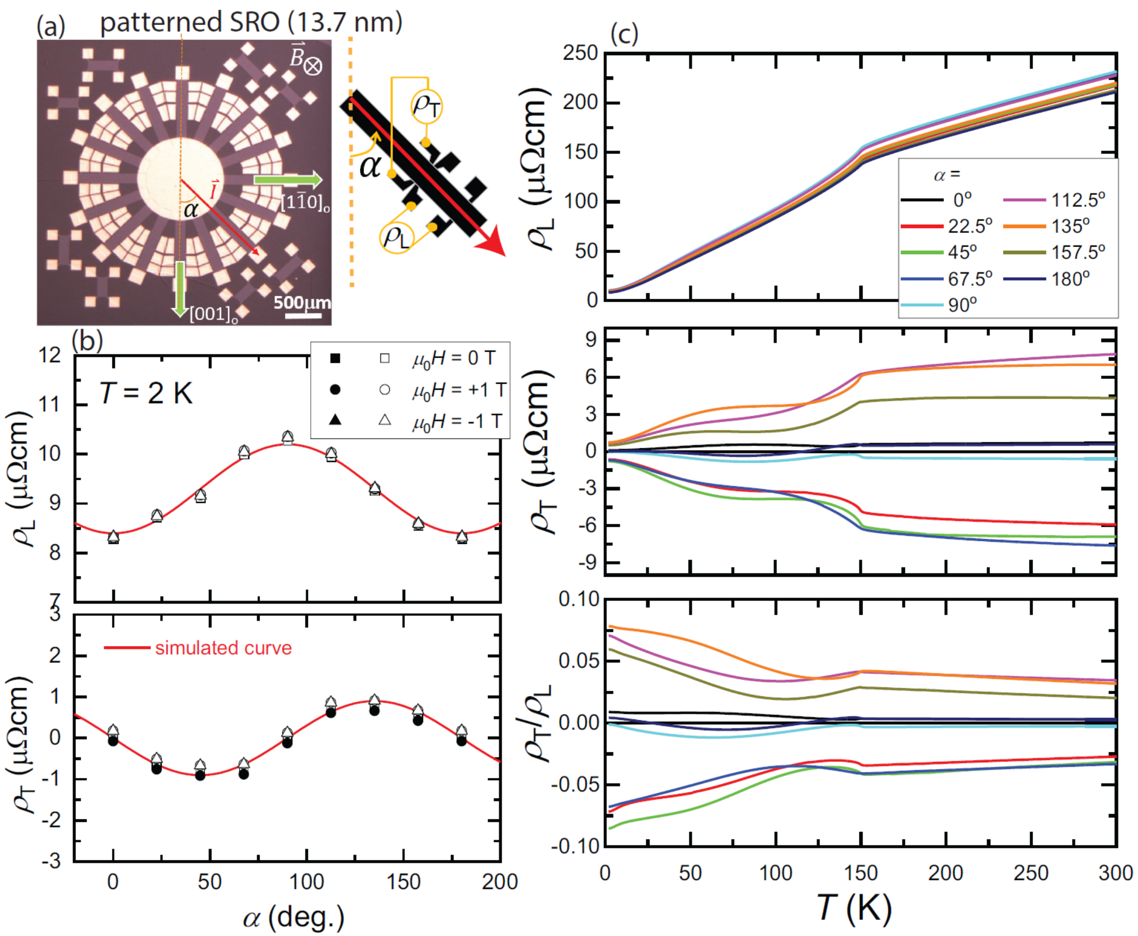
(a) patterned SRO (13.7 nm)
α
ρT
ρL
[1-10]o
[001]o
500μm
(b)
T = 2 K
μ0H = 0 T
μ0H = +1 T
μ0H = -1 T
ρL (μΩcm)
ρT (μΩcm)
simulated curve
α (deg.)
(c)
ρL (μΩcm)
α =
0°
22.5°
45°
67.5°
90°
112.5°
135°
157.5°
180°
ρT (μΩcm)
ρT/ρL
T (K)

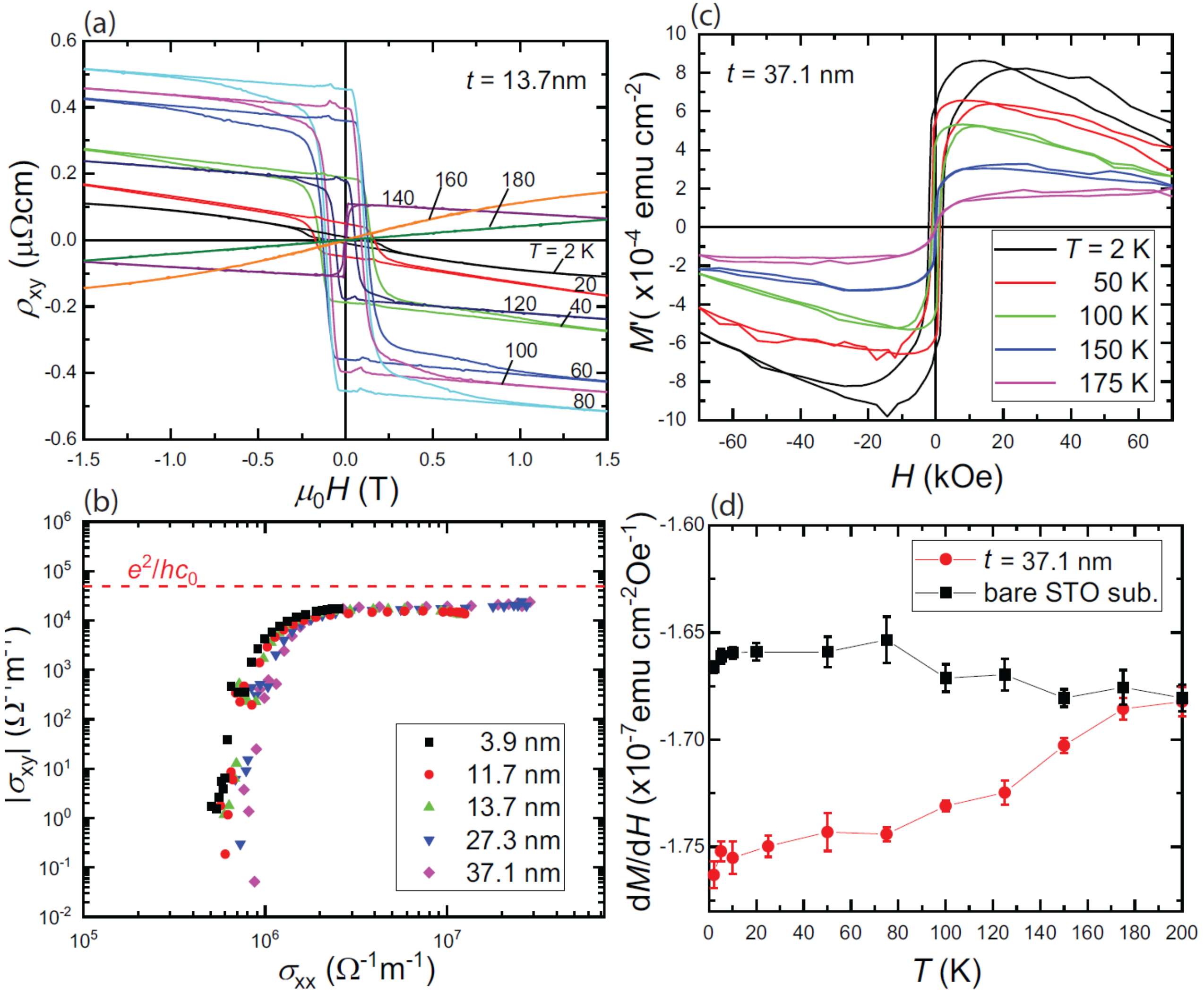
(a)
t = 13.7nm
ρxy (μΩcm)
μ0H (T)
T = 2 K
20
40
60
80
100
120
140
160
180
(b)
e2/hc0
|σxy| (Ω-1m-1)
σxx (Ω-1m-1)
3.9 nm
11.7 nm
13.7 nm
27.3 nm
37.1 nm
(c)
t = 37.1 nm
M'(x10-4 emu cm-2)
H (kOe)
T = 2 K
50 K
100 K
150 K
175 K
(d)
t = 37.1 nm
bare STO sub.
dM/dH (x10-7emu cm-2Oe-1)
T (K)

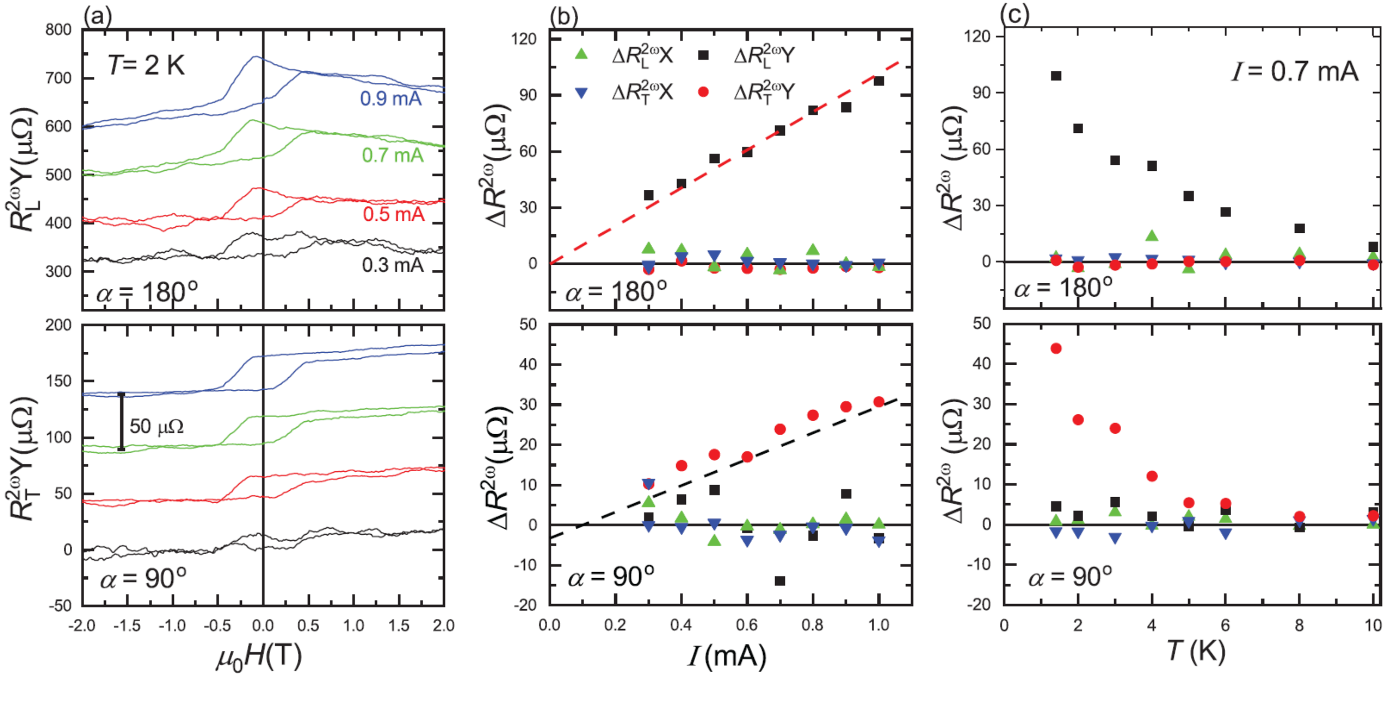

(a)
(b)
(c)
T= 2 K
0.9 mA
0.7 mA
0.5 mA
0.3 mA
α = 180°
α = 90°
50 μΩ
$R_L^{2\omega}Y(\mu\Omega)$
$R_T^{2\omega}Y(\mu\Omega)$
μ_0H(T)
$\Delta R_L^{2\omega}X$
$\Delta R_L^{2\omega}Y$
$\Delta R_T^{2\omega}X$
$\Delta R_T^{2\omega}Y$
$\Delta R^{2\omega}(\mu\Omega)$
I (mA)
I = 0.7 mA
T (K)

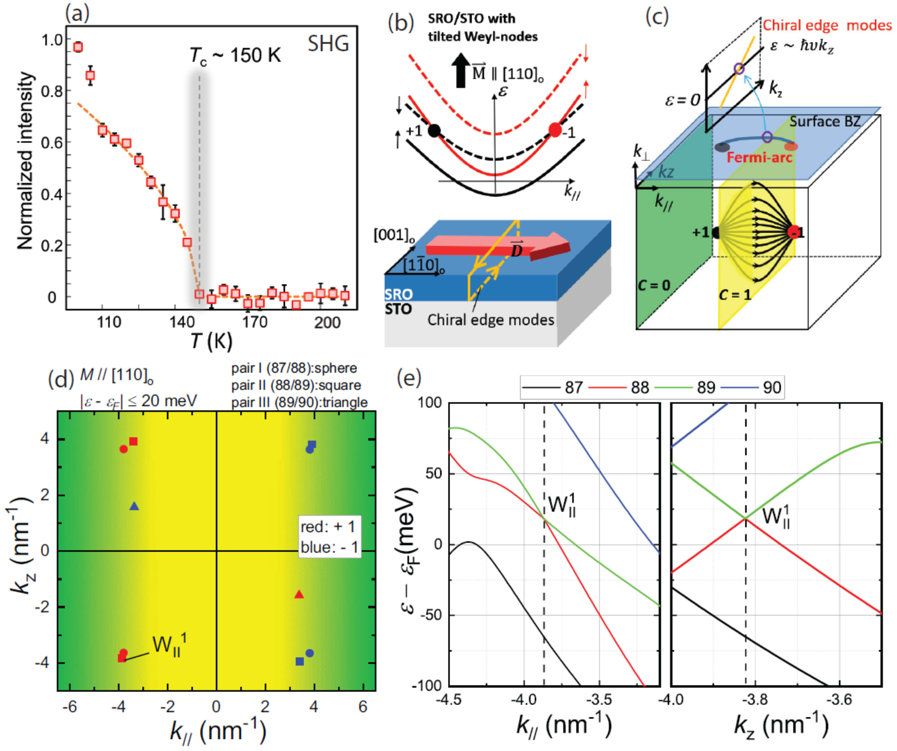

(a)
SHG
T_c ~ 150 K
Normalized intensity
T (K)
(b)
SRO/STO with
tilted Weyl-nodes
M ∥ [110]o
ε
+1
-1
$k_{//}$
[001]o
[1$\bar{1}$0]o
SRO
STO
Chiral edge modes
(c)
Chiral edge modes
ε ~ ħυk_z
ε = 0
k_z
Surface BZ
Fermi-arc
$k_\perp$
$k_{//}$
+1
-1
C = 0
C = 1
(d)
M // [110]o
|ε - ε_F| ≤ 20 meV
pair I (87/88):sphere
pair II (88/89):square
pair III (89/90):triangle
red: + 1
blue: - 1
W_{II}^1
k_z (nm^{-1})
$k_{//}$ (nm^{-1})
(e)
87
88
89
90
ε − ε_F(meV)
W_{II}^1
$k_{//}$ (nm^{-1})
k_z (nm^{-1})

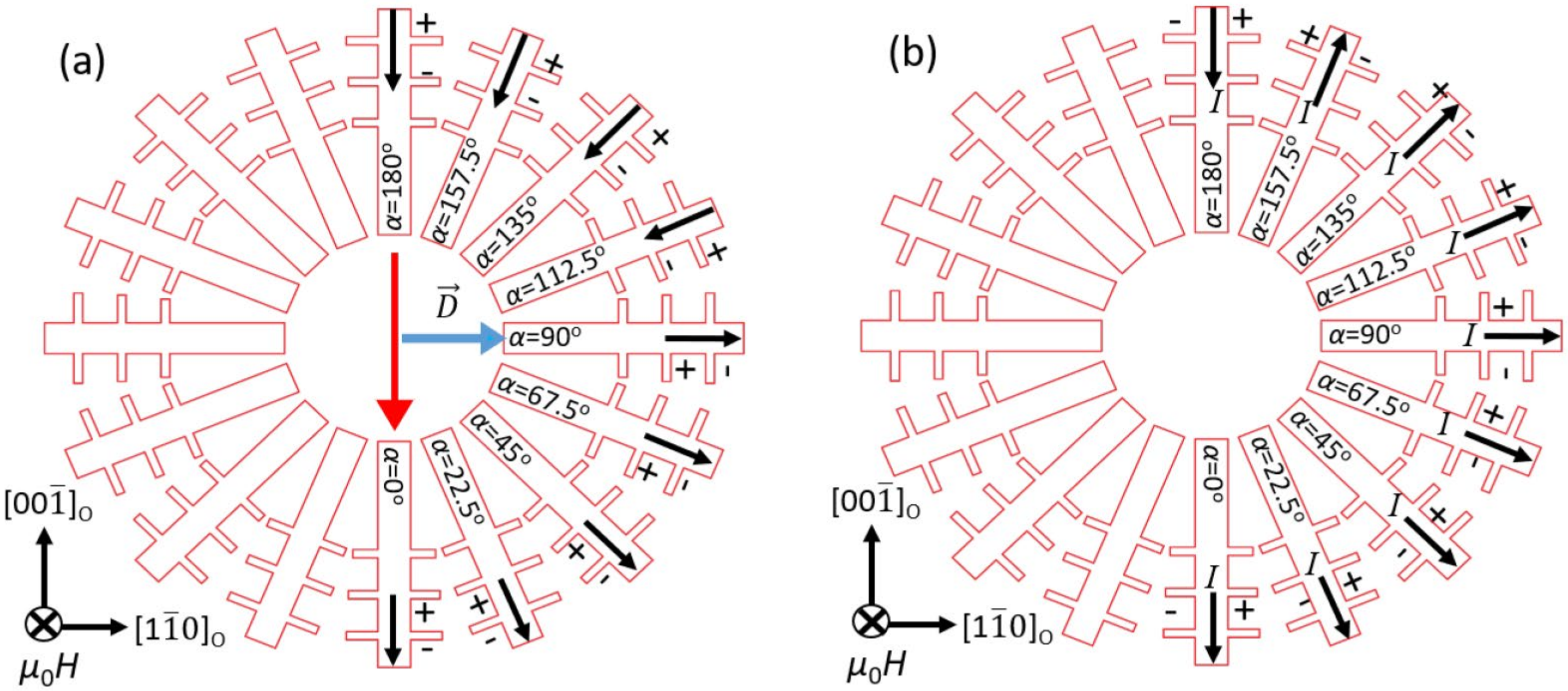

(a)
α=180°
α=157.5°
α=135°
α=112.5°
α=90°
α=67.5°
α=45°
α=22.5°
α=0°
$\vec{D}$
$[00\bar{1}]_O$
$[1\bar{1}0]_O$
$\mu_0 H$
(b)
α=180°
α=157.5°
α=135°
α=112.5°
α=90°
α=67.5°
α=45°
α=22.5°
α=0°
I
$[00\bar{1}]_O$
$[1\bar{1}0]_O$
$\mu_0 H$

Supporting information end